SQT

E.9-10.199
CR-158511

A STUDY OF
MINNESOTA LAND AND WATER
RESOURCES USING REMOTE SENSING

December 31, 1978
NASA GRANT 24-005-263 VOL. XII

ORIGINAL CONTAINS
COLOR ILLUSTRATIONS

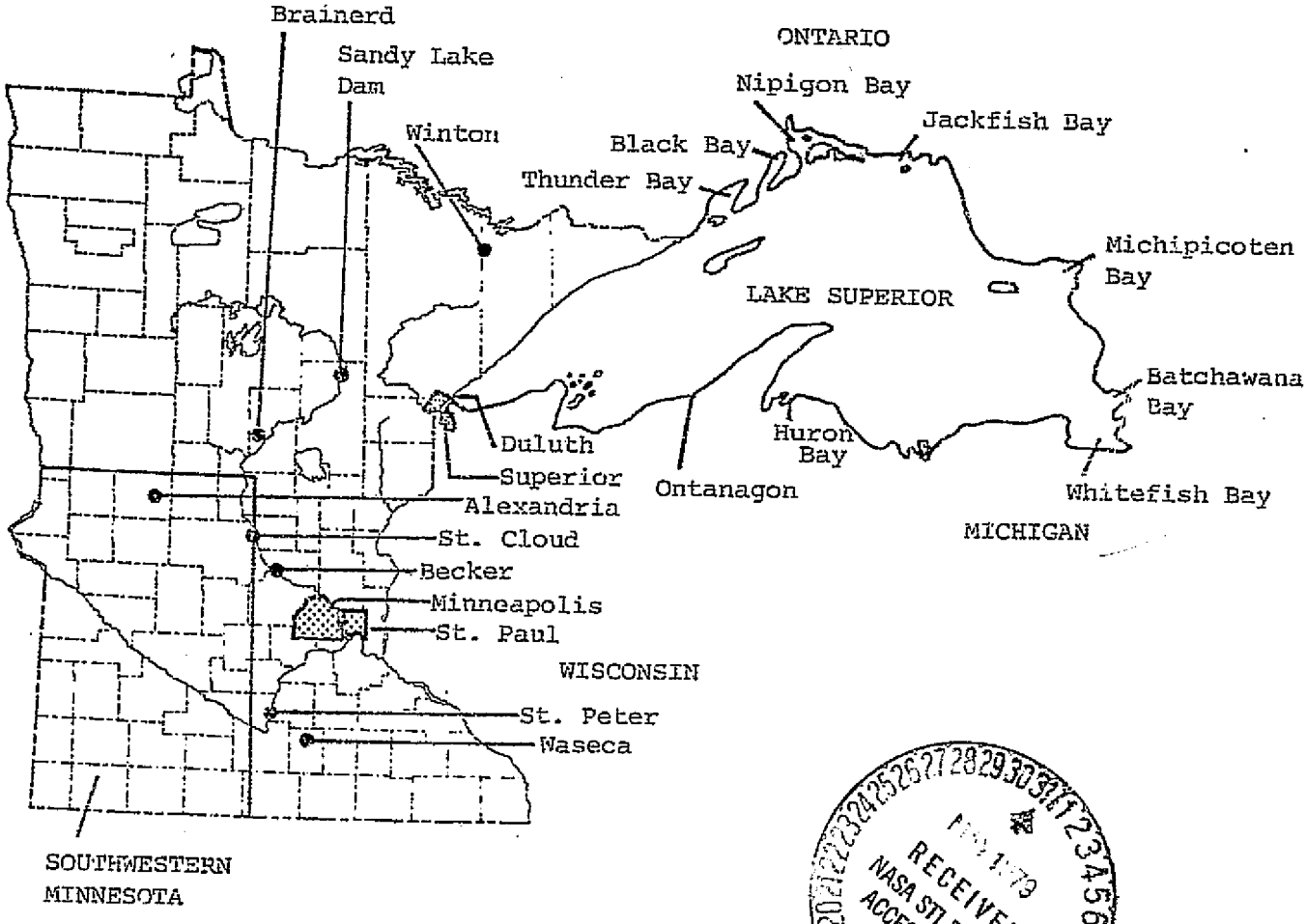

SPACE SCIENCE CENTER

University of Minnesota

Minneapolis, Minnesota 55455

A STUDY OF MINNESOTA LAND AND WATER RESOURCES USING REMOTE SENSING

PROGRESS REPORT

January 1, 1979

Supported By:

NASA GRANT NGL 24-005-263

Submitted to:

NATIONAL AERONAUTICS AND SPACE ADMINISTRATION

Washington, D.C. 20546

TABLE OF CONTENTS

Introduction..... 1

Dr. William Shepherd
Director, Space Science Center
University of Minnesota, Minneapolis

LANDSAT Applications to Wetlands Classification in the Upper Mississippi River Valley..... Section A

T. M. Lillesand and L. F. Werth
College of Forestry
University of Minnesota, St. Paul

A Project to Evaluate Moisture Stress and Weather Modification Procedures in Corn and Soybean Areas of Western and Southwestern Minnesota..... Section B

Dr. Richard Rust and Pierre Robert
Department of Soil Science
University of Minnesota, St. Paul

Synergistic Relationship Between Lineaments Located on LANDSAT Imagery and Traditional Sources of Topographic Information..... Section C

Drs. Matt Walton and Joseph Goebel, Mr. Lawrence Batten
Minnesota Geological Survey
St. Paul, Minnesota

Determination of Detectability Limits for Particulates in Lake Superior Through the Use of LANDSAT Data..... Section D

Dr. Michael Sydor
Physics Department
University of Minnesota, Duluth

Ice Coverage of Minnesota Lakes -- Assessment of Freeze-Over from LANDSAT Imagery and Weather..... Section E

Dr. H. Stefan and Alec Fu
Department of Civil and Mineral Engineering
St. Anthony Falls Hydraulic Laboratory
University of Minnesota, Minneapolis

Space Science Center

Progress Report

January 1979

INTRODUCTION

This report covers research at the University of Minnesota during the twelve month interval from January 1, 1978 to December 31, 1978.

Section A by T. M. Lillesand and L. F. Werth summarizes progress made during the first six months of a study of LANDSAT Applications to Wetland Classification in the Upper Mississippi River Valley.

The study aimed at assessing the applicability of multitemporal LANDSAT digital image processing to the task of classifying and mapping surface cover types in freshwater wetlands. In an earlier investigation, single-data LANDSAT data had been used to classify broad cover types in wetlands occurring on five contiguous 7.5-minute quadrangles in the Twin City 7-County Metropolitan Area. Overall test field accuracy in the single-date analysis was approximately 72% after a single iteration of a supervised classification procedure. The average class accuracy was only 41%. In the current study, two-date data have been geometrically registered and analyzed using a hybrid classification process. Overall test field accuracy of five broad cover types (Water, Aquatics, Emergents, Forest, and Non-Wetland) has been improved to about 80% using the multitemporal approach. Average class accuracy has risen to 66%. Under the spectrally and spatially complex site conditions characterizing the geographical area of this study, additional accuracy improvement appears to be precluded by the constraints of LANDSAT's spectral and spatial resolution. This has led to the preliminary assessment of

digitized color infrared aerial photography as an alternative data source. The coarse spectral resolution of the photography continues to limit the accurate differentiation of certain wetland and non-wetland cover types when an entire image is analyzed. However, when classification with the photographic data is limited to wetland areas only, spectral differentiation is achieved at high levels of specificity (Duckweed, Lily, Cattail, Reed Canary Grass, Water) with 87% accuracy.

In the remaining six months of the current grant it is expected that the analysis of the LANDSAT classification results will be completed including summary statistics on a cover type basis for each of the study quadrangles.

Section B is a report by Richard H. Rust and Pierre C. Robert on the continuation of the study "Evaluation of Soil Moisture Stress in Western and Southwestern Minnesota." The preceding report on this study described the steps undertaken to establish a ground truth network in the area under study which would provide information on leaf and soil moisture, precipitation events and crop signatures to be correlated with remote sensing information. In addition to the field data, preliminary greenhouse studies were undertaken to provide data on plant water stress under controllable conditions.

The current report presents an evaluation of the utility of remote sensing data from color infrared photography, LANDSAT imagery and reflected spectral intensity in assessing the effects of soil water stress on corn and soybeans evidenced by the leaf water potential. Correlations were sought between plant conditions in field studies and in a controlled situation in a greenhouse. Significant differences in leaf temperatures, measured radiometrically, between stressed and unstressed

plants have been observed suggesting that thermal infrared can be a valuable tool in assessing plant water status.

Section C is a report by Joseph E. Geobel, Matt Walton and Lawrence G. Batten entitled "Synergistic Relationships Between Lineaments Located on LANDSAT Imagery and Traditional Sources of Topographic Information." This represents a continuation of their use of LANDSAT imaging as a synoptic tool in correlating information derived over time from a variety of sources to provide a more complete and detailed understanding of the geology of the State of Minnesota than any one of the basic information sources provides alone. As the authors point out in their report, they have found remote sensing an increasingly important tool in the operations of the Minnesota Geological Survey.

Section D, a report by Michael Sydor entitled, "Determination of Detectability Limits for Particulates in Lake Superior through the use of LANDSAT Data", describes the program followed to determine the steady state background levels of turbidity of Lake Superior required to set the boundary conditions for the numerical modelling of the dispersion of particulate matter in the lake. He also describes the development of a quick, inexpensive method for analysis of the suspended solids in water samples ("ground truth").

From these findings he has determined the detectability limits for particulates in Lake Superior using LANDSAT data. The conlusion is that the detectability limits by LANDSAT are at the limit of usefulness for particulate budget studies of western Lake Superior and not useful mid-lake where the steady state particulate concentrations are low. However, he concludes that LANDSAT observations can provide the geometric resolution and concentration level measurements necessary to establish

the initial boundary conditions for the numerical modelling of the time dependent particulate budget studies. He concludes that these together with NIMBUS G data, which provide higher accuracy at low signal levels, will make possible the verification of the correctness of the model of the dispersal process.

Section E is a final report of a study by Professor Stefan of the use of LANDSAT imagery in assessing the validity of a model for predicting the freeze over of Minnesota lakes.

LANDSAT observations confirmed that the model was an excellent prediction. This is an important result in the management of lake water quality and fisheries.

SECTION A

LANDSAT APPLICATIONS TO WETLANDS CLASSIFICATION IN THE UPPER MISSISSIPPI RIVER VALLEY

Dr. T.M. Lillesand and Lee F. Werth
Institute of Agriculture
University of Minnesota
St. Paul, Minnesota

o

INDEX

Abstract..... A1
Background..... A2
Current LANDSAT Effort..... A3
Digitized Photography..... A4
Synopsis..... A11
Continuing Research Activities..... A12

o

LANDSAT APPLICATIONS TO WETLANDS CLASSIFICATION IN THE UPPER MISSISSIPPI RIVER VALLEY

Investigators: Dr. Thomas M. Lillesand
Lee F. Werth
Institute of Agriculture
St. Paul, Minnesota

ABSTRACT

This report summarizes progress made during the first six months of a study aimed at assessing the applicability of multitemporal LANDSAT digital image processing to the task of classifying and mapping surface cover types in freshwater wetlands. In an earlier investigation, single-date (July 5, 1976) LANDSAT data had been used to classify broad cover types in wetlands occurring on five contiguous 7.5-minute quadrangles in the Twin City 7-County Metropolitan Area. Overall test field accuracy (% of all test field pixels classified correctly) in the single-date analysis was approximately 72% after a single iteration of a supervised (maximum likelihood) classification procedure. The average class accuracy (sum of all classes accuracies/number of classes) was only 41%. In the current study, two-date data (July 5, 1976 and August 7, 1975) have been geometrically registered and analyzed using a hybrid classification process (LARS modified block clustering). Overall test field accuracy of five broad cover types (Water, Aquatics, Emergents, Forest, and Non-Wetland) has been improved to about 80% using the multitemporal approach. Average class accuracy has risen to 66%. Additional accuracy improvement appears to be precluded by the constraints of LANDSAT's spectral and spatial resolution. This has led to the preliminary assessment of digitized color infrared high altitude photography as an

alternative data source. The coarse spectral resolution of the photography continued to limit the accurate differentiation of certain wetland and non-wetland cover types in "full scene" analyses. However, when classification with the photographic data was limited to wetland areas only, spectral differentiation was achieved at the dominance type level of specificity (Duckweed, Lily, Cattail, Reed Canary Grass, Water). The overall classification accuracy was 87% in the photographic analysis.

BACKGROUND

Accurate classification and mapping of wetland cover types is essential to effective implementation of a number of Federal, State, and local legislative mandates and resource management programs. The task of mapping wetlands on a statewide basis is challenging (particularly in Minnesota); that of mapping the wetlands of the U.S. is monumental. Hence, automated processing of the timely, synoptic and machine-amenable data from LANDSAT would appear to be an attractive approach to the classification and mapping process. This was supported by the results of a preliminary LANDSAT application study undertaken by the IAFHE Remote Sensing Laboratory during 1978. The test site for this study was within the Twin City 7-County Metropolitan Area. This entire area had been previously mapped by the Remote Sensing Laboratory under contract with a consortium of funding agencies.[1] The preliminary LANDSAT investigation was supported by in-house funds.[2]

---

[1] The Minnesota Department of Natural Resources, the U. S. Army Corps of Engineers, the U. S. Fish and Wildlife Service, the USDA Soil Conservation Service, and the Twin Cities Metropolitan Council.

[2] The University of Minnesota Agricultural Experiment Station and the College of Forestry.

The preliminary LANDSAT study involved analysis of digital data acquired on a single date (July 5, 1976). The data were analyzed at the Purdue University Laboratory for Application of Remote Sensing (LARS). A coarse geometric correction was applied to the data and a single training iteration through a supervised, maximum likelihood, classification process was performed over five contiguous 7.5-minute quadrangles. Overall classification accuracy (% of all training area pixels classified correctly) was promising at 72%, but not at the desired, 85-90%. In addition, residual positional errors of image pixels ranged from two to four pixels.

CURRENT LANDSAT EFFORT

Under the current grant, LANDSAT data from two dates (July 5, 1976 and August 7, 1975) have been analyzed under subcontract to LARS. A precision geometric correction has been applied to all data contained in the five quadrangles used in the previous study. All data have been resampled using both a nearest neighbor and cubic convolution resampling procedure. Classification of the geometrically registered data has been accomplished using a hybrid (modified block cluster) classification process. This involved clustering training areas and merging appropriate spectral classes prior to implementation of a maximum likelihood classifier. In this process, a total of 14 spectral classes were needed to typify five information classes: Water, Aquatics, Emergent Wetland Vegetation, Forest, and Non-Wetland. The LARSYS feature selection process was employed to judge which subsets of the eight bands of sensing would be optimum for subsequent classification. LANDSAT Band 5 and 6 for both dates were found to be best suited for the classification.

At this juncture, all preprocessing, training, and classification tasks have been performed. Likewise, a preliminary assessment of test field accuracy has also been completed. This involved choosing some 450 test fields that varied in size from one to nine pixels. Then cover types were verified using photointerpretation (and site visit in ambiguous cases). All errors of omission and commissions for each class are being tabulated on a quadrangle by quadrangle basis. Tables are also being prepared to express the comparative overall percentage area of each cover type on each quadrangle as measured through photointerpretation, the single date LANDSAT analysis, and the two-date analysis. Preliminary figures indicate that overall test field accuracy of approximately 80% has been obtained with the multitemporal approach. This represents about an 8% improvement over the results of the single-date analysis and the application of the precision geometric correction has reduced average residual positioning errors to less than 1 to 1.5 pixels. Average class accuracy has risen from 41% to 66%. Hence, work to date has indicated a measurable increase in the accuracy and geometric integrity of the classified LANDSAT data. However, additional classification accuracy appears to be precluded by the limiting spatial and spectral resolution of the LANDSAT MSS for the application at hand.

DIGITIZED PHOTOGRAPHY

Having realized improved, yet unacceptable classification accuracy with the multitemporal LANDSAT data, an experimental digital analysis of color infrared photography of a portion of the study area has been undertaken. This effort was not envisioned in the original proposal for this research, but it represents a logical extension of the LANDSAT in-

vestigation in two respects. First, the digitized photography virtually removes the spatial resolution restrictions from the automated classification process, thereby enabling more thorough study of the spectral characteristics of the cover types of interest. On one hand, this is important to judging the potential applicability of LANDSAT data analysis in wetland areas which are less complex spatially than those in the Twin Cities study area. In addition, the photographic research is providing a "first look" at the potential utility of using digitized color infrared photography per se as a data source for wetland mapping in complex areas.

For the purposes of this preliminary assessment, digital analysis was limited to a single frame of existing 70mm, 1:50,000 color infrared (Kodak type 2443) aerial photography. The photography had been taken with a Hasselblad 500 EL (f=50mm) camera on July 21, 1977, in support of other wetlands research efforts conducted by the Remote Sensing Laboratory. The image was digitized using a modified P-1700 Optronics drum scanner made available by the University of Wisconsin Environmental Monitoring and Data Acquisition Group (UW/EMDAG). Density readings from (0-3) Density Units were digitized into 256 levels and recorded on computer compatible tape. Spectral filters were used to scan each of the three film layers. A measurement spot size of 50μm was employed such that each pixel represented a ground area approximately 2.5m square. Since a calibration step wedge image was not available for the analysis film, all data analysis was done with the "raw" gray scale values, rather than with calibrated film exposure values.

The image data set was analyzed using a supervised maximum likelihood classification algorithm made available by UW/EMDAG. Initially,

all cover types in the entire scene were placed in the following 13 categories: Duckweed, Water Lily, Cattail, Reed Canary Grass, Willow, Pasture, Cropland, Bare Soil, Roof Top, Asphalt, Forest, Shadow, and Water. A total of 35 training areas was used to develop the statistics for the intended full-scene classification. However, an analysis of the classification accuracy of the various training area pixels indicated that, as with the LANDSAT data, many of the cover types present in the scene were not spectrally separable.

Table 1 indicates the confusion matrix expressing the accuracy of classification in the initial training areas. Note that for some classes, the accuracy of classification in the training areas was excellent (e.g., Lily = 100%). Other classes (e.g., Willow = 5%) were very poorly classified. Of particular note is the fact that all wetland classes except Willow were mutually separable. That is, errors of omission and commission in each wetland class (except Willow) were primarily attributable to the spectral confusion between wetland and non-wetland cover types, rather than between wetland cover types themselves.

Because of the spectral confusion between the wetland and non-wetland cover types, it was hypothesized that if the training and classification procedures were limited to only wetland areas and cover types, the classification accuracy would improve greatly. Hence, the training process was repeated in wetland areas only, using the following classes: Duckweed, Water Lily, Cattail, Reed Canary Grass, and Water. Table 2 indicates the classification accuracy obtained for the "wetland only" training areas. Note the high accuracy of training area classification which results when non-wetland classes (and Willow) are eliminated from the analysis.

Table 1. Classification Performance for Training Fields Used in Full Scene Analysis.

Known Cover Types			% Classified As Indicated Cover Type												
Cover Type	No. of Training Sets	No. of Pixels	Duckweed	Lily	Cattail	Reed Canary	Willow	Pasture	Cropland	Bare Soil	Roof Top	Asphalt	Forest	Shadow	Water
Duckweed	4	113	98					1							1
Lily	2	164		100											
Cattail	9	426			86	2	4		8						
Reed Canary	5	821			2	96			2						
Willow	1	21			62	5	5		28						
Pasture	2	690		1				98		1					
Cropland	3	713			14	23			62						1
Bare Soil	1	162	1					9		83	4	1	2		
Roof Top	1	96	1							5	93	1			
Asphalt	1	44						2				98			
Forest	1	52	2		19	10		3	10	6		4	44		2
Shadow	1	40											5	95	
Water	4	677												1	99

Table 2. Classification Performance for Training Fields Used in Wetland Areas Only.

Known Cover Types			% Classified As Indicated Cover Type				
Cover Type	No. of Training Sets	No. of Pixels	Duckweed	Lily	Cattail	Reed Canary	Water
Duckweed	1	20	100				
Lily	1	98		98		2	
Cattail	3	116			99	1	
Reed Canary	3	533			2	98	
Water	2	348					100

Test field accuracy for the "wetland only" classification process was also evaluated. For this purpose, the boundaries of eight wetland test units were defined by polygons whose vertexes were expressed by their pixel row and column number obtained from line printer output of the image data. The accuracy of classification in each of the eight test areas was obtained by comparing the computer-derived classification to that obtained by photointerpretation. This was done for all pixels in the eight areas (approximately 33,000). In those cases where the photointerpretation was ambiguous, a field visit to the site was made to be certain of the correct identification of the cover type present.

The results of the pixel-by-pixel accuracy assessment are given in Table 3. A number of observations can be made from these results. First, the test area results are generally lower than the training area results. This derives from the introduction of scene variability which is not necessarily accommodated in the selection of training areas. It is felt that the classification accuracy of the Lily and Reed Canary classes could be improved somewhat with additional training. Most of the Lily/Reed Canary confusion occurred in an area of the scene which was not used for training. This problem was not realized before-the-fact because: (1) the subtle spectral variability in these classes could not be detected on the original photograph through visual observation, and (2) the line printer output of the original digital image data was very difficult to interpret at a detailed level due to geometric uncertainties and difficulty in detecting small areas of spectral differences from the printer character rendering of the data.

Errors in the classification of Duckweed and Water are believed to be caused by edge effects, in which a given pixel actually overlays two

Table 3. Classification Performance in Eight Wetland Areas.

Known Cover Type		% Classified As Indicated Cover Type				
Cover Type	No. of Test Pixels	Duckweed	Lily	Cattail	Reed Canary	Water
Duckweed	984	95	3	2		
Lily	2,240	11	72	1	16	
Cattail	13,586			81	19	
Reed Canary	9,920	1	5	2	92	
Water	6,173	2			1	97

Ave. Class Accuracy = 87%

cover types near a boundary between the two types. To some extent, this effect enters into the accuracy problems for Lily as well.

The errors in classification of Cattail are believed to be due to the presence of mixed Cattail/Willow in many areas. A sparse scattering of Willow occurred in many areas of both the Cattail and the Reed Canary cover types. Wherever present, Willow tended to cause misclassification due to the highly variable spectral characteristics of this cover type. These difficulties may be resolvable by the inclusion of a "texture" variable in the analysis process.

SYNOPSIS

Progress made to date in this research has shown that:

1. Precision geometric correction, iterative training analysis, and the use of multitemporal data has improved average wetland classification accuracy in the test area by 25% (from 41% to 66%).
2. Under the spectrally and spatially complex site conditions characterizing the geographical area used in this study, further improvement in wetland classification accuracy is apparently precluded by the spectral and spatial resolution restrictions of the LANDSAT MSS.
3. Full scene analysis of scanning densitometer data from color infrared photography has failed to permit discrimination of many wetland and non-wetland cover types.
4. When classification of the photographic data was limited to wetland areas only, detailed classifications were made with average classification accuracy of 87%.

5. The integration of conventional image interpretation (to simply delineate wetland boundaries) and machine-assisted classification (to discriminate among cover types present within a wetland area) appears to warrant further research. Though both the delineation of wetland boundaries and the development of valid training area statistics are labor-intensive tasks, the results from the combined approach appear to be quite accurate. Additional research is needed to study the feasibility and cost of extending this methodology over a large area using small scale photography.

CONTINUING RESEARCH ACTIVITIES

In the remaining grant period, the following tasks will be undertaken:

1. Analysis of the LANDSAT classification results will be completed. This will include summary statistics on a cover type basis for each of the study quadrangles.
2. A final report describing the background, methods, results, and conclusions of both the LANDSAT and the digitized photographic approaches used in the study will be prepared.

SECTION B

A PROJECT TO EVALUATE MOISTURE STRESS AND WEATHER MODIFICATION PROCEDURES IN CORN AND SOYBEAN AREAS OF WESTERN AND SOUTHWESTERN MINNESOTA

Dr. R.H. Rust and Pierre Robert
Department of Soil Science
University of Minnesota
St. Paul, Minnesota

o

INDEX

Introduction..... B1
Procedures..... B1
  Ground Data..... B1
  Aerial Color Infrared Photographs..... B4
  Greenhouse Experiment..... B9
  Experiment at the Sand Plain Research Farm (Becker)..... B11
  Precipitation Event Maps..... B12
Previous Results..... B13
  1977 Ground Data..... B13
  Remote Sensing Imagery Acquired..... B13
  LANDSAT Spectral Band Evaluation..... B14
  Differential of Well and Poorly Drained Soils
    Using LANDSAT Imagery..... B14
  Use of Thermal Infrared..... B14
Results to Date..... B14
  1978 Season on Site Records..... B14
  Imagery..... B15
  Greenhouse Experiments..... B16
  Sand Plain Research Farm Experiment..... B23
Conclusions and Future Research..... B32
Acknowledgements..... B33
Literature Cited..... B33

o

A PROJECT TO EVALUATE MOISTURE STRESS IN CORN AND SOYBEAN AREAS OF WESTERN AND SOUTHWESTERN MINNESOTA

Investigators: Dr. Richard H. Rust
Pierre C. Robert
Department of Soil Science
University of Minnesota
St. Paul, Minnesota

INTRODUCTION

In a previous report (Rust and Robert, 1978) it was noted that southwestern and western Minnesota had been for several successive years under soil water stress conditions resulting in variable but important crop yield losses. Since this part of the state has a drought history, the ability to detect water stressed areas using remote sensing techniques, LANDSAT imagery or color infrared photography would be valuable. In this past season, as may be observed in Table 1, amount and distribution of precipitation was adequate and crop conditions were as good as in the 1977 season. Current research has included gathering ground data information and crop spectral signature under controlled conditions (greenhouse and experimental field).

PROCEDURES

Ground Data

In addition to the twelve representative sites (figure 1) of various southwestern Minnesota soil landscapes selected in 1977, the Sand Plain Farm (Becker) was included in the 1978 ground data network. This site, located on a coarse sandy plain, is most susceptible to water stress on

B2

Table 1. 1978 Growing Season Monthly Precipitation and Normals for Some Weather Stations of SW Minnesota.*

		April	May	June	July	August	Sept.	October	Total
Montevideo	Normal	2.29	3.31	4.72	3.48	3.69	2.92	1.62	22.03
	1978	3.95	4.46	3.17	1.62	2.67	6.05	.08	22.00
Marshall	Normal	2.46	3.3	4.49	3.95	2.68	2.7	1.61	21.19
	1978	3.58	3.44	1.4	3.99	1.7	3.96	.09	18.16
Pipestone	Normal	2.22	3.6	4.62	3.35	2.96	3.2	1.73	21.68
	1978	3.5	4.21	1.31	4.19	2.15	4.39	.43	20.18
Redwood Falls	Normal	2.22	3.25	3.92	3.86	3.24	2.42	1.74	20.65
	1978	3.7	3.04	1.64	3.65	2.39	3.96	.27	18.65
Windom	Normal	2.35	3.61	4.5	3.74	3.3	3.54	1.7	22.74
	1978	3.39	2.81	3.51	5.10	2.25	1.41	.42	18.89
Average	Normal	2.30	3.41	4.45	3.67	3.17	2.96	1.68	21.66
	1978	3.62	3.59	2.21	3.71	2.23	3.95	0.26	19.58

* Climatological data - Minnesota - Environ. Data Inf. Serv., National Climatic Center, Asheville, N.C.

Figure 1. LANDSAT coverage of Southwest Minnesota and twelve ground data site locations.

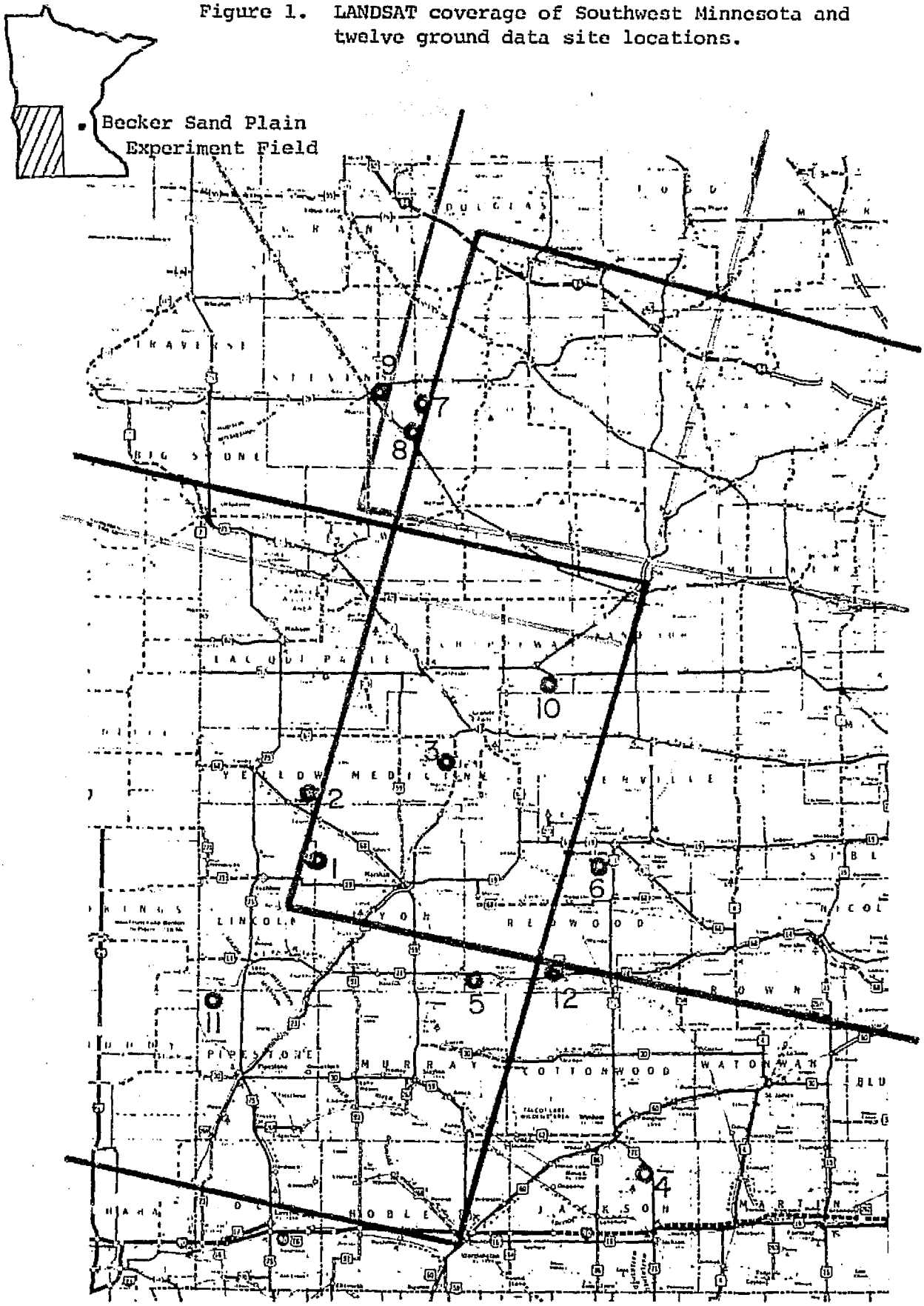

non-irrigated crops, thus enabling the study of spectral signature changes in droughty conditions.

The SW Minnesota sites are each composed of two homogenous areas larger than 10 acres. They are representative of well drained (Udolls and Ustolls) and poorly drained (Aquolls) soils. Two SW Minnesota sites and the Becker Farm contrast irrigated and non-irrigated conditions. All sites were planted in corn or soybeans.

Soil water content was determined on all sites from the surface to the rooting zone throughout the growing season in coincidence with the LANDSAT overpass (Figure 2). The gravimetric method was used. The sampling was accomplished by field soil scientists of the Soil Conservation Service located at Lakefield, Marshall, Montevideo, Pipestone, Redwood Falls and cooperators of the West-central and Southwest Experiment Stations. (Samples were processed at the Soil Science Department).

Field information (Table 2) such as phenologic data, farming operations, crop treatments, precipitation events were recorded. Soil surveys and field crop maps were gathered or prepared for all sites.

Crop condition, and particularly stress conditions were recorded for all the soil sampling dates and measured using a pressure chamber (Figure 3). Since soil water conditions were generally favorable this year, only two measurements (July 23-25 and August 8-10) were performed on most sites. Crop yields were also measured for all cases; two rows 20 feet long were sampled in triplicate at each site. Shelled corn yields are expressed at 15.5% moisture content, and soybeans, as oven dry weight.

Aerial Color Infrared Photographs

Seventy-mm color infrared positive transparencies at a scale of 1:50,000 were obtained for the SW Minnesota sites on the following dates

Table 2. Field record example

MOISTURE STRESS PROJECT

FIELD INFORMATION

Date: 1978
Field #: 12.a Holmberg
Soil: Ves

Date: May, June, July, August

Month, day hour (1)	Crops (2)	Stage of growth (3)	Height (cm) (4)	Cover (%) (5)	Leaves shape and color (6)	Treatment (7)	Soil Moisture Rooting Zone (8)	Soil Moisture Surface (9)	Leaf Moisture (10)	Additional Information (11)
5/16 12:00	Corn	Planted May 1	0	0	--	10 lbs	High-- Moderate	Moderate	--	Rainfall April 3.05"
5/22	Corn	Emergence	5,0	2-3	Light green Turgid	2,4-D Broadcast	Moderate	Moderate	--	Slide #20
6/09 10:00	Corn	Pre-tassel	35.0	20	Light green	--	Moderate	Moderate	--	-
6/27	Corn	Pre-tassel	85.0	35-40	Slight rolling grayish green	--	Moderate	Low	--	Slide #14
7/05 10:00	Corn	Starting to tassel	150.0	65.0	Rolled upright grayish green	--	Moderate	Moderate	--	Slide #12
8/02 9:30	Corn	Tasseling cobs: 20 cm	187.0	90.0	Slight rolling upright grayish green	--	Moderate	Moderate to low	--	Slide #17
8/21 10:15	Corn	Cobs: 23-24.5 cm	225.0	90.0	Wind damage grayish green	--	Moderate	Low	--	Cob beginning to dry out (leaves)

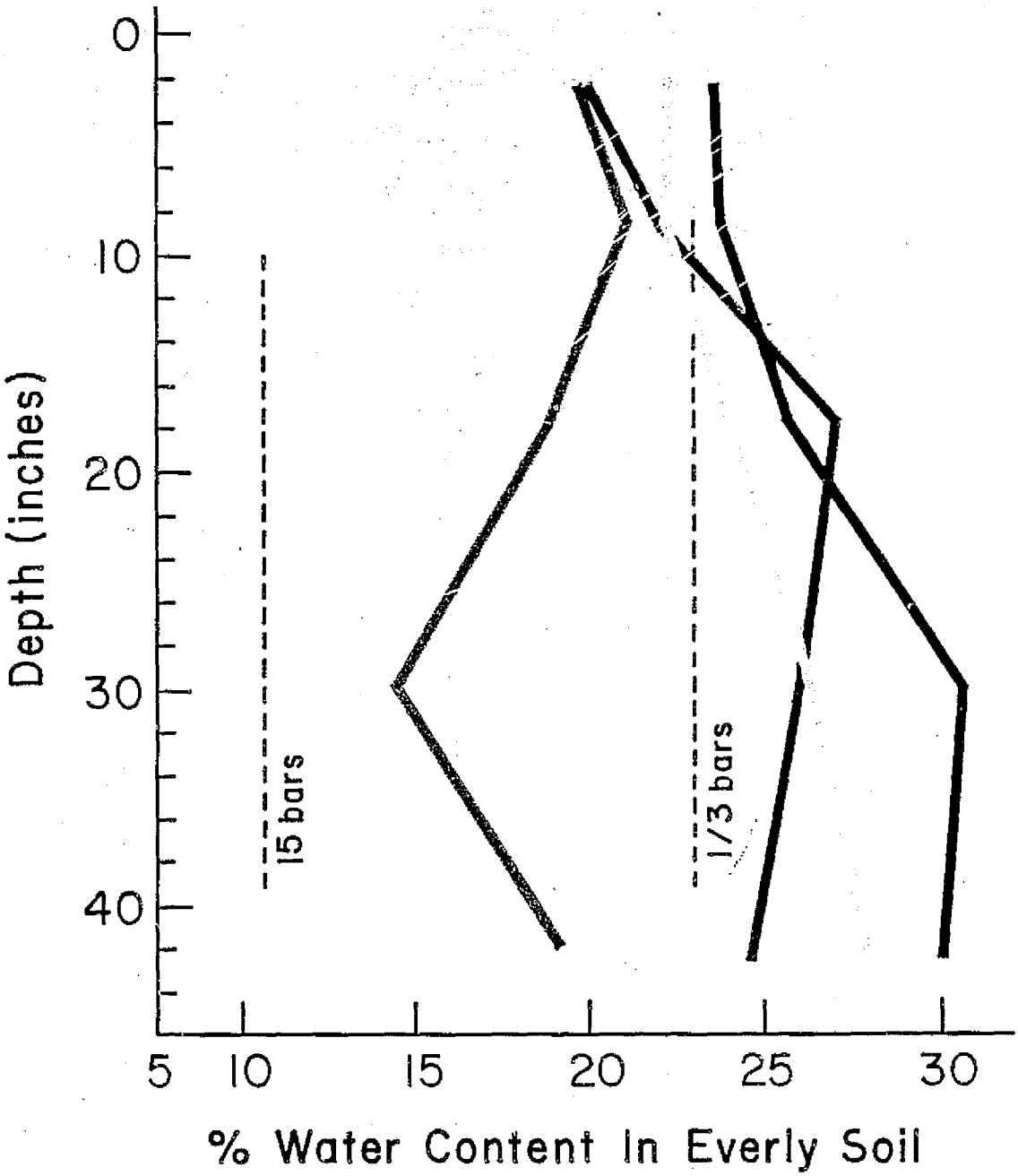

Figure 2. Water-content distribution profiles of selected dates during the growing season. The one-third bar water content represents the maximum of water in the rooting zone that the soil retains against gravity. The 15-bar water content is the water remaining in the rooting zone at the wilting point of most crops. Water content in excess of 1/3 bar indicates a saturated condition.

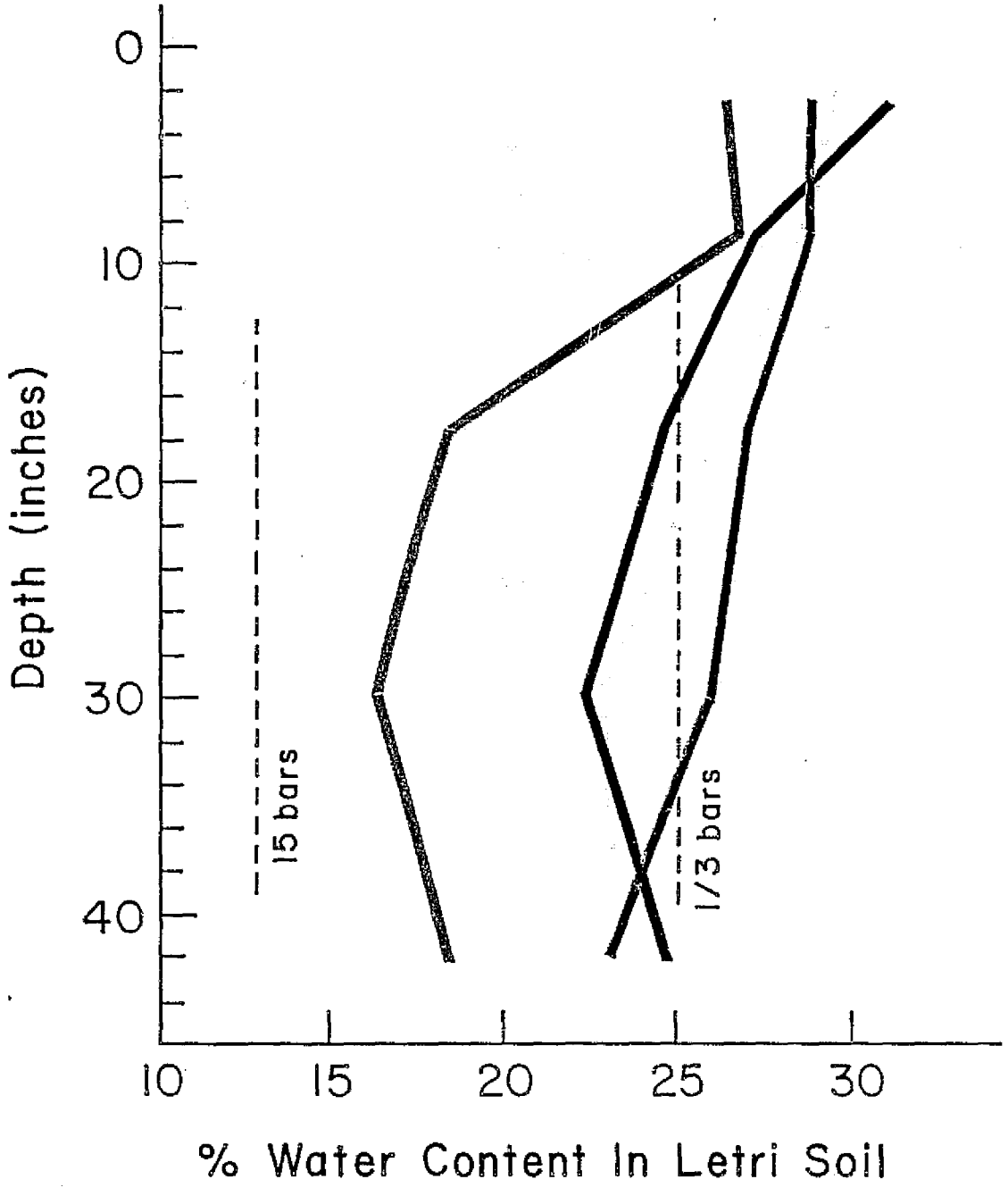

Figure 2 (cont.)

DATES

05 16 78

06 08 78

08 02 78

09 25 78

Figure 3. Pressure chamber and "remote sensing platform."

in 1978: May 18, July 11, September 8. A fourth flight was scheduled in August but continuous cloud cover prevented its execution. In 1978, 70 mm film was used instead of 35 mm because it is larger scale and has less image distortion. The following photographic specifications were used: lens, 50 mm; film, Kodak 2443; filter, 15; shutter speed, 1/500; f/no, 5.6.

The Sand Plain Research Farm (Becker) plots were flown between 9:00 and 10:30 a.m. on 4 dates in 1978: July 19, August 7, August 20 and September 4. Vertical 35 mm color infrared slides at a 1:10,000 scale were processed.

Greenhouse Experiment

Corn and soybean plants were grown to maturity from fall 1977 to spring 1978. The corn variety was a hybrid especially adapted to greenhouse culture. The soybean variety was Hodgson. Corn was grown in 12" pots and soybeans in 6" pots, filled with the coarse sandy soil of the surface horizon from the Becker Research Farm. The temperature was maintained at 25°C. Fluorescent and incandescent lights were used, respectively, 14 and 15 hours a day. Plants were watered with tap water. A standard Hoagland solution was the main nutrient source. Different pesticides were tried to control, with variable success, aphids, red spiders and thrips.

In the case of corn, three pots were always kept in similar soil water condition. To simulate a drought cycle on three plants watering was terminated whereas three others were normally watered. A similar procedure was followed for soybeans with six plants instead of three kept in similar condition.

Only one leaf of one plant was selected to initiate a series of irradiance measurements whereas most of the leaves of the two other plants were taken for leaf water potential, i.e., plant stress evaluation. Measurements were performed after tasseling (corn) or early seed development (soybeans).

The use of a pressure chamber or pressure bomb (Figure 3) was tested to determine leaf or plant water status. Boyer (1966) and others demonstrated that leaf water potential* can conveniently be evaluated from the

---

* Water demand and water potential are properties (or conditions) of the plant at given stages in its development. Water demand is the amount of water needed by the plants for all physiologic activity. Water potential is the energy status of the contained water in the leaves (or other plant parts) expressed in units of pressure (- bars).

measurement of the sap pressure. Results indicate the pressure chamber is suitable for estimating leaf water potential of corn (DeRoo, 1969) and soybeans (Boyer, 1971). Principal advantages of the pressure bomb are its ease of use and its field capability (and portability).

The pressure chamber is simple in operation. After a segment of the leaf blade (corn) is cut from the plant a short length of the midvein area is placed between the smooth surface of a halved silicon rubber stopper previously coated with silicone stopcock grease. Then, the stopper is inserted into the cover that is screwed to the cylinder of the bomb. Sufficient pressure is applied from a cylinder of compressed nitrogen to return the meniscus of the xylem sap to the cut surface of the leaf blade which is protruding a few millimeters from the split stopper.

In the case of soybeans, the petiole is sealed in the chamber top so that the cut end of the petiole projected a few millimeters to the outside but most of the petiole and the leaf blade were subjected to the pressure within the chamber. Care was used to reduce the two main sources of errors: sample preparation and rate of pressure increase in the chamber.

A spectroradiometer and thermoradiometer were used to measure individual leaf (greenhouse) and field (Becker Research Farm) reflected energy intensity (spectral intensity) in the visible, near infrared and thermal infrared.

Some principal specifications of the ISCO spectro-radiometer are:

- *wavelength range:* *visible, 380-750 mm*
  near infrared, 750-1050 mm
- *bandwidth:* *approximately 15 mm (380-750 mm range)*
  30 mm (750-1050 mm range)

- *continuous scanning by a unique wedge-interference filter system*
- *fiber optic extension head for closed or special measurements*
- *highly portable unit*
- *units of energy rate intensity per bandwidth (microwatts per sq cm per nm)*
- *sensitivity:* *8 ranges from 0.3 to 1000 uw cm^{-2} nm^{-1}*
- *accuracy:* *7 to 10%*
- *programmed scanner and recorder available.*

The fiber-optic extension head was always used and a cylinder 5 cm long was added to focus the head exclusively on the leaf section. In the greenhouse, the opening of this extension was always kept 2 cm from the leaf blade and perpendicular to its surface.

The thermoradiometer, a Barnes PRT-10L infrared field thermometer has the following specifications:

Temperature scales: -10^{o} *to* $+60^{o}C$

Temperature sensitivity: $\pm$ $0.2^{o}C$ *at* $20^{o}C$

Spot size: 7^{o} *field of view*

Spectral sensitivity: *6.9 to 20 microns*

The calibration of the instrument in the absolute mode is done by setting up the absolute scale with a pocket reference target. Indeed, continuous calibration was required for accurate measurement. This is a major inconvenience. In the greenhouse, the PRT-10L was held perpendicular to the leaf, at a distance shorter than 2 cm.

Experiment at the Sand Plain Research Farm (Becker)

Corn and soybean field reflected energy intensity measurements were conducted throughout the growing season using the spectroradiometer and

thermoradiometer described in the previous section. Measurements were taken from a stepladder installed on a pick-up truck platform (Figure 3). The instrument was about 3 meters above the ground and was held in a slightly oblique direction. All the measurements were done from the same location, at approximately the same hour, parallel to the rows, with clear sky and with the sun at the back.

Soil water content was recorded by the gravimetric method and plant water status, using the pressure chamber. At least 3 leaves, at the ear node, were sampled each time from corn and the uppermost fully mature trifoliate (central leaflet) in the case of soybeans.

All four plots were located on a flat terrain with a slight micro relief. The soil is a Hubbard sandy loam (Udorthentic Haploboroll). Size of the soybean plots was about 1 acre. Similar farming operations were used. One plot of each crop was irrigated as required, until maturation. Although the irrigated corn was replanted on June 9 (original planting May 5) the amount of growth at the time of measurements, was essentially equal on irrigated and non-irrigated plots.

Aerial color infrared photographs were taken 4 times at a 1:10,000 scale.

Precipitation Event Maps

The capability of producing computerized precipitation maps for any region and any period of time has been developed (J.W. Enz, Soil Science Dept., U of Minnesota; E.L. Kuehnast, Climatology Office, D.N.R.; D.G. Baker, Soil Science Dept., U of Minnesota; St. Paul Computing Center Staff, U of Minnesota). When available for the 1978 growing season, precipitation maps corresponding to the time interval separating two available LANDSAT scenes will be generated.

PREVIOUS RESULTS

1977 Ground Data

Soil water content, field record and crop condition, on-site amount and distribution (computerized maps) of precipitation were recorded for the SW Minnesota sites.

Precipitation was well-distributed during the season and soil water content was always adequate or in excess. Several poorly drained soils had excess moisture for some period of time. This could be deduced by tone variations on the color infrared photograph of July 18. Good growing conditions were reflected in the 1977 corn yields: 75 to 150 bu/a, compared to almost zero bu/a in 1976. As a result, no general "drought signature" was observed. Crop signatures on well drained and poorly drained sites were very similar, as viewed from the color infrared photographs, particularly in case of corn.

Remote Sensing Imagery Acquired

Aerial color infrared 35 mm coverage of the SW Minnesota sites was obtained in June, July and August 1977.

Black and white LANDSAT transparencies corresponding to the study area were obtained for the following dates in 1977: June 23, July 11, July 16, July 29 and September 9 with the following specifications: 1:1,000,000 scale, band 5 and 7, cloud free (less than 10%).

After the study of these products, three LANDSAT computer compatible tapes (C.C.T.) corresponding to the best conditions were selected. After considerable delay the tapes for the 1977 growing season were obtained in June 1978.

Color slides were also taken at several sites and dates. Daily color slides of the growing corn were taken at the Southwest Experiment Station.

LANDSAT Spectral Band Evaluation

The 1:1,000,000 scale imagery, corresponding to the bands 5 (red) and 7 (near infrared), available for the 1977 growing season, was evaluated. At this scale, band 7 was found better for our purpose.

Differentiation of Well and Poorly Drained Soils Using LANDSAT Imagery

Analysis of 1976 and 1977 LANDSAT 1:1,000,000 scale, band 5 and 7 imagery was performed using a density slicer (V.P. 8) and a supervised approach (Frazee, et al., 1972). A section of the New Ulm Minnesota Soil Atlas map was used as "ground truth". A very satisfactory location of well vs. poorly drained soils was obtained when using the imagery corresponding to the period of maximum drought development (August, 1976).

Use Of Thermal Infrared

A preliminary experiment conducted at the St. Paul experimental field (July-August 1977) using a Barnes PRT-10L thermoradiometer indicated that absolute temperature readings are affected by sky condition, wind speed, crop height and measurement direction. It also gave promising results since a differential increase of as much as $7^{o}C$ was measured on a stressed corn field as compared to a non-stressed area.

RESULTS TO DATE

1978 Season On-Site Records

The analysis of the soil water content of the different sites show that conditions during the critical growing periods were generally adequate. Some excess was recorded in some poorly drained soils, but,

again, as in 1977, no drought situations were observed. The "field information records" (Table 2) confirmed good crop conditions reflected in the high yields. Furthermore, leaf water potential measurements (Table 3) taken at different periods of time, and for example, in mid-August, a period of maximum water demand, show similar water potential values between well drained (WD) and poorly drained (PD) soils, i.e., there was no drought stress.

On-site and county information related to hail damage and soil drainage were also collected.

Imagery

The three 1:50,000 scale, 70 mm color infrared images obtained for all the SW Minnesota sites are of very good quality. The three dates of flight in 1978 represent bare soil (May 18), maximum "green condition" (July 11) and mature plants (September 8). These photographs will be a valuable reference when analyzing the LANDSAT computer tapes.

Since the time lapse between LANDSAT 2 and 3 is nine days, twenty different images were expected. But, as a result of the cloudy conditions, only nine scenes present less than 10% cloud cover. The following 1:1,000,000 scale, band 7, black and white LANDSAT transparencies will be analyzed: May 21, June 18, July 15, August 10, August 24, September 15 of 1978. Computer compatible tapes corresponding to two or three scenes will be studied.

Since the LANDSAT 3 infrared sensor does not work properly, we will not be able to use this waveband which, according to the ground experiment, seems very promising in the study of water stress.

Table 3. Leaf water potential of corn measured at some SW Minnesota sites.

	Sites	Date	Time	Crop[1]	Leaf water potential[2] WD[3]	PD
					-bars	
02	Porter	8/09/78	1:30P	S	14	13
03	Hanley Falls	8/09/78	3:30P	C	12	12
06	Redwood Falls	8/10/78	11:30A	S	14	13
10	Clara City	8/10/78	2:30P	C	8.4	9.6
11	Pipestone	8/09/78	10:30A	S	9.0	6.0
12	Vesta	8/10/78	9:30A	C	7.4	4.5

[1]S - soybeans

C - corn

[2]Average of several measurements

[3]WD - Well drained sites

PD - Poorly drained sites

Greenhouse Experiments

The purpose of the greenhouse experiment was to test some ground data measurement techniques and to perform preliminary measurements useful for the interpretation of the remote sensing products.

The pressure chamber was adapted to corn leaves; its sensitivity, the repeatability of measurements and the sources of error in a controlled drying cycle were studied. Also, during the same cycle, the corn and soybean individual leaf variations in the visible, near infrared and thermal infrared were recorded.

The pressure chamber used was originally designed for tree leaves or needles and employed a plate type receptor. In order for the chamber top to accept soybean petioles, a new leaf holder was constructed to accept soybean petioles and the broad midvein of corn leaves without gas leak. The design was inspired by A. Blum, et al. (1973). A brass flange accommodated a soft silicon rubber stopper on one side (sliced into two halves), and a brass disc having a narrow slit on the other side to allow the leaf sample to pass through. The flange and the disc were held in place by a threaded brass cover (Figure 4). With this arrangement, only very slight pressure on the leaf sample was observed.

The new cover has been tested by measuring soybean leaf water potentials with both plate and silicon stopper systems. Table 4 shows that the silicon rubber stopper gives results similar to the plate stopper for various levels of leaf water potential.

The effect of leaf number upon leaf water potential was investigated. Table 5 gives results of a soybean experiment performed at three different water states. It shows that water potentials of the middle medium leaves are fairly constant. A practical result is that as long as there is no shading interference, middle leaves can be interchanged without affecting the results.

A soybean leaf is composed of three leaflets. The central top leaflets only were used for the measurements since it was found that water potential varies greatly according to the leaflet utilized. In the case of corn, the top 1/3 of the leaf was used. Identical results were obtained when using whole leaf, 2/3 or 1/3 leaf segments. Since it is more convenient to use a small leaf portion and a thin midvein, the 1/3 top section was selected.

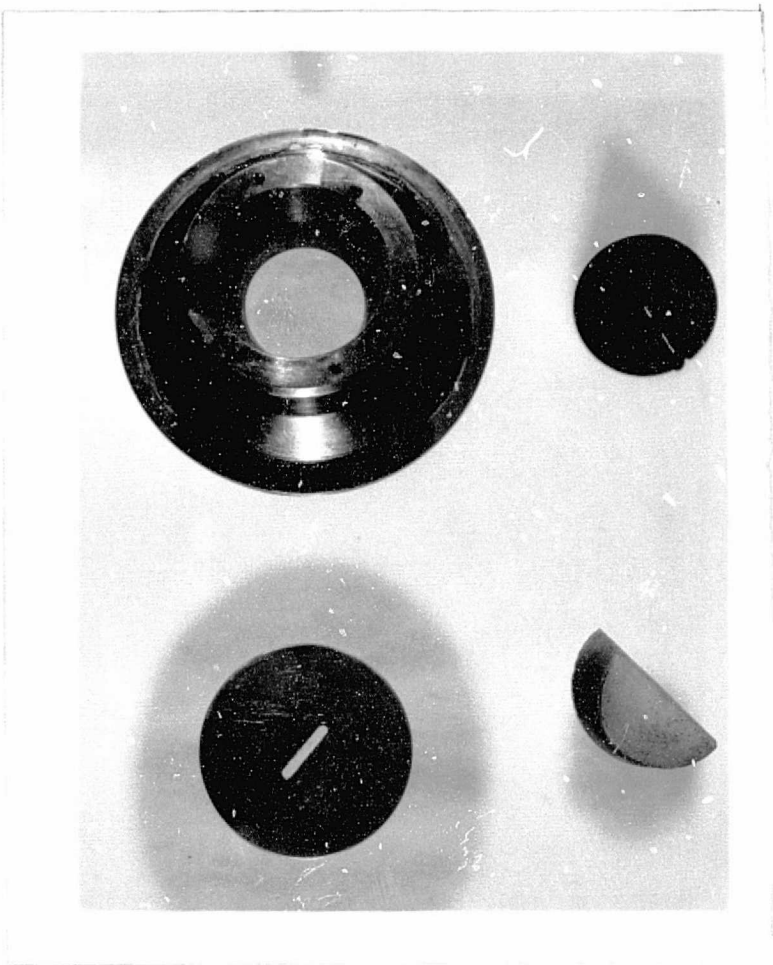

Figure 4. Modification of the pressure chamber leaf holder to accommodate corn and soybean leaves.

Leaf reflected energy intensity. The effect of droughty conditions on crop signature, or more precisely, the effect of leaf water status on corn and soybean leaf reflected energy intensity in the visible, near infrared, and thermal infrared parts of the spectrum were investigated in a controlled environment. Figure 5 gives an example of energy intensity variation from 400 to 1000 nm for a turgid and a stressed soybean leaf. Table 6 gives the normalized differential energy intensity between a progressively stressed soybean leaf and a turgid leaf at 575, 750 and 850 nm. To compensate for changes in incoming radiation intensity, the energy intensity values measured were normalized by divid-

Table 4. Comparisons of the leaf water potential determinations for soybean plants using two different pressure chamber sample holders.

		Leaf water potential (-bars)						
	Leaf number*	5	6	7	8	9	10	Avg.
Pot 1	Plant 1							
	Plate	-	5.60	5.73	-	-	-	5.66
	Silicon stopper	-	-	-	5.73	5.46	4.93	5.37
	Plant 2							
	Plate	-	5.73	5.60	5.73	-	-	5.69
	Silicon stopper	-	-	-	-	5.60	5.33	5.46
Pot 2	Plant 1							
	Plate	14.8	-	17.33	-	16.67	-	16.27
	Silicon stopper	-	16.27	-	17.2	-	16.4	16.62
	Plant 2							
	Plate	-	15.73	-	15.87	-	-	15.80
	Silicon stopper	16.13	-	15.87	-	15.07	-	15.69
Pot 5	Plant 1							
	Plate	-	-	-	13.2	-	12.53	12.86
	Silicon stopper	-	-	-	-	13.06	-	13.06
	Plant 2							
	Plate	-	-	-	12.53	-	-	12.53
	Silicon stopper	-	-	-	-	12.8	-	12.80

*Leaves numbered beginning at the bottom of a given plant. Leaves selected are from mid-portion of the plant.

Table 5. Leaf water potential variability with leaf number under different water stress conditions

		Plant Condition					
		No Stress		Stress		Extreme Stress	
Date		4/11/78		4/12/78		4/13/78	
		Plant 1	Plant 2	Plant 1	Plant 2	Plant 1	Plant 2
		(-bars)					
Leaf #	4	2.00	5.33	-	16.67	-	-
	5	8.00	5.33	16.67	14.00	20.00	-
	6	8.67	12.70	16.67	13.33	21.33	19.87
Series 1	7	6.67	8.67	16.67	14.00	21.33	19.07
	8	7.33	9.33	16.67	14.33	21.33	21.20
	9	-	8.00	-	-	21.47	20.93
Leaf #	4	6.67	6.67	-	16.67	18.00	-
	5	6.53	6.67	-	15.33	16.67	19.33
	6	8.67	8.00	16.67	16.67	20.00	18.93
Series 2	7	8.00	8.00	15.33	15.67	20.00	-
	8	8.00	6.67	16.00	-	20.00	-
	9	-	6.67	-	-	21.20	-

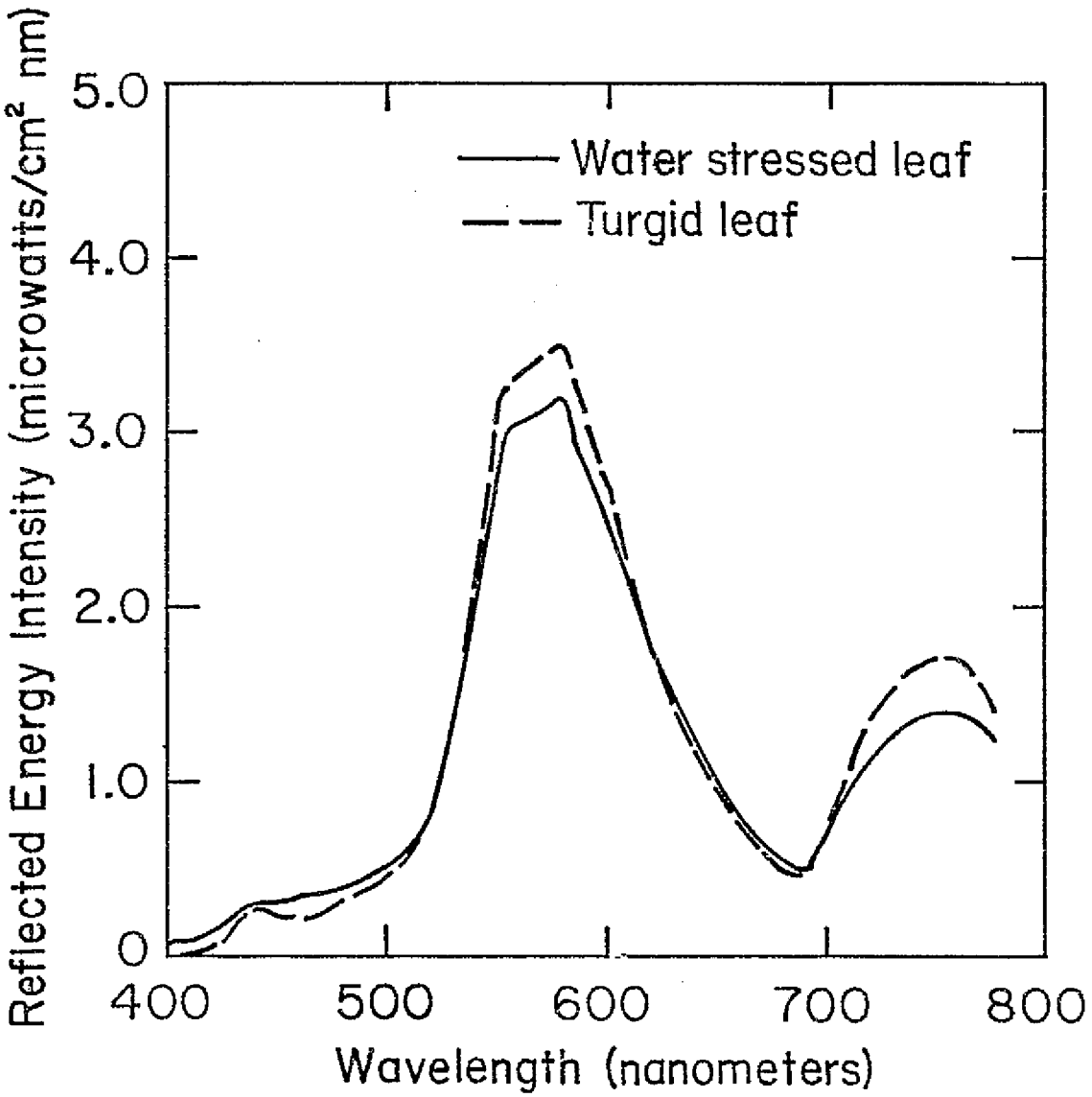

Figure 5. Reflected energy intensity of turgid and water stressed soybean leaves.

Table 6. Tabulated results for Differential Leaf Water Potential (DLWP), Visual Leaf Conditions (VLC) and Differential Normalized Reflected Energy (DNRE)* from observations made on leaves of turgid and progressively stressed soybean plants.

Date	4/23	4/24	4/26		4/27	
Time	9:15	9:30	11:00	6:00	9:00	4:30
DLWP (- bars)	0	0	10	14	22.14	23.33
VLC	green	green	green	green	yellowish	yellowish
DNRE (x 100)						
575 nm	-1.8	-4.5	-3.0	+5.8	+12.9	+15.0
750 nm	-1.8	-6.2	-6.5	+2.9	+2.9	+3.0
850 nm	----	----	-1.5	+0.7	+0.4	+1.5

$$* \text{ DNRE} = \frac{\text{Energy intensity of stressed Leaf}}{\text{Energy intensity of standard (600 nm)}} \text{ minus } \frac{\text{Energy intensity of turgid Leaf}}{\text{Energy intensity of standard (600 nm)}}$$

Example for 575 nm above (readings from Figure 5)

$$\text{DNRE} = \frac{3.2}{17} - \frac{3.5}{17} = -1.8 \times 10^{-2}$$

Energy intensity of standard for this example was 17 μw at 600 nm

ing the observed values by the energy intensity of a standard (magnesium oxide) at 600 nm. During the drying of the leaves, differential reflected energy intensity increases at all wavelengths. The absolute increase is progressively greater mainly in the 550-575 but also in the 725-750 nm wavebands.*

Similar results were obtained with corn leaves.

Sand Plain Research Farm Experiment

Purposes of this experiment were to establish a link between the artificial conditions of a greenhouse and the SW sites; to study crop signatures and spectral reflectance of known plant and soil water status and [illegible] sure droughty conditions. Spectral signatures of these irrigated and non-irrigated plots can can also be used as references for the SW sites.

Since amount and distribution of precipitation were also favorable at Becker, non-irrigated corn and soybean plots, not only matured but had significant yields (Table 7). Furthermore, except at the end of the growing season, non-irrigated plants did not show stress symptoms - such as rolling or tipping over leaves - much more frequently than irrigated

---

* The leaf water potential is taken as a measure of the state of the plant. A plant in the turgid state would show a lower leaf water potential than a plant under stress. It should be noted that for two plants presumably in the same unstressed state there is a variation in the leaf water potential. This has significance when determinations are made of the differential reflected energy intensity between plants in various states of stress and a plant in the turgid state which is taken as a "standard". The state of the turgidity lies in a range and it should not be surprising that negative values can appear in the differential reflected energy intensity between a "standard" plant and another presumably in a turgid state; also variations may occur in this general trend since plant material depends upon many other factors than water potential.

Table 7. Sand Plain Research Farm (Becker) 1978 yields. Irrigated and non-irrigated corn and soybean fields

		Yields (bu/a)	Average yield (bu/a)
Soybeans irrigated	1	54.2	50.0
	2	47.1	
	3	48.8	
Soybeans non-irrigated	1	22.8	26.0
	2	26.3	
	3	28.0	
Corn irrigated			84.0
Corn non-irrigated			64.0

plants. However, leaf water potential (Table 8) of corn and soybeans on non-irrigated plots were always higher.

Since the differences were much greater in the morning than in the afternoon, the LANDSAT overpass between 10:00 and 11:00 a.m. appears to be satisfactory for our purpose. In summer, afternoon plant stress may be more a result of hot, windy condition than soil water availability.

Field reflected energy intensity of irrigated and non-irrigated corn and soybean plots are shown in Tables 9 and 10. The values correspond to the difference between the irrigated and non-irrigated reflected energy intensity. As observed in the greenhouse experiment, best differentiation occurs in the wavebands 550-575, 650-675, and 800-850 nm. But in the field experiment, maximum differentiation occurs in the near infrared band instead of the 575 nm (green) band. The result would recommend the use of LANDSAT band 7 or color infrared photographs to differentiate crop water status in regard to soil water content. The two last measurements

Table 8. Sand Plain Research Farm - Plant water potential of irrigated and non-irrigated plots.

Date		Crop	Time	Leaf Water Potential[1] (-bars) Irrigated		Non-irrigated	
8/11/78	Clear sky	Soybeans	9:00	7	no stress[2]	17.3	stress
			1:30	13		18.8	stress
		Corn	9:30	4.8		13.2	
			2:00	7.2		18.4	stress
8/25/78	Overcast, foggy	Soybeans	9:15	3.9	no stress	5.9	no stress
			1:00	10.7		12.8	no stress
		Corn	10:00	2.1		4.3	no stress
			1:45	5.3		-	no stress
8/30/78	Clear sky	Soybeans	9:50	6.8	no stress	13.3	no stress
			3:30	12.8		14.9	some stress
		Corn	10:30	7.2		--	dried out
			4:00	7.4		--	dried out
9/7/78	Clear sky	Soybeans	9:45	9.1	no stress	10.0	no stress
			2:30	12.3		14.2	slight stress
		Corn	10:15	7.1		--	dried out
			3:30	10.8		--	dried out

[1]Average of several measurements.

[2]Visually estimated.

Table 9. Differential reflected energy intensity and temperature between irrigated and non-irrigated soybeans. Sand Plain Research Farm.

Date		8/7	8/11	8/13	8/17	8/30	9/7	9/11
Time (a.m.)		10:00	11:00	10:15	10:15	10:45	10:45	9:45
		Differential reflected energy (10^{-1} uw)						
Wavelength (nm)								
Visible	500	+ .5	+1.3	+ .2*	+ .4	0	+ .9	+1.4
	25	+ .6	+2.2	+ .1	+1.1	+ .7	+ .9	+1.2
	50	+ .8	+2.7	+ .5	+1.7	+1.3	+2.3	+1.2
	75	+ .7	+2.8	+ .3	+1.7	+1.2	+2.8	+1.9
	600	+ .7	+2.5	- .1	+1.4	+1.1	+3.9	+2.5
	25	+ .8	+2.6	0	+1.1	+1.0	+4.5	+2.9
	50	+ .6	+2.3	- .1	+. 9	+ .7	+4.7	+3.2
	75	+ .4	+1.8	0	+ .5	+ .4	+3.4	+3.2
	700	+ .2	+1.8	+ .1	+1.0	+ .9	+3.7	+2.1
	25	- .2	+1.2	-1.0	+ .5	+ .5	-1.0	0
	50	-1.3	+ .8	-2.1	-1.0	-1.1	-2.6	- .8
	760	-1.4	+1.6	-1.5	-1.2	-1.0	-2.3	-
Near Infrared	760	-1.6	+2.7	-3.6	-2.1	-1.5	-2.7	-1.3
	800	-2.8	+2.1	-4.3	-3.2	-2.1	-3.7	-1.0
	50	-2.2	+2.2	-4.2	-3.2	-2.0	-3.5	- .6
	900	-1.8	+1.6	-3.3	-2.5	-1.4	-2.5	+1.0
	50	-1.1	+1.8	-1.4	- .7	- .6	-1.1	0
	1000	- .9	+1.0	-1.3	- .7	- .7	-1.1	+ .2
		Differential temperature (°C)						
Thermal Infrared		5*	7	0	0	0	-	-
Differential Leaf Water Potential (- bars)		-	10	-	-	-	-	-
Leaf Condition (non-irrigated)		Slight Stress	Stress	No Stress	No Stress	Yellow-ing	1/2 leaves lost	most leaves lost

*Plus values indicate higher reflected energy intensity on non-irrigated plots; minus values, higher on irrigated plots.

Table 10. Differential reflected energy intensity and temperature between irrigated and non-irrigated corn. Sand Plain Research Farm.

Date		8/3	8/7	8/11	8/17	8/30	9/11
Time (a.m.)		9:45	9:45	11:45	10:45	11:15	11:15
		Differential reflected energy (10^{-1} uw)					
Wavelength (nm)							
Visible	500	+1.2*	+ .5	+ .2	+1.0	+2.2	+2.6
	25	+1.6	+ .8	0	+1.4	+2.3	+2.3
	50	+2.6	+1.2	- .1	+2.1	+2.5	+2.5
	75	+3.3	+1.4	+ .2	+2.8	+3.4	+3.2
	600	+2.9	+1.5	+ .6	+3.1	+4.4	+4.1
	25	+2.7	+1.4	+ .6	+3.0	+4.9	+4.8
	50	+2.6	+1.3	+1.2	+3.3	+5.0	+5.3
	75	+1.9	+1.1	+1.1	+3.0	+4.9	+4.4
	700	+2.3	+1.2	+ .6	+2.8	+3.9	+4.1
	25	+2.1	+1.0	-1.9	+1.3	- .5	+ .2
	50	+ .9	0	+2.6	-1.1	-4.0	+2.8
	760	- .3	- .2	+3.1	-1.3	-3.9	—
Near Infrared	760	+ .7	- .8	-8.9	-2.3	-5.5	-5.0
	800	+ .6	-1.3	-8.7	-3.9	-7.1	-6.0
	50	+1.0	-1.1	-10.4	-3.5	-7.2	-6.0
	900	+ .5	- .6	-7.2	-1.6	-5.4	-4.3
	50	- .3	- .2	-2.4	- .9	-2.7	-1.6
	1000	+ .4	- .5	-2.3	- .4	-1.7	- .2
		Differential temperature (°C)					
Thermal Infrared		1*	2	5	3	-	-
Differential Leaf Water Potential (- bars)		-	-	6	-	-	-
Leaf Condition (non-irrigated)		No Stress	No Stress	Slight Stress	No Stress	Drying	Drying

* Plus values indicate higher reflected energy intensity on non-irrigated plots; minus values, higher on irrigated plots.

(August and September) correspond to mature conditions in the case of non-irrigated plots. At this stage, plants are drying out and water potential is no longer a good indicator of leaf water status but reflected energy intensity is representative of plants under droughty conditions.

Thermal infrared, according to the data in Tables 9 and 10, seems to be a valuable tool in assessing plant water status. Values seem to be correlated with plant water potential measurements. Morning differential values of 0° to 7°C were recorded. Morning observations seem more appropriate than afternoon for the reason noted.

Color infrared photographs. Figures 6a-6d are color infrared products. It is well to note the color shift from ordinary color to color infrared images. For example, a dark green color becomes brownish red, green becomes red, light green becomes bright red or pink; thus a bare soil becomes dark green to light blue-green depending upon its darkness, surface water content, and texture.

The analysis of the photographs shows that crop signature varies significantly with plant water status. Soil moisture stress related to excess or drought condition can be detected.

Hail damage was mapped and dated by soil surveyors from information given by district conservationists and Federal Crop Insurance officers. These observations will be correlated with the LANDSAT imagery when the 1978 tape imagery is available.

Yield forecasting. Yield values of the well drained and poorly drained sites confirm the generally favorable conditions of the 1978 season (Table 11). If lower yields are related to soil water, it was not drought conditions but some excess of water in 1978 since the lower yields are observed on non-tiled, poorly drained, soils.

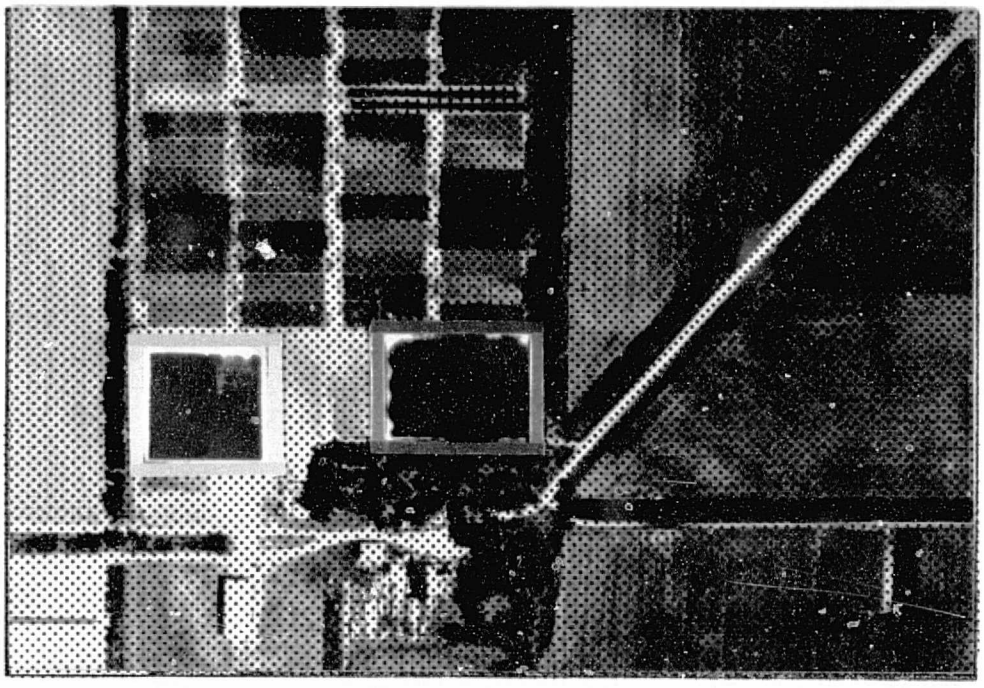

a. July 19; non-irrigated, irrigated soybeans

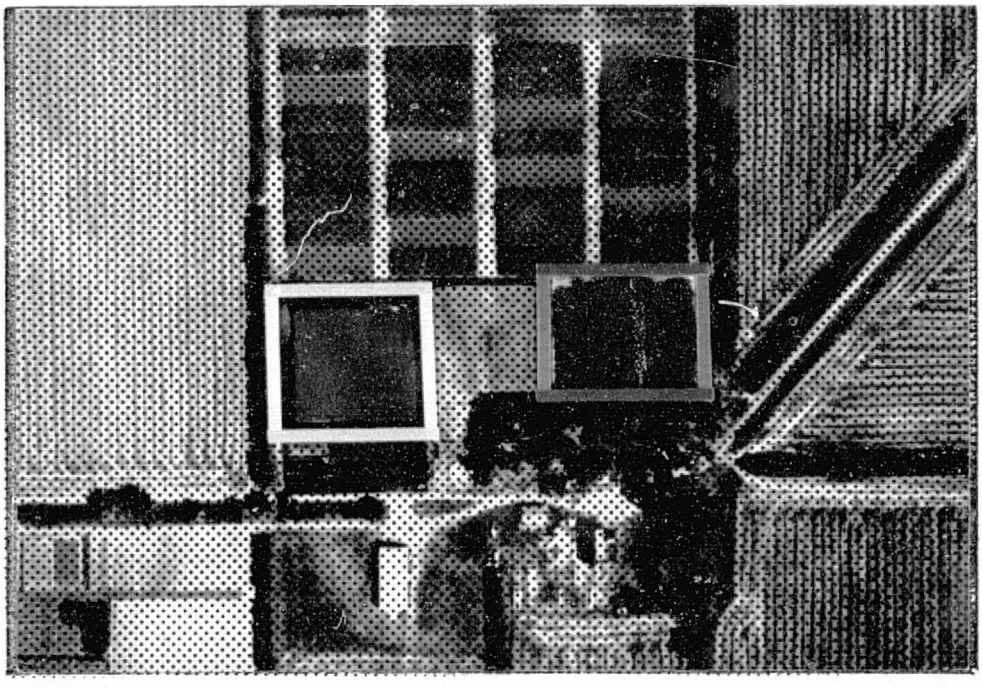

b. August 7;..... non-irrigated,....irrigated

Figure 6. Sand Plain Research Farm (Becker). Color infrared photographs illustrating changing spectral reflectance on irrigated and non-irrigated plots during the 1978 growing season.

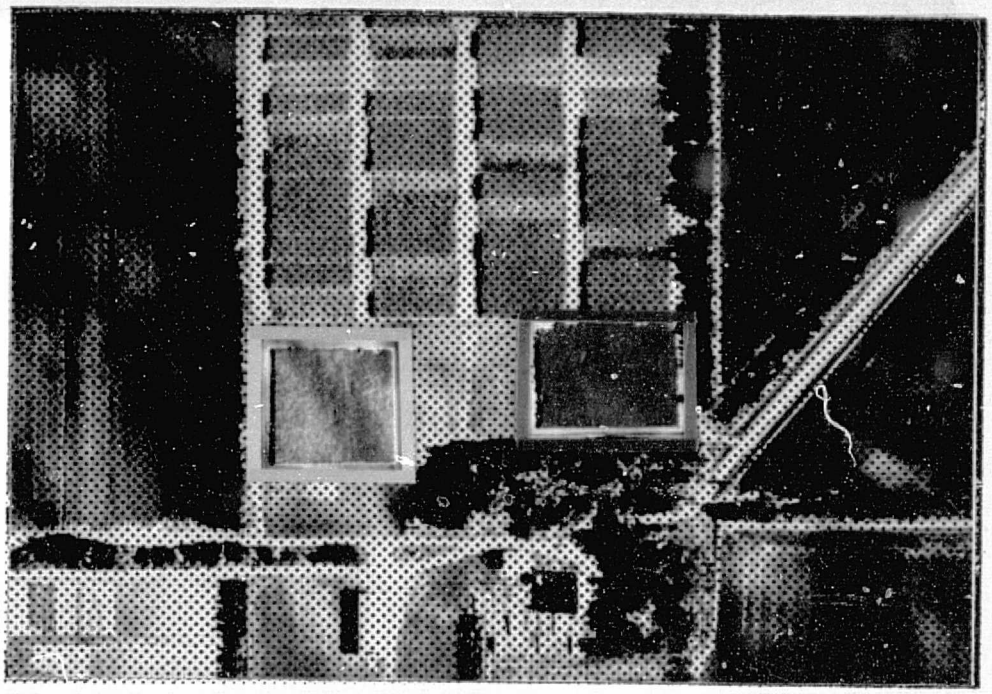

C. August 20;.....non-irrigated, irrigated soybeans

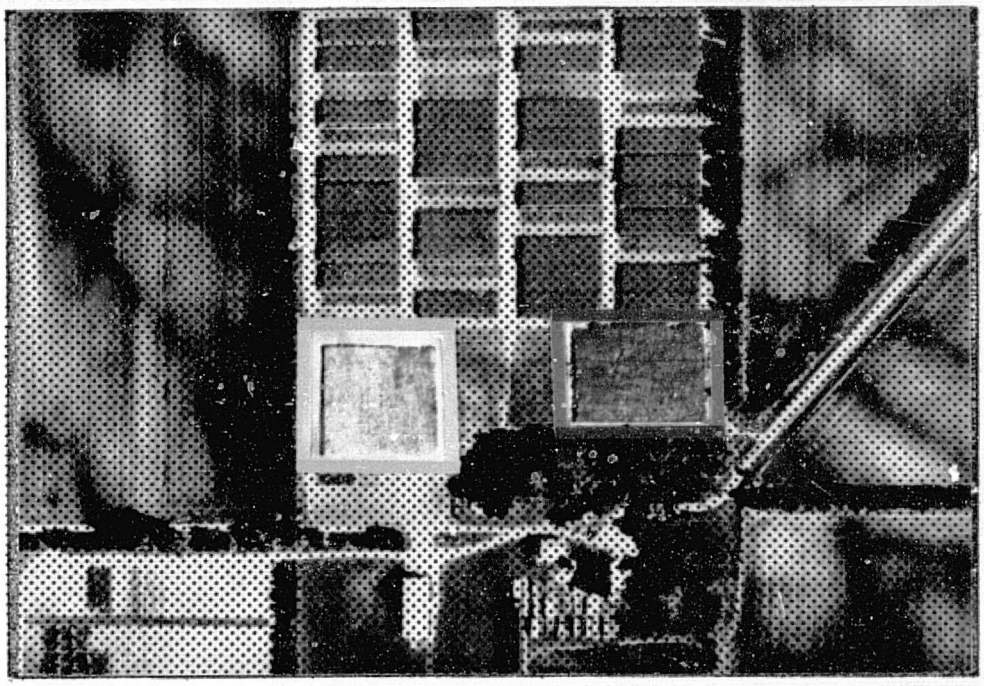

d. September 4,.....non-irrigated, irrigated soybeans

Table 11. Corn and soybean yields obtained in 1978 on sites in SW Minnesota selected for LANDSAT and other imagery studies.

Sites	Soils well drained	Crop[1]	Yield (bu/a)	Soils poorly drained	Crop	Yield (bu/a)	Tiling
Porter	Ves	S	43.1	Canisteo	S	29.7	No
Bergen	Clarion	C	140.5	Webster	C	125.5	No
Tracy	Everly	C	130.0	Letri	C	157.0	Yes
Redwood Falls	Everly	C	130.0	Okoboji	C	154.0	Yes
Clara City	Tara	C	121.8	Colvin	C	121.2	Yes
Pipestone	Kranzburg	C	135.6	Hidewood	C	113.2	No
Vesta	Everly	C	129.0	Canisteo	C	140.0	Yes
	Soil	Non-Irrigated			Irrigated		
Hanley Falls	Seaforth	C	106.0		C	136.0	No

[1]S - soybeans, C - corn

CONCLUSIONS AND FUTURE RESEARCH

Ground data, basic to remote sensing interpretation, were gathered during the 1977 and 1978 growing seasons. Soil water content, field information such as phenologic data, farming operations, precipitation events, crop stress status were recorded.

Greenhouse experiments have shown that a pressure chamber equipped with an original leaf holder gives satisfactory measurements of corn and soybean water stress and that water stressed leaves have a significantly different spectral signature. This was confirmed in a controlled field experiment (Becker Research Farm) when analyzing spectral intensity in the visible, near infrared, thermal infrared and with color infrared photographs. It was found that corn and soybean stressed plots can be best differentiated in the near infrared and thermal infrared wavebands.

Future research will analyze 70 mm and 35 mm color infrared positive film by densitometry techniques to study site variability in spectral signatures. Computer processing using a digitizer and desk-top computer system will be tested to compare low altitude color infrared digitized imagery and LANDSAT digital tapes. Their capability to differentiate corn and soybean fields, evaluate crop condition, localize well and poorly drained soils, map hail damage, and assess drainage efficiency will be evaluated.

Since a general drought condition has not occurred in the study area during the past two seasons, a third ground data collection, on a limited number of sites, should be continued.

ACKNOWLEDGEMENTS

The cooperation of the following persons and agencies is gratefully acknowledged:

W. Brug, H. Hokansen, E. Loll, J. Murray, G. Nelson, P. Rem, K. Steffen, S. Vlieger, soil scientists of the Cooperative Soil Survey;

D.G. Baker, Department of Soil Science;

S. Evans, West-Central (Morris) Experiment Station;

A. Frenkel, Department of Botany;

O. Gundersen and G. Holcomb, Agricultural Extension Service;

L.D. Hanson, Department of Soil Science;

M. Meyer and T. Lillesand, Institute of Agriculture, Forestry and Home Economics, Remote Sensing Laboratory;

W. Nelson, Southwest (Lamberton) Experiment Station

LITERATURE CITED

Blum, A., et al., 1973. On the pressure chamber technique for estimating leaf water potential in sorghum. Agron. J. 65:337-338.

Boyer, J.S. and S.R. Ghorashy. 1971. Rapid field measurement of leaf water potential in soybeans. Agron. J. 63:344-345.

Boyer, J.S. 1966. Leaf water potentials measured with a pressure chamber. Plant Physiol. 42:133-137.

DeRoo, H.C. 1969. Leaf water potentials of sorghum and corn estimated with the pressure chamber. Agron. J. 61:969-970.

Frazee, C.J. 1972. Density slicing techniques for soil survey. Soil Sci. Soc. Amer. Proc. 36:693-695.

Rust, R.H., and P. Robert. 1978. Evaluation of soil moisture stress in western and southwestern Minnesota. Section F in NASA Progress Report (NGL 24-005-263).

SECTION C

SYNERGISTIC RELATIONSHIP BETWEEN LINEAMENTS LOCATED ON LANDSAT IMAGERY AND TRADITIONAL SOURCES OF TOPOGRAPHIC INFORMATION

Drs. Joseph E. Goebel, Matt Walton
and Mr. Lawrence G. Batten
Minnesota Geological Survey
St. Paul, Minnesota

o

INDEX

Introduction..... C1
Status of Remote Sensing at the Minnesota Geological Survey..... C1
Growth of Remote Sensing at the Minnesota Geological Survey..... C1
Review of Specific Application of Remote Sensing by the Minnesota Geological Survey in 1978..... C2
Interpretation of Lineaments on Aerial Photographs in Northeastern and Southeastern Minnesota..... C2
The Investigation of Karst Processes in Southeastern Minnesota..... C3
Present Study--Inventory of Lineaments of Minnesota..... C3
Introduction..... C3
Materials..... C4
Methods..... C5
Preliminary Lineaments Maps..... C10
Coincident Lineaments Maps..... C29
Signigicant Coincident Lineament Maps..... C36
Results..... C39
Discussion..... C39
Indicative Lineaments Map..... C40
Maps of Indicative Lineaments and Geologic Conditions..... C42
Literature Cited..... C50

o

SYNERGISTIC RELATIONSHIP BETWEEN LINEAMENTS LOCATED ON LANDSAT IMAGERY AND TRADITIONAL SOURCES OF TOPOGRAPHIC INFORMATION

Investigators: Dr. Joseph E. Goebel
Dr. Matt Walton
Mr. Lawrence G. Batten
Minnesota Geological Survey

INTRODUCTION

Status of Remote Sensing at the Minnesota Geological Survey.

Remote sensing now serves a more important function at the Minnesota Geological Survey than it had previously. Minnesota Geological Survey applies remote sensing in a variety of ways. One of the applications is the identification of surficial geology, both at the state-wide level and at the more detailed county level. Also we are using it for the location of faults and fractures in northeastern and southeastern Minnesota. Further, it is used to locate such mineral resources as iron, copper, nickel, and gravel. Remote sensing helps us evaluate sites for waste disposal and road and building locations. It is also useful in field research projects. It helps us study geological processes involved in karst formation, subsurface hydrology, geotectonics, glaciology, and geomorphology. One of its more significant contributions is the accurate identification and location of geological features.

Growth of Remote Sensing at the Minnesota Geological Survey

For a long time geological base information was quite restricted. Sources of data were limited to drill hole logs, well drilling cuttings, cores, rock outcrops, and a limited number of topographic maps.

The situation has improved. The current sources of interpretable information have expanded to include all of the things listed above, as

well as aerial photographs, LANDSAT imagery, natural seismology, geomagnetics, and geogravity. In the near future, the Minnesota Geological Survey expects to be able to use all of the available sources of information as well as some new sources. We anticipate the use of radar imagery, high resolution gravity data, induced seismology, GEOSAT imagery and airborne electrical resistivity data to clarify our geological perspectives. With this improved perspective we are better able to understand the surficial unconsolidated glacial drift and the underlying rock strata.

REVIEW OF SPECIFIC APPLICATIONS OF REMOTE SENSING BY THE MINNESOTA GEOLOGICAL SURVEY IN 1978

During the last year many kinds of remote sensing have been applied to the following five geologic studies. The first of these is the study of some interesting relationships among geologic and remote sensing data sources for lineaments of the state. The second is the collection of data for further synergistic studies. Third, we assisted in evaluating the peat resources of Aitkin County. Fourth is the interpretation of lineaments on aerial photographs in northeastern and southeastern Minnestota. Fifth is the investigation of karst processes in southeastern Minnesota.

Interpretation of Lineaments on Aerial Photographs in Northeastern and Southeastern Minnesota.

Dr. G.B. Morey is engaged in an extended project to log the lineaments on the Hibbing Geologic Sheet as an outgrowth of Dr. Roger Cooper's work in the same area.

Ramesh Venkatakrishnan mapped lineaments from aerial photographs for

the St. Paul Geologic Sheet in southeastern Minnesota as part of karst investigations. This study has increased our understanding of the fracture patterns and cave locations buried by glacial drift, loess, and bedrock.

The Investigation of Karst Processes in Southeastern Minnesota.

Dr. E. Calvin Alexander and Dr. George Shaw used remote sensing to study karst in southeastern Minnesota. They used aerial photographs to locate sinkholes, limestone fracture patterns, and the inlets and outlets for cave water.

PRESENT STUDY--INVENTORY OF LINEAMENTS OF MINNESOTA

Introduction

The purpose of this study was to compare remote sensing data with traditional sources of geologic information. Specifically we identified and classified lineaments that appear on both satellite imagery and topographic maps. We were particularly interested in lineaments that appeared to relate to geologic conditions.

We define a lineament as a real landscape feature, such as slopes and channels, approximately 10 km long or longer, that appears as a smooth narrow line or edge on imagery or on maps. For this study we assumed that certain topographic contour lines indicated lineaments. We assume that lineaments occur in nonrandom patterns that are related to geologic causes. Although some strong lineaments appear on topographic maps, they are difficult to recognize on the ground and their significance is not readily apparent on these maps. We are beginning to suspect that lineaments may provide us with a sort of window through the thick cover of glacial drift

that hampers investigation of subsurface geology in Minnesota. They seem to reflect subsurface control even when they occur within thick drift. Thus, we decided to assemble an inventory of Minnesota lineaments and examine their relationship to geology.

Materials

As we collected the materials we kept in mind that the inventory of lineaments should record all the lineaments under the defined conditions. It should group them into logical categories and evaluate their significance. The lineaments fell into two natural groups; rectilinears and curvilinears. Rectilinears are relatively straight lines with less than 10° arc. Curvilinears are smooth curves with more than 10° arc. We divided each group of lineaments into those associated with rivers, lakes, physiographic areas, tonal stripes from LANDSAT imagery, and 50-foot contour lines.

We identified lineaments from the following sources: winter scenes band 7 LANDSAT imagery; spring scenes false color composite LANDSAT imagery; the lakes and rivers plate of the U.S.G.S. 1:500,000 topographic map of Minnesota and the 50-foot contours plates of the U.S.G.S. 1:250,000 topographic map series, which we reduced to 1:500,000. Lineaments identified were superimposed on: the Geologic Map of Minnesota - Quaternary geology, State Map S-4; the generalized geologic map of Minnesota - bedrock geology; the simple Bouguer gravity map of Minnesota, the aeromagnetic map of Minnesota, isopach map of the thickness of the unconsolidated sediments of Minnesota, a map of faults and buried valleys in Minnesota, and the map of bedrock topography of Minnesota.

Methods

Using spring and winter LANDSAT imagery, the lakes and rivers plate and the 50-foot contour lines, we derived a group of preliminary maps of rectilinear and curvilinear lineaments. Rivers, lakes, topographic contour lines, tonal stripes, and contacts between physiographic areas may all appear as lineaments. We combined the preliminary lineament maps to identify the lineaments that coincided from one map to another for at least two of the data sources. We then combined all of the preliminary lineaments that had this coincidence to generate a map of lineaments that are most likely to provide information about the geology of Minnesota. We have called these lineaments indicative lineaments. Finally, the map of indicative lineaments was superimposed on various maps of gravity, magnetic and geologic conditions which could have caused the lineaments.

Separate identification of rectilinear and curvilinear lineaments was critical throughout the inventory. We drafted lines of the winter LANDSAT scenes where rivers appeared to meet the definition of rectilinear lineaments (for scene locations see Figure 1). We placed this LANDSAT imagery under a sheet of mylar which had been punch registered to and placed under the base map of rivers and lakes, thereby registering the imagery to the base map. We removed the base map and interpreted the LANDSAT image without it to avoid biasing the study. We repeated the procedure for curvilinear lineaments associated with rivers revealed on winter imagery.

Evaluation of the spring imagery for rivers was conducted in the same way (for scene location see Figure 2). We repeated this procedure for lineaments associated with contacts between physiographic areas expressed

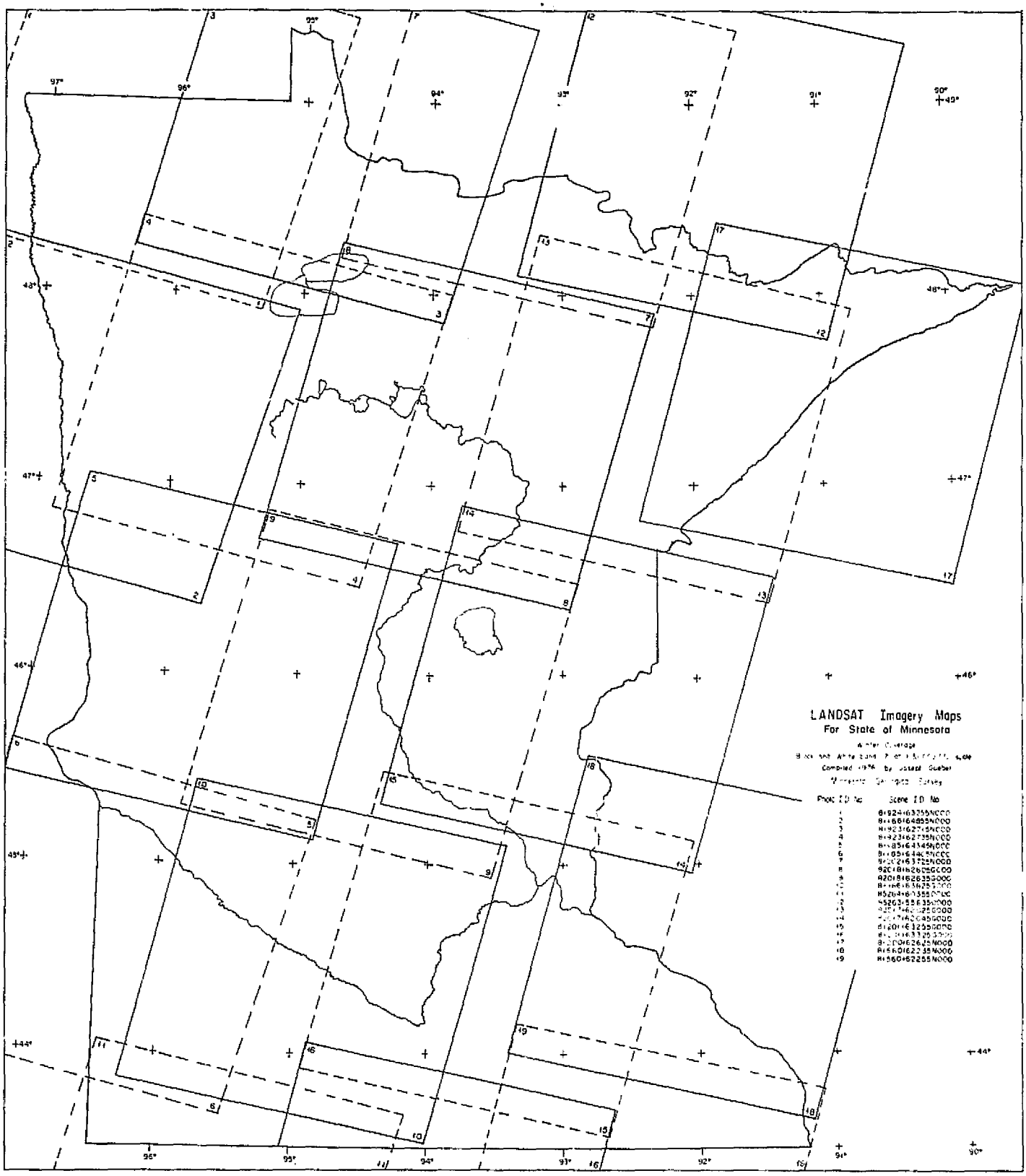

Figure 1: LANDSAT imagery index map of winter band 7 scenes of Minnesota.

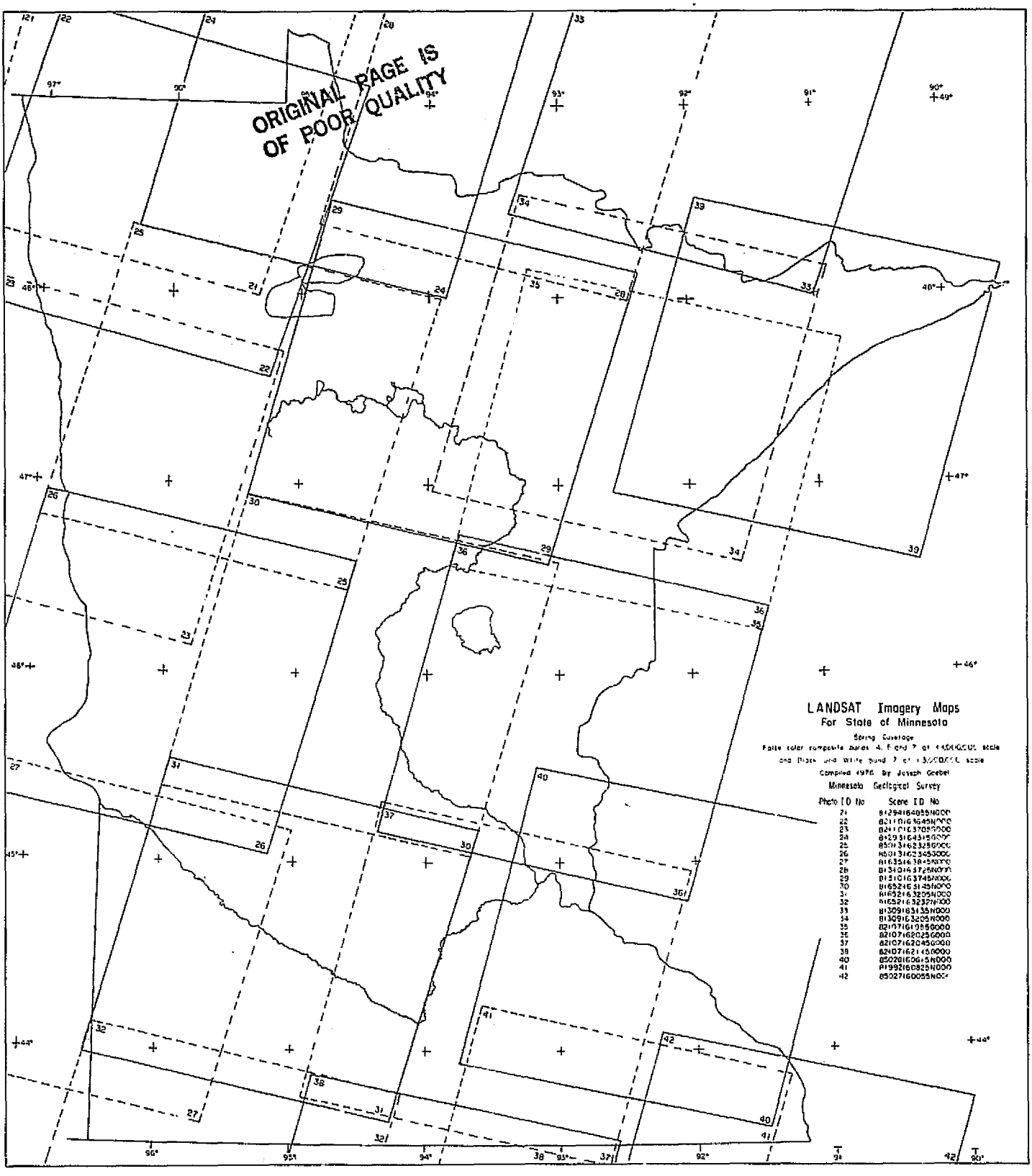

Figure 2: LANDSAT imagery index map of spring false color composites imagery of Minnesota.

as color changes on the imagery. In the case of lineaments associated with lakes and tonal stripes the procedure was the same, except we noted both the rectilinears and curvilinears at the same time on the same mylar sheet. In all cases we assessed the base maps of lakes, rivers and topographic contours for the lineaments without the assistance of the imagery to avoid biasing the study. With this procedure we generated the following maps of the preliminary lineaments.

Preliminary lineaments of rectilinear rivers on the rivers and lakes base, Figure 3.

Preliminary lineaments of rectilinear contours on the 50-foot topographic contours, Figure 4.

Preliminary lineaments of rectilinear rivers on winter LANDSAT imagery, Figure 5.

Preliminary lineaments of rectilinear rivers on spring LANDSAT imagery, Figure 6.

Preliminary lineaments of rectilinear contacts between physiographic areas on winter LANDSAT imagery, Figure 7.

Preliminary lineaments of rectilinear contacts between physiographic areas on spring LANDSAT imagery, Figure 8.

Preliminary lineaments of tonal stripes on winter LANDSAT imagery, Figure 9.

Preliminary lineaments of tonal stripes on spring LANDSAT imagery, Figure 10.

Preliminary lineaments on lake base, Figure 11.

Preliminary lineaments along lakes on winter LANDSAT imagery, Figure 12.

Preliminary lineaments along lakes on spring LANDSAT imagery, Figure 13.

Preliminary lineaments of curvilinear rivers on the river base, Figure 14.

Preliminary lineaments of curvilinear contours on the 50-foot topographic contours, Figure 15.

Preliminary lineaments of curvilinear rivers on winter LANDSAT imagery, Figure 16.

Preliminary lineaments of curvilinear rivers on spring LANDSAT imagery, Figure 17.

Preliminary curvilinear contacts between physiographic areas on winter LANDSAT, imagery, Figure 18.

Preliminary curvilinear contacts between physiographic areas on spring LANDSAT imagery, Figure 19.

We began to select lineaments with supporting evidence from more than one source. Lineaments that were essentially superimposed or closely parallel were classed as coincident. Abutting lineaments, one of which terminated at the point of contact with the other, were included in this class. We looked first for any rectilinear lineaments from winter and spring LANDSAT imagery that coincided with or abutted lineaments from the base map of rivers and lakes. We used solid lines to indicate them, with one exception: we drafted dashed lines where rivers shown on the imagery but not on the rivers base map indicated lineaments that had supporting evidence from another source. Curvilinear lineaments associated with rivers received the same treatment.

We compared the rectilinear lineaments indicated on winter or spring imagery by sharp color contacts between physiographic areas with those indicated by the 50-foot contour lines. Lineaments indicated by both sources were drafted as solid lines, and the same procedure was followed for curvilinear lineaments.

We compared the tonal stripe lineaments of the winter and spring imagery to the 50-foot contours lines. Since the curvilinear and rectilinear lineaments had been drafted on the same overlay sheet for each season, an occasional curvilinear lineament appeared on the map of coincident rec-

Preliminary Lineaments Maps

The maps in Figures 3 through 19 show the lineaments identified on the original sources, i.e., 50-foot topographic contours; rivers and lakes base map; LANDSAT band 7 winter imagery and false color composites of spring imagery.

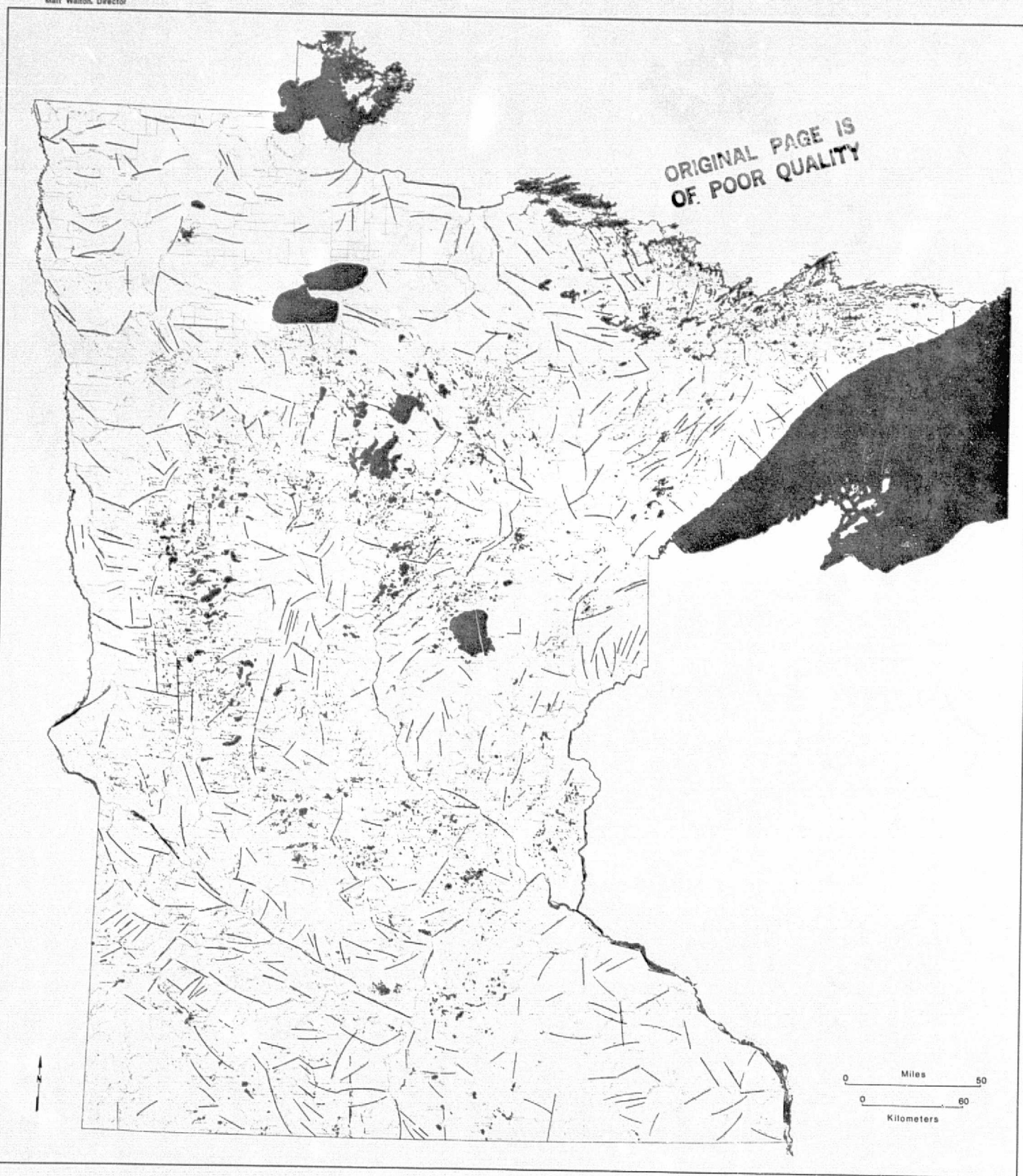

Figure 3: Preliminary linaments of rectilinear rivers on the river base.

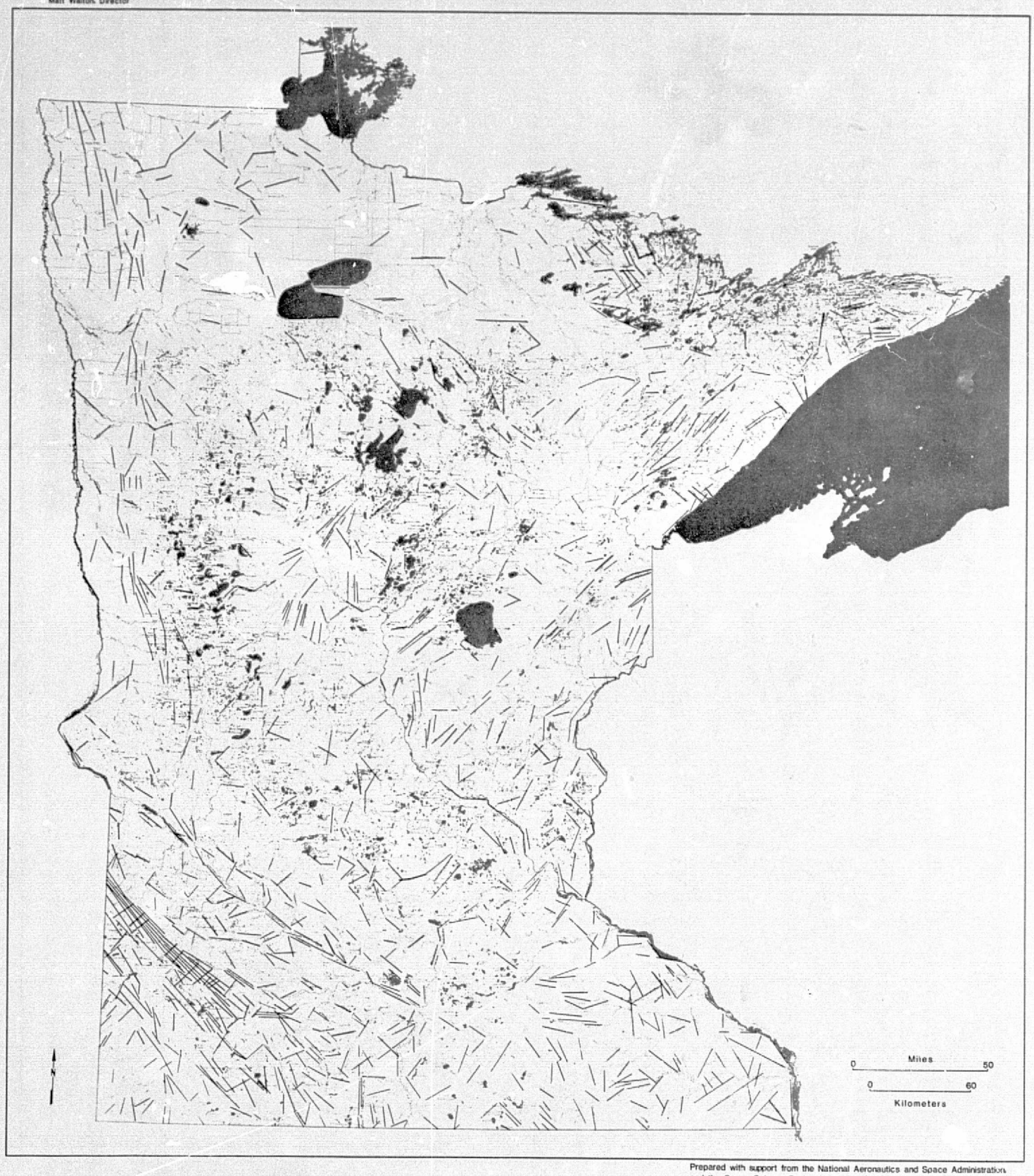

Figure 4: Preliminary lineaments of rectilinear contours on the topographic base.

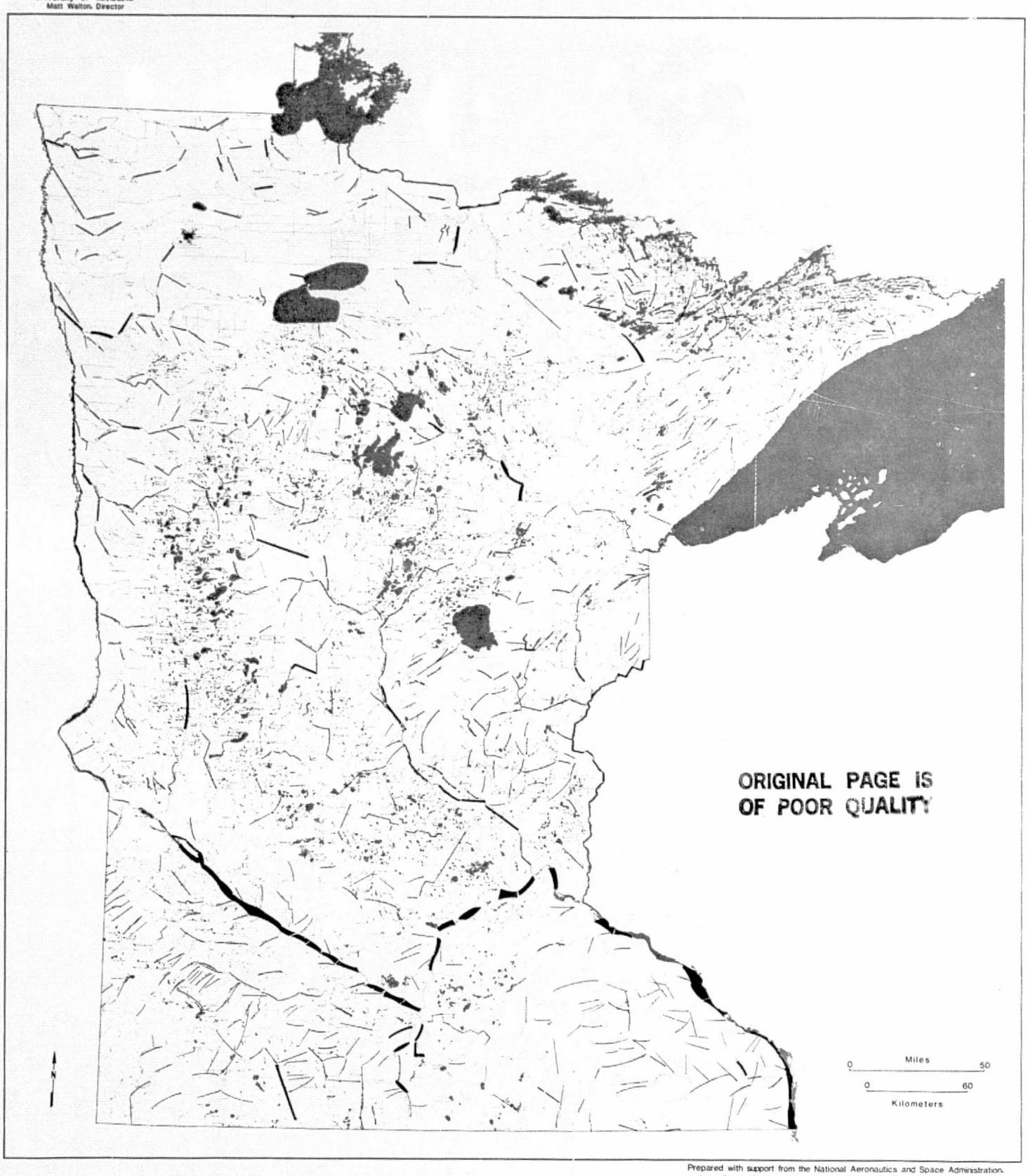

Figure 5: Preliminary lineaments of rectilinear rivers on winter LANDSAT imagery.

C14

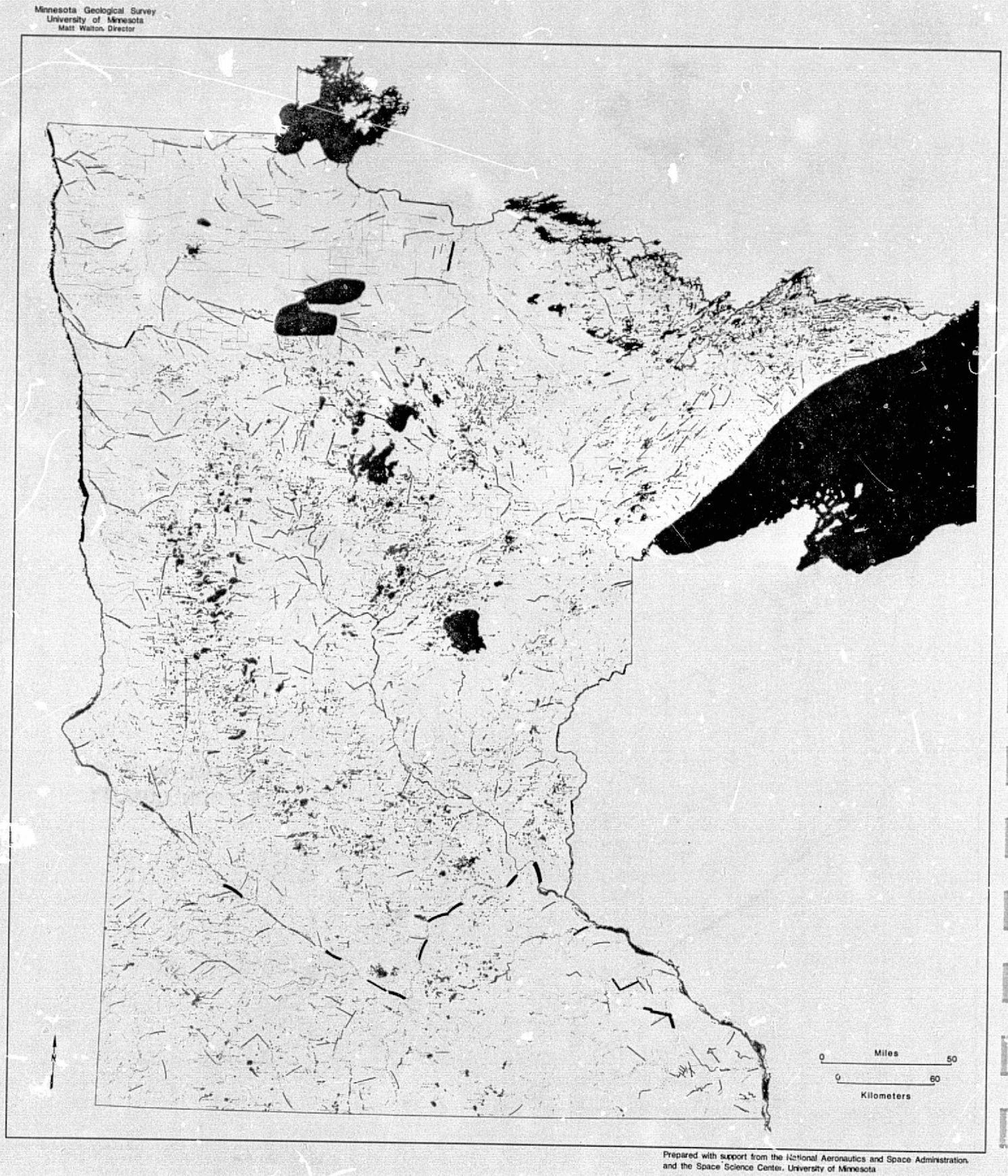

Figure 6: Preliminary lineaments of rectilinear rivers on spring LANDSAT imagery.

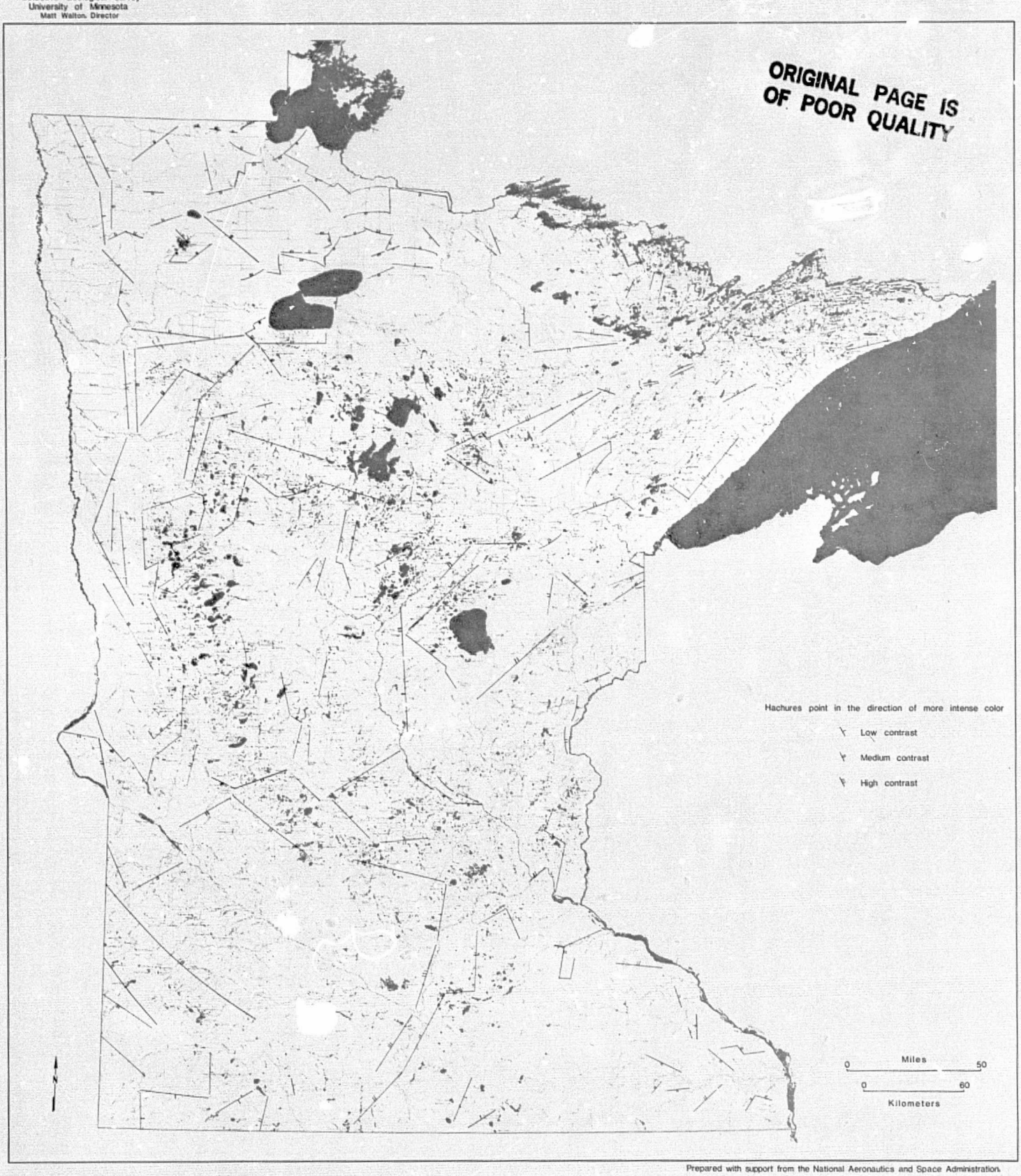

Figure 7: Prelinimary lineaments of rectilinear contacts between physiographic areas on winter LANDSAT images.

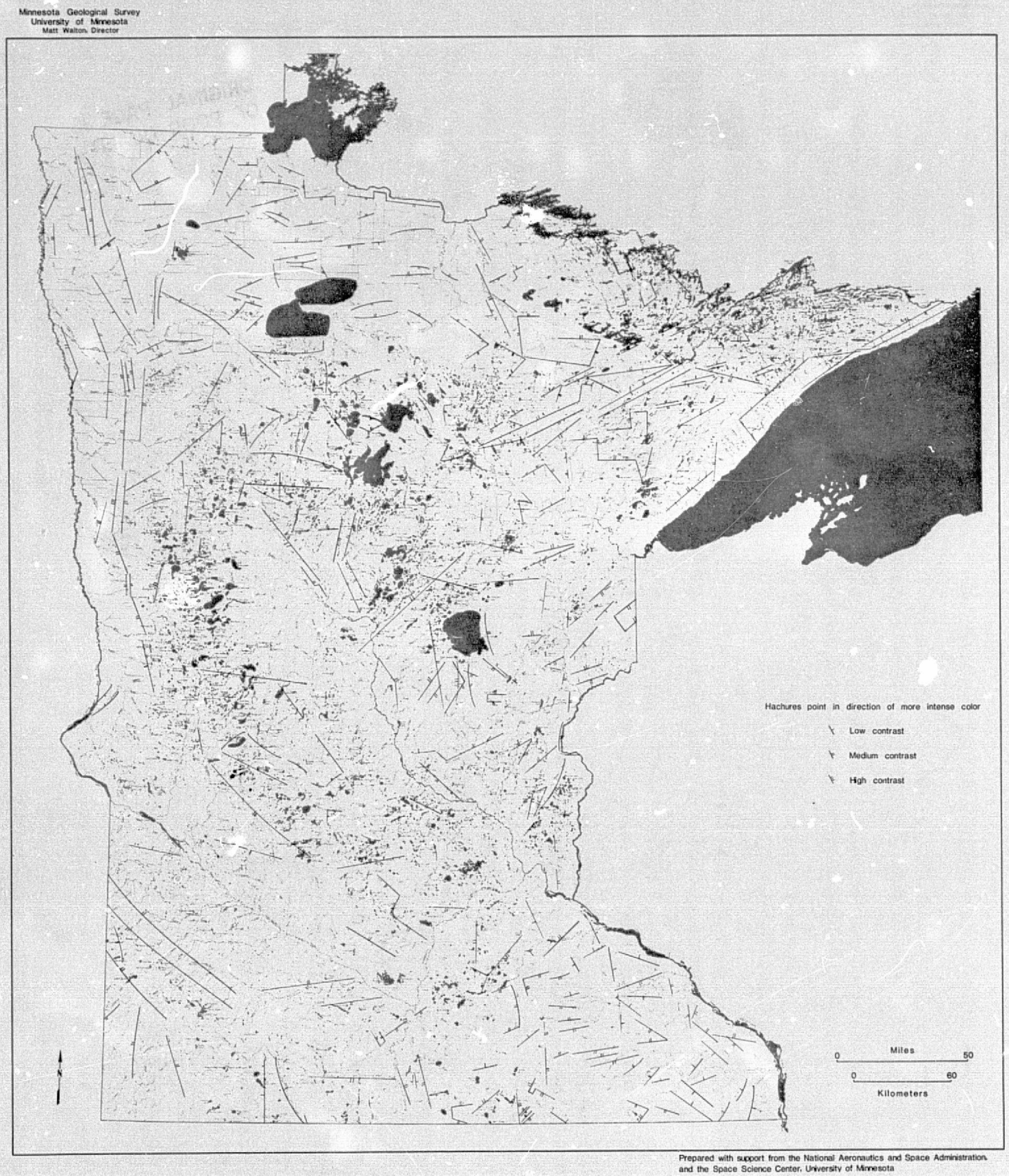

Figure 8: Preliminary lineaments of rectilinear contacts between physiographic areas on spring LANDSAT images.

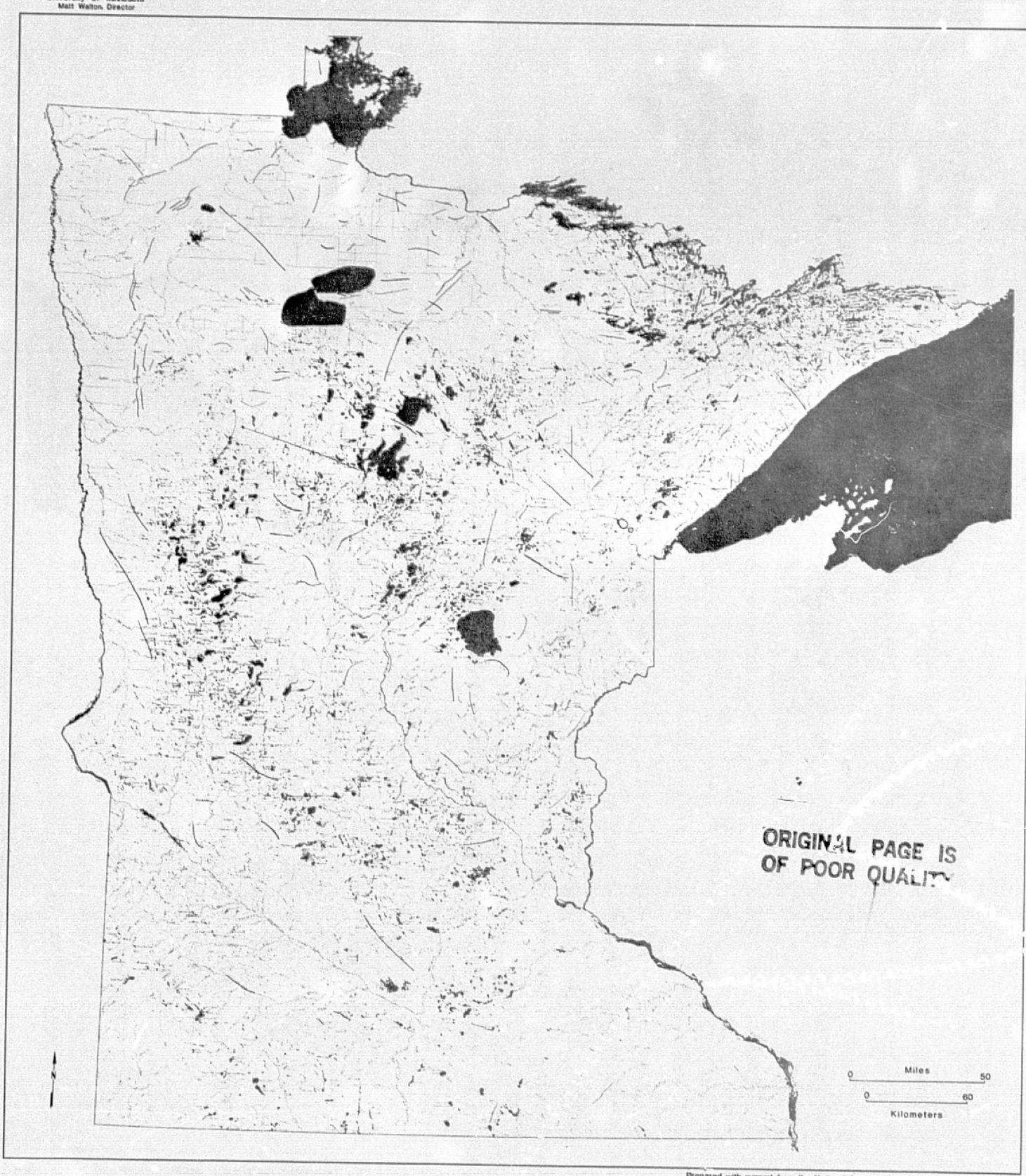

Figure 9: Preliminary lineaments tonal stripes on winter LANDSAT imagery.

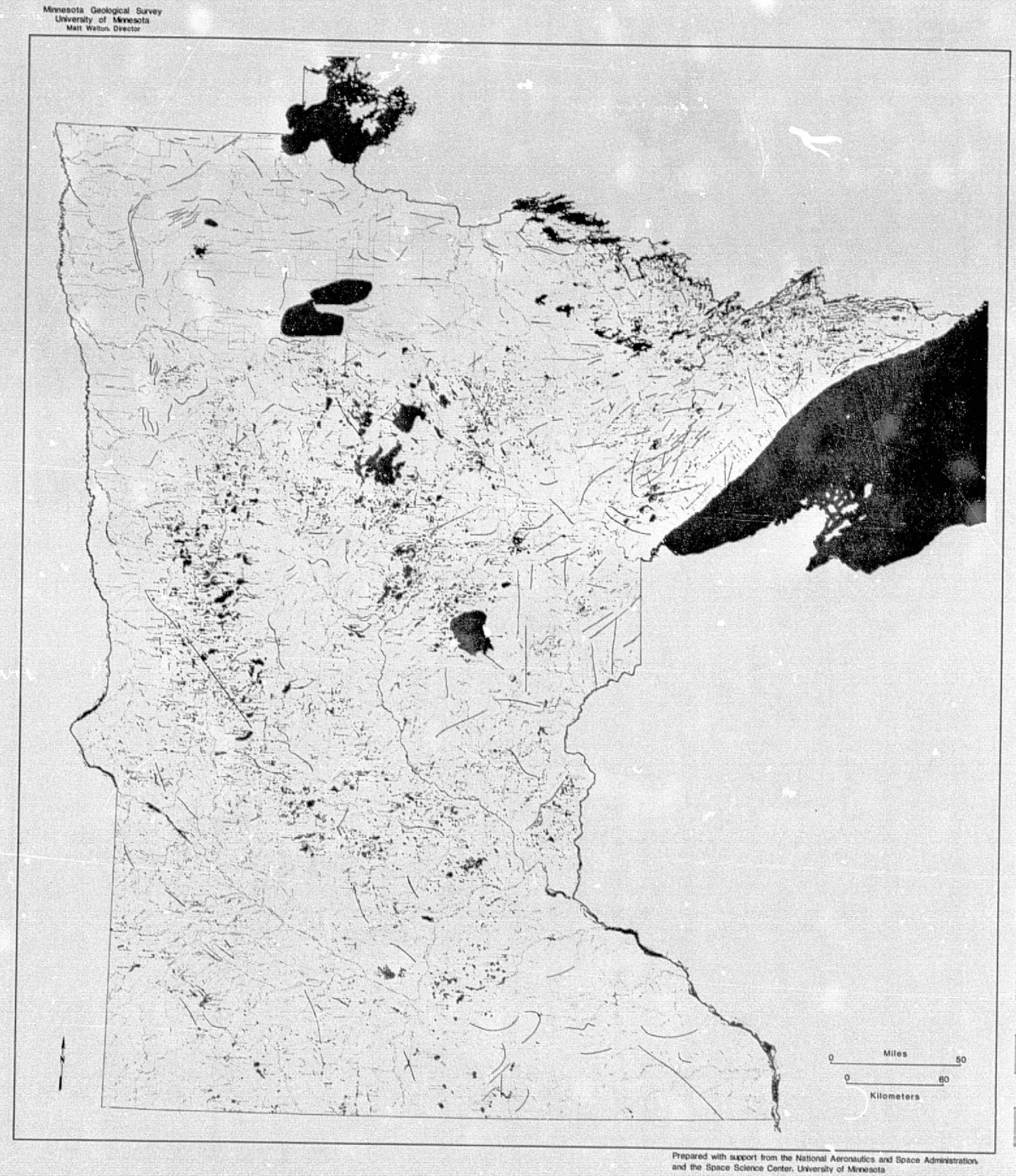

Figure 10: Preliminary lineaments tonal stripes on spring LANDSAT imagery.

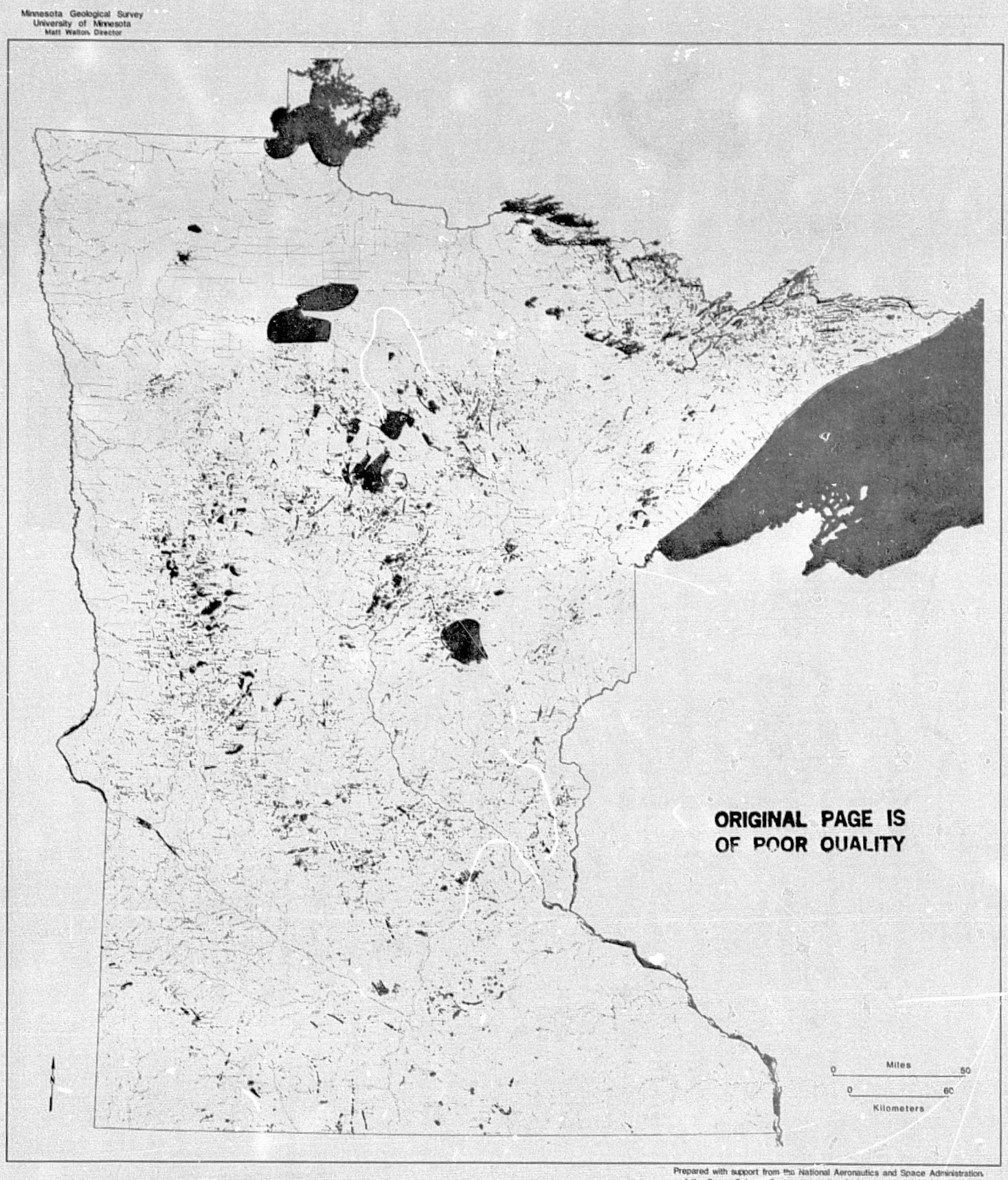

Figure 11: Preliminary lineaments on lake base.

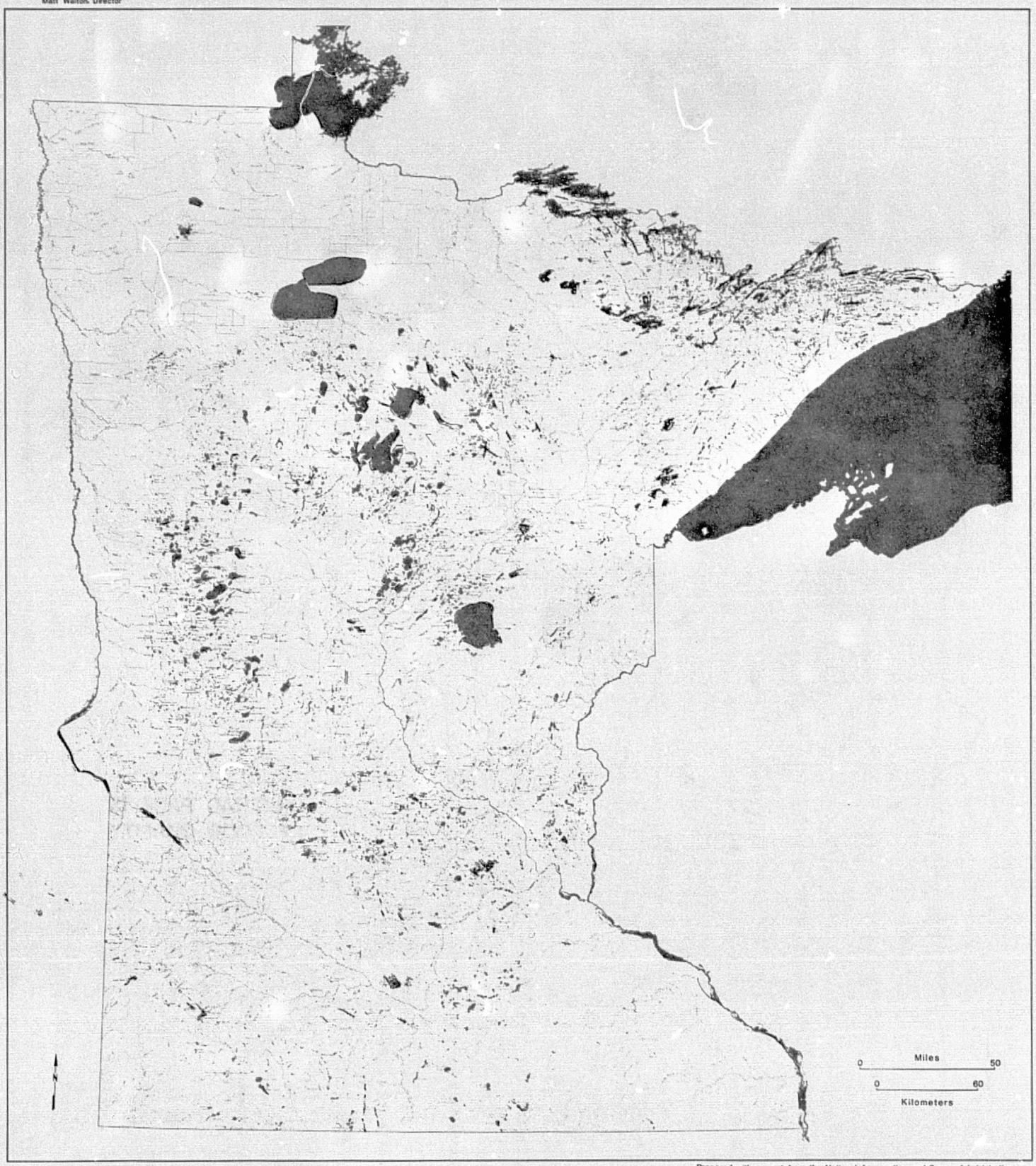

Figure 12: Preliminary lineaments along lakes on winter LANDSAT imagery.

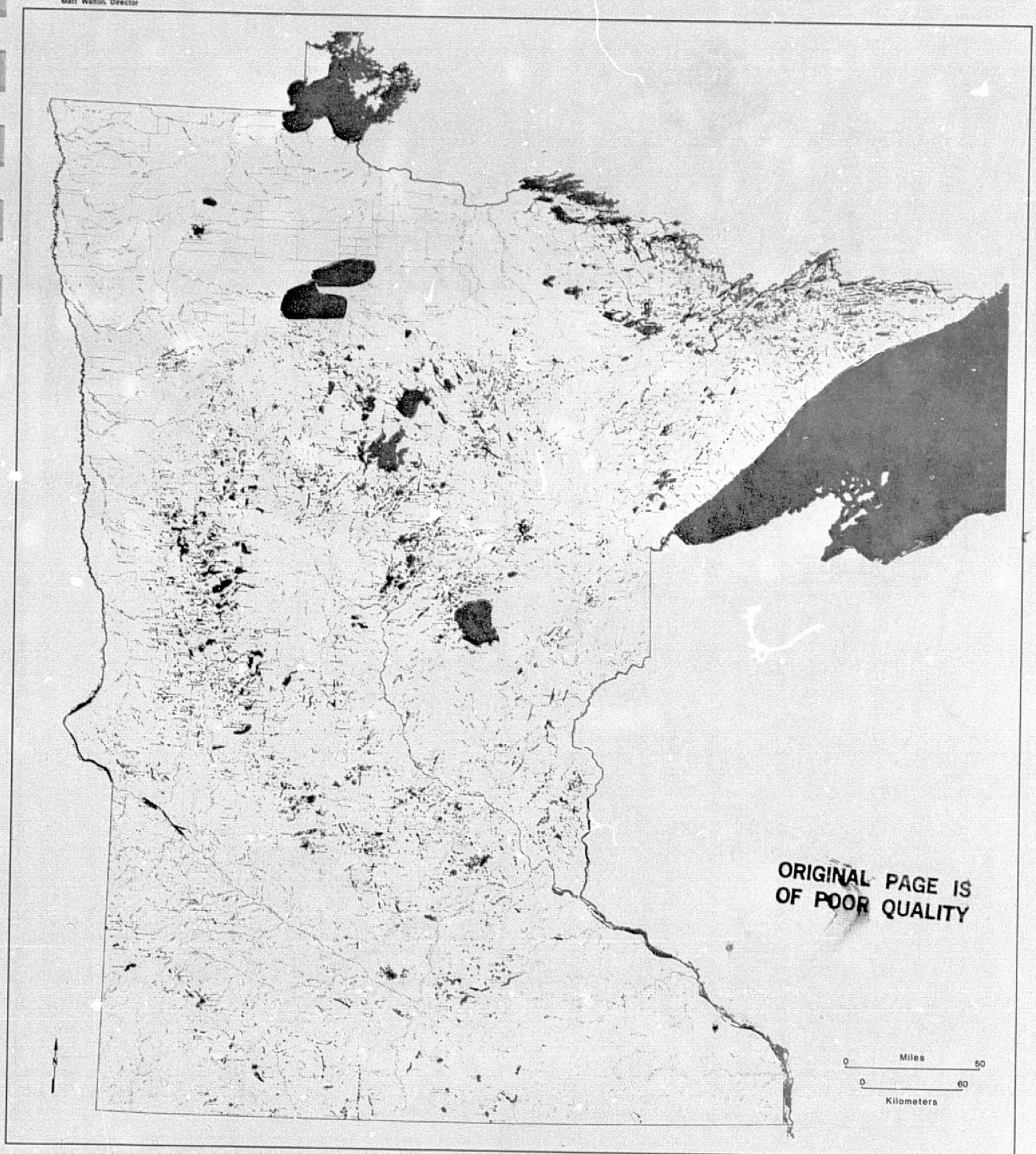

Figure 13: Preliminary lineaments along lakes on spring LANDSAT imagery.

C22

Minnesota Geological Survey
University of Minnesota
Matt Walton, Director

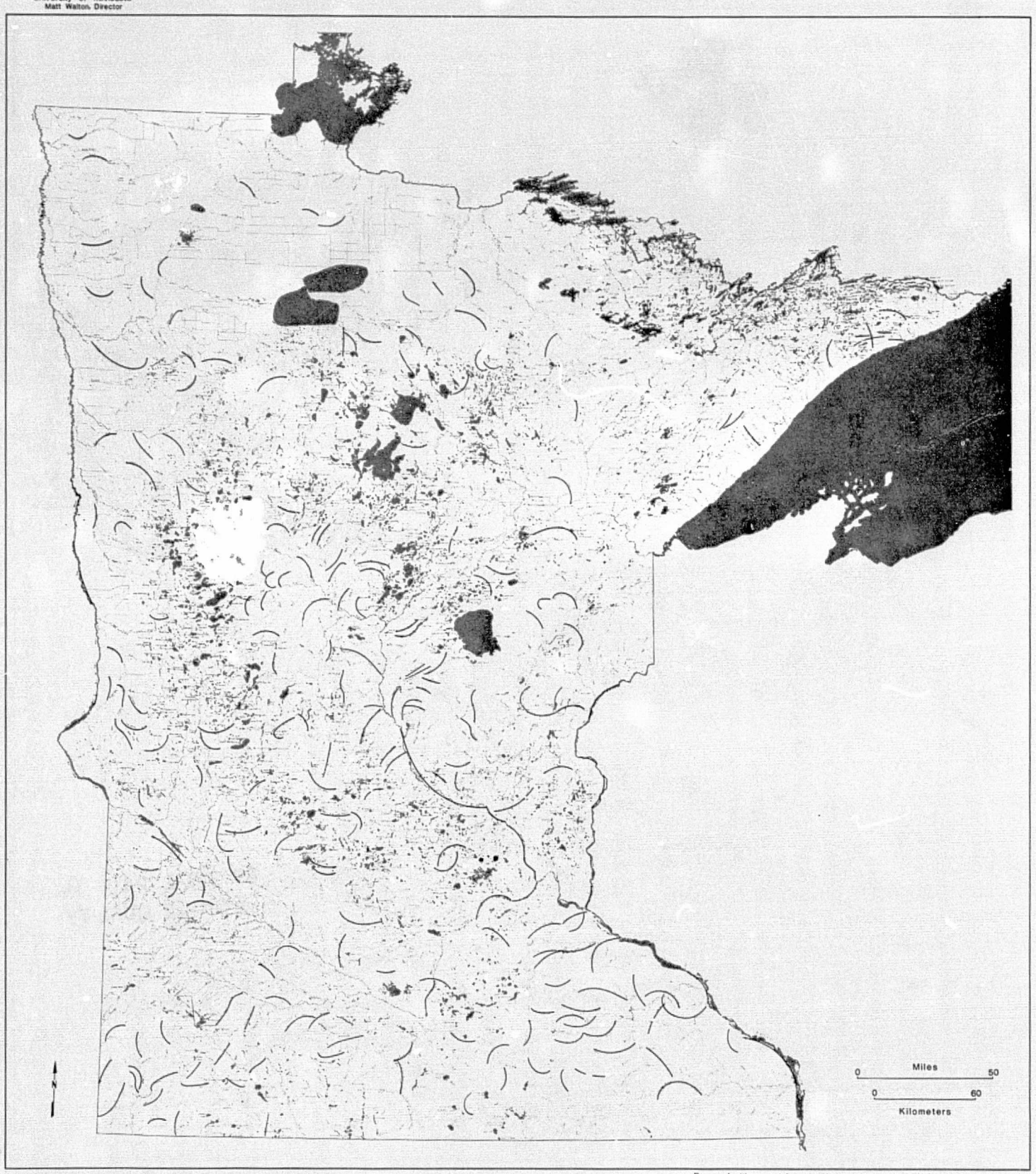

Prepared with support from the National Aeronautics and Space Administration and the Space Science Center, University of Minnesota

Figure 14: Preliminary lineaments of curvilinear rivers on the river base.

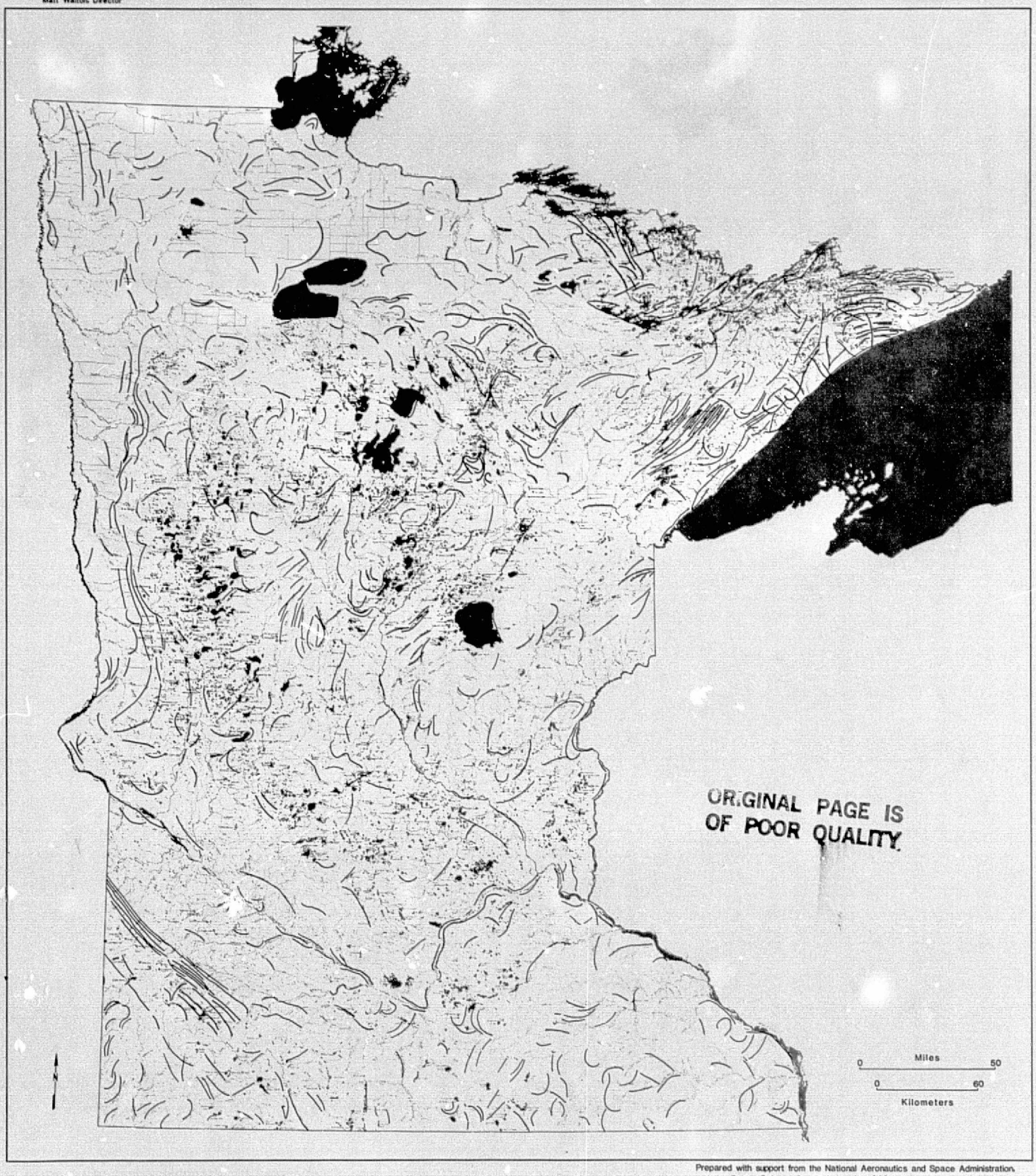

Figure 15: Preliminary lineaments of curvilinear contours on the topographic base.

C24

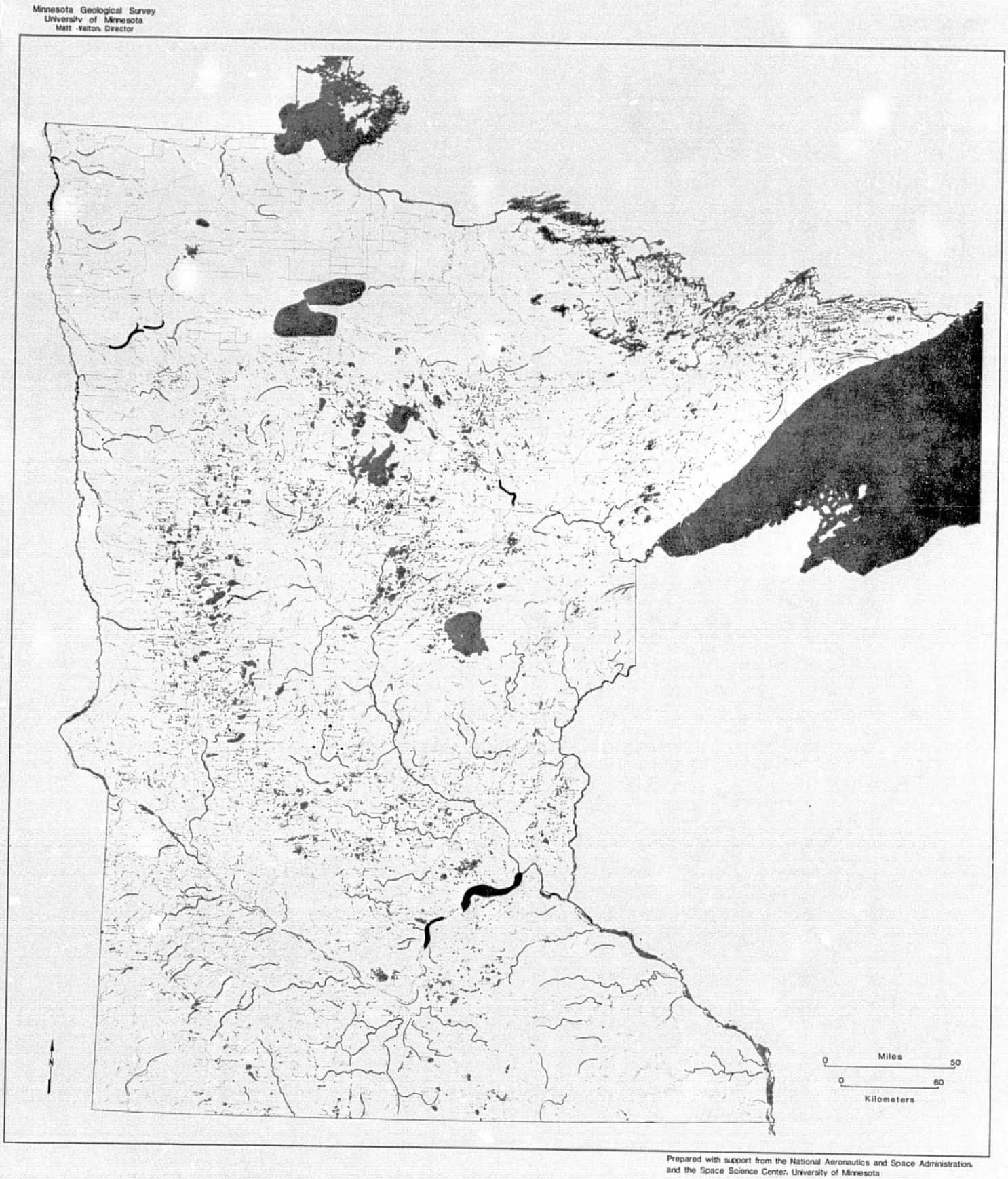

Figure 16: Preliminary lineaments of curvilinear rivers on winter LANDSAT imagery.

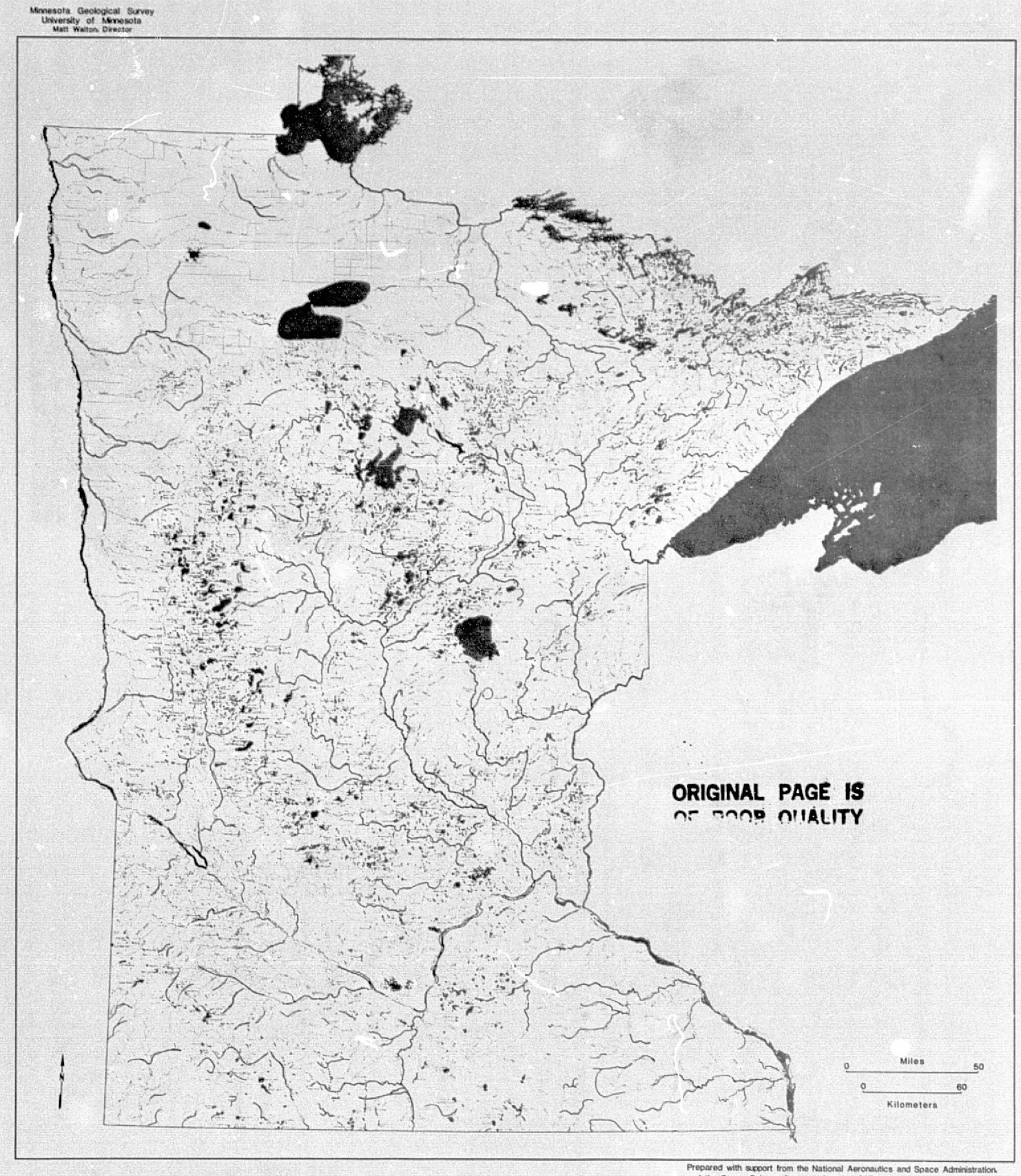

Figure 17: Preliminary lineaments of curvilinear rivers on spring LANDSAT imagery.

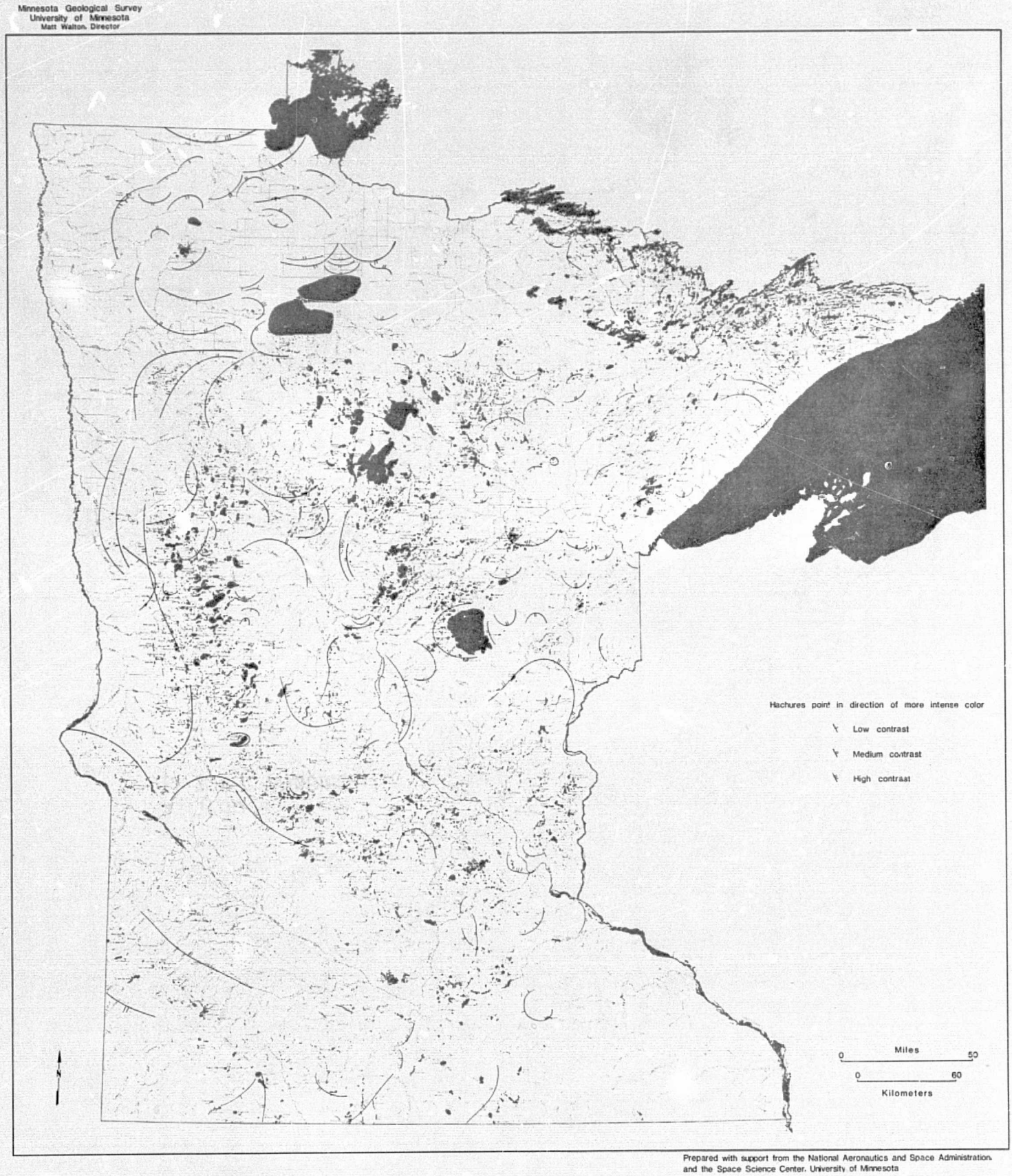

Figure 18: Preliminary curvilinear contacts between physiographic areas on winter LANDSAT imagery.

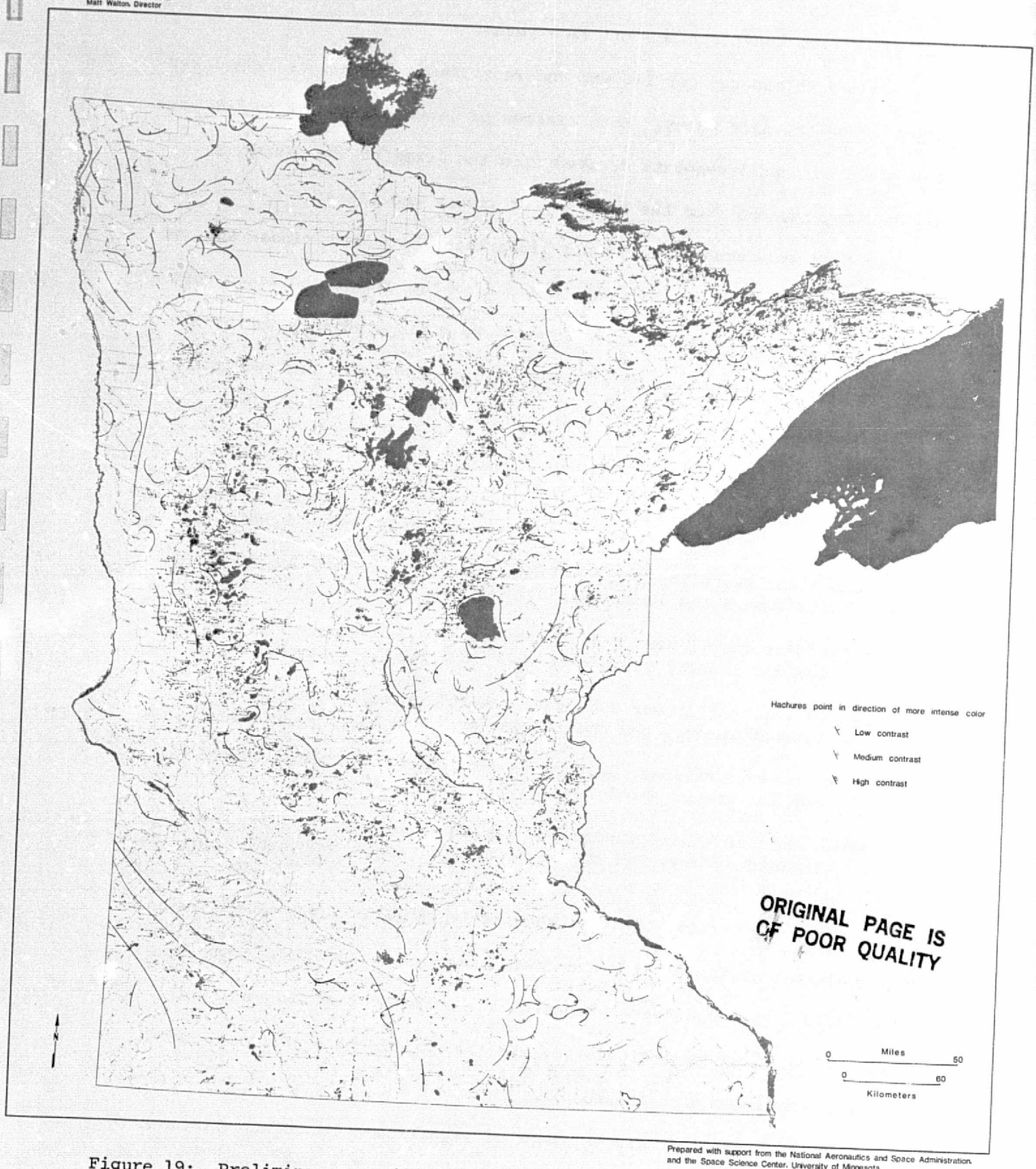

Figure 19: Preliminary curvilinear contacts between physiographic areas on spring LANDSAT imagery.

tilinears from tonal stripes and vice versa.

We had to map the curvilinear and rectilinear lineaments from lakes together on the same sheet. Both classes of lineaments occur on the same map of coincident lineaments derived from the lakes on the winter or spring imagery, and from the base map of rivers and lakes.

We then generated a map of all lineaments, both curvilinear and rectilinear, that coincided with any others from the rivers and lakes base and the 50 foot topographic contour map. We designated this map as the base map for the selection of all significant lineaments derived from LANDSAT imagery.

The following is a list of maps showing coincident lineaments.

Coincident rectilinear and curvilinear lineaments from the rivers and lakes base map and the 50-foot topographic contours, Figure 20.

Coincident rectilinear river lineaments from LANDSAT imagery and the rivers and lakes base, Figure 21.

Coincident rectilinear contacts between physiographic areas from LANDSAT imagery and the 50-foot topographic contours Figure 22.

Coincident rectilinear and curvilinear lineaments from lakes on LANDSAT imagery and the rivers and lakes base, Figure 23.

Coincident curvilinear lineaments from rivers on LANDSAT imagery and the rivers and lakes base, Figure 24.

Coincident curvilinear contacts between physiographic areas on LANDSAT imagery and the 50-foot topographic contours, Figure 25.

After we generated the maps showing this first level of coincidence, we combined them to identify and draft the significant coincident lineaments. Two maps, were prepared--the coincident significant rectilinear lineament map, Figure 26; and the coincident significant curvilinear lineament map, Figure 27.

Next we compared these two maps of significant coincident lineaments

Coincident Lineaments Maps

The maps in Figures 20 through 25 are composed from the preliminary lineaments maps and depict those lineaments which coincided on two or more of the independent sources of lineaments.

Minnesota Geological Survey
University of Minnesota
Matt Walton, Director

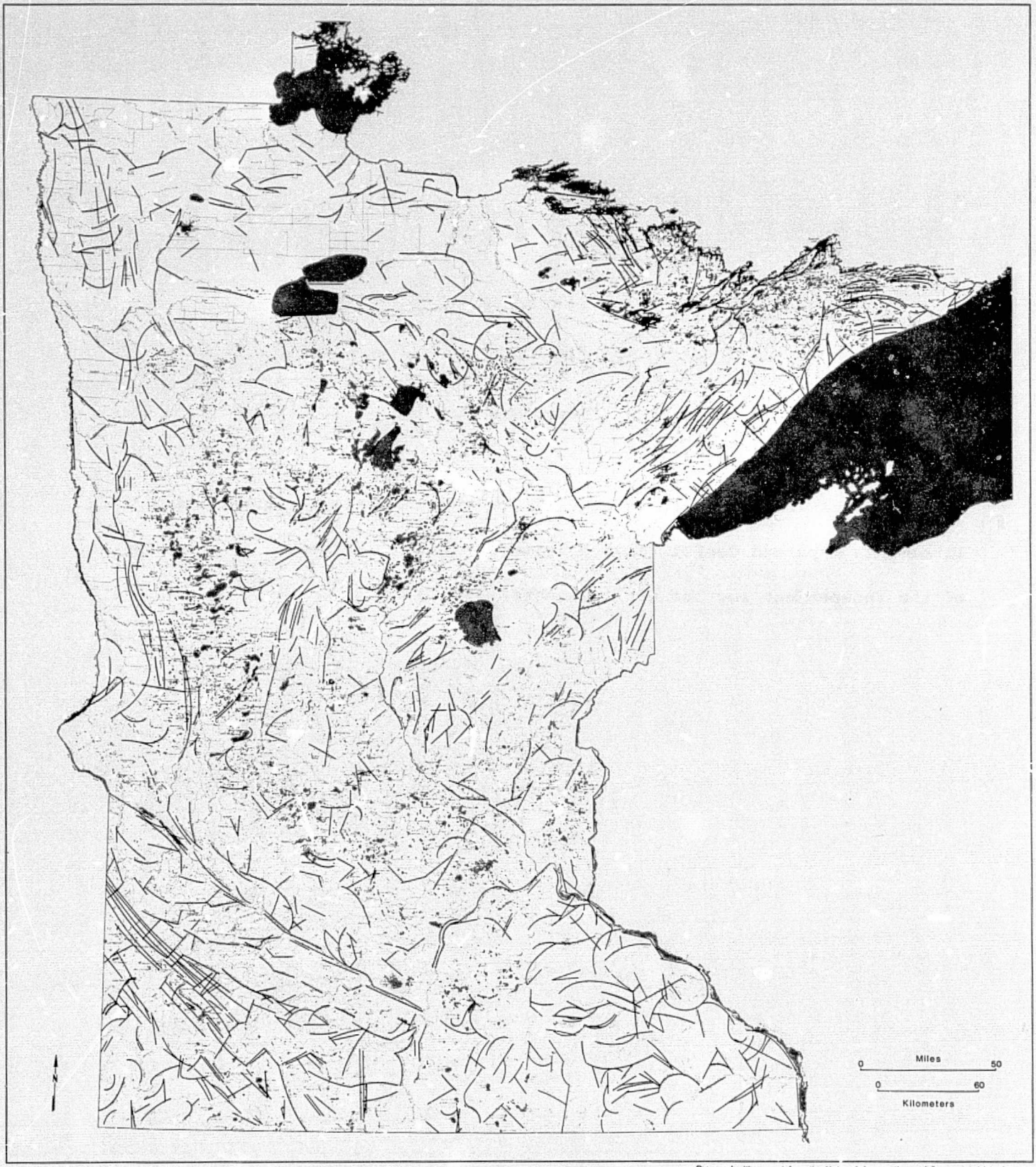

Prepared with support from the National Aeronautics and Space Administration and the Space Science Center, University of Minnesota

Figure 20: Coincident rectilinear and curvilinear lineaments between the rivers, lakes and topographic bases.

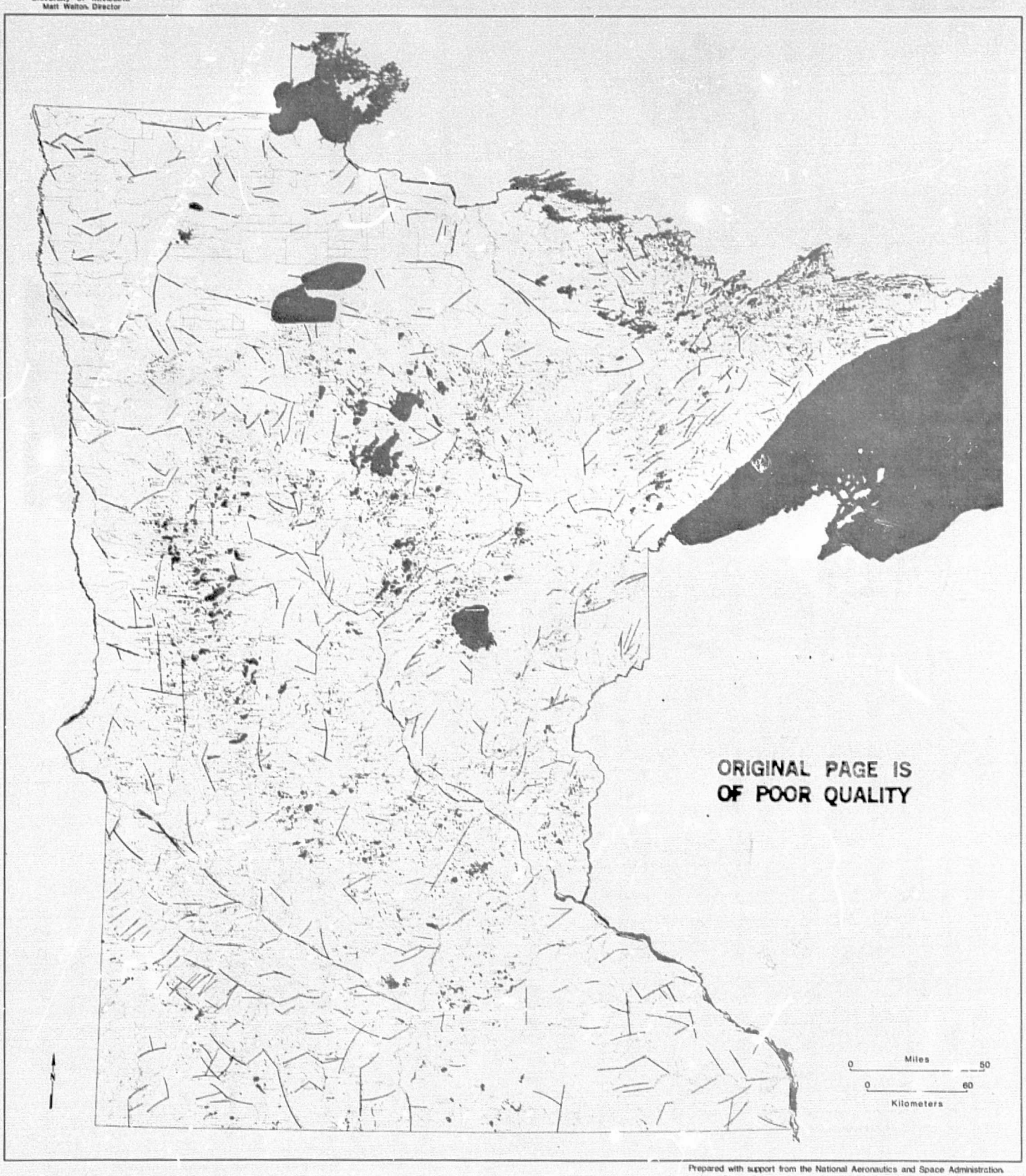

Figure 21: Coincident rectilinear river lineaments between LANDSAT imagery and the river base.

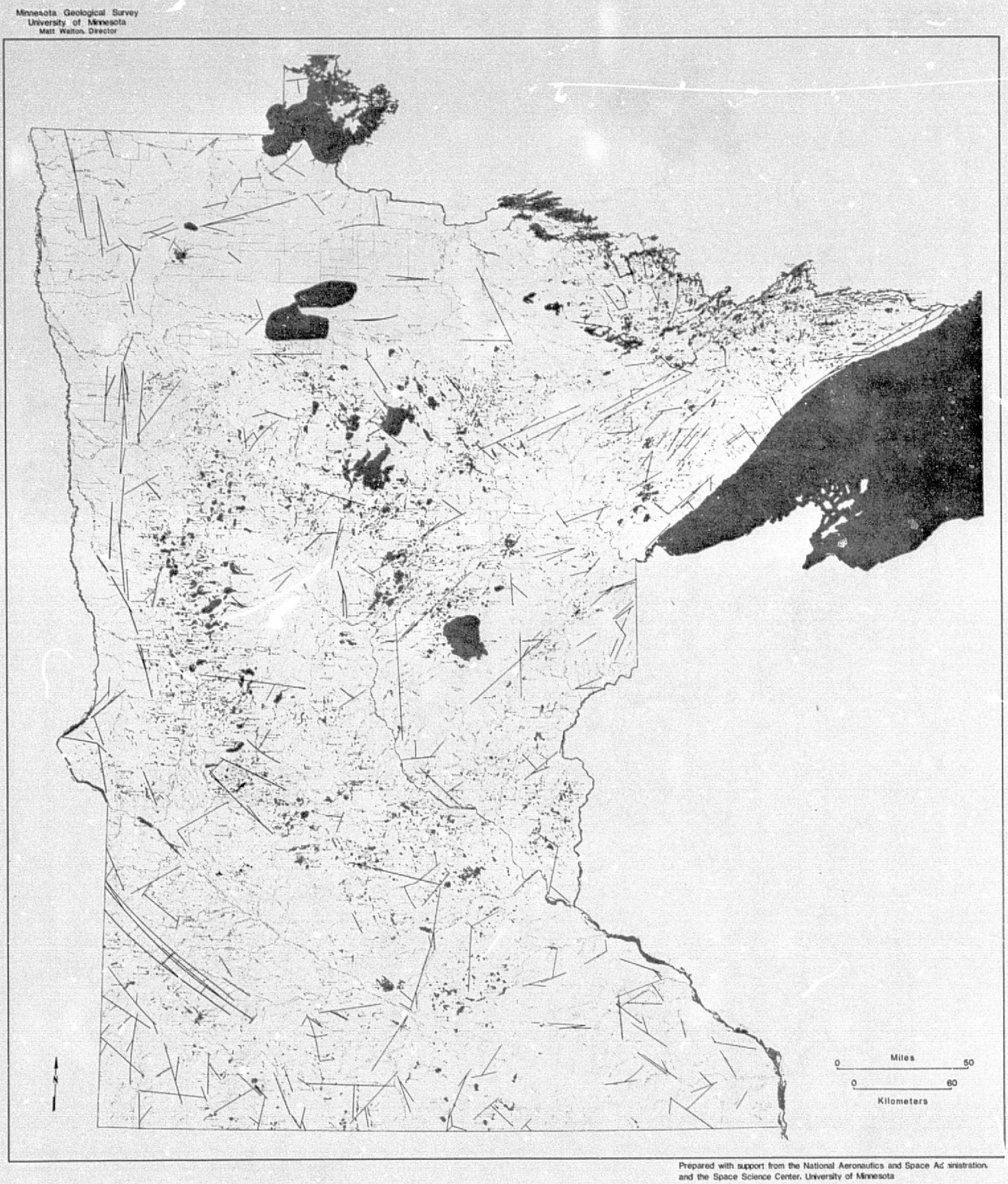

Figure 22: Coincident rectilinear contacts between physiographic areas of LANDSAT imagery and the topographic base.

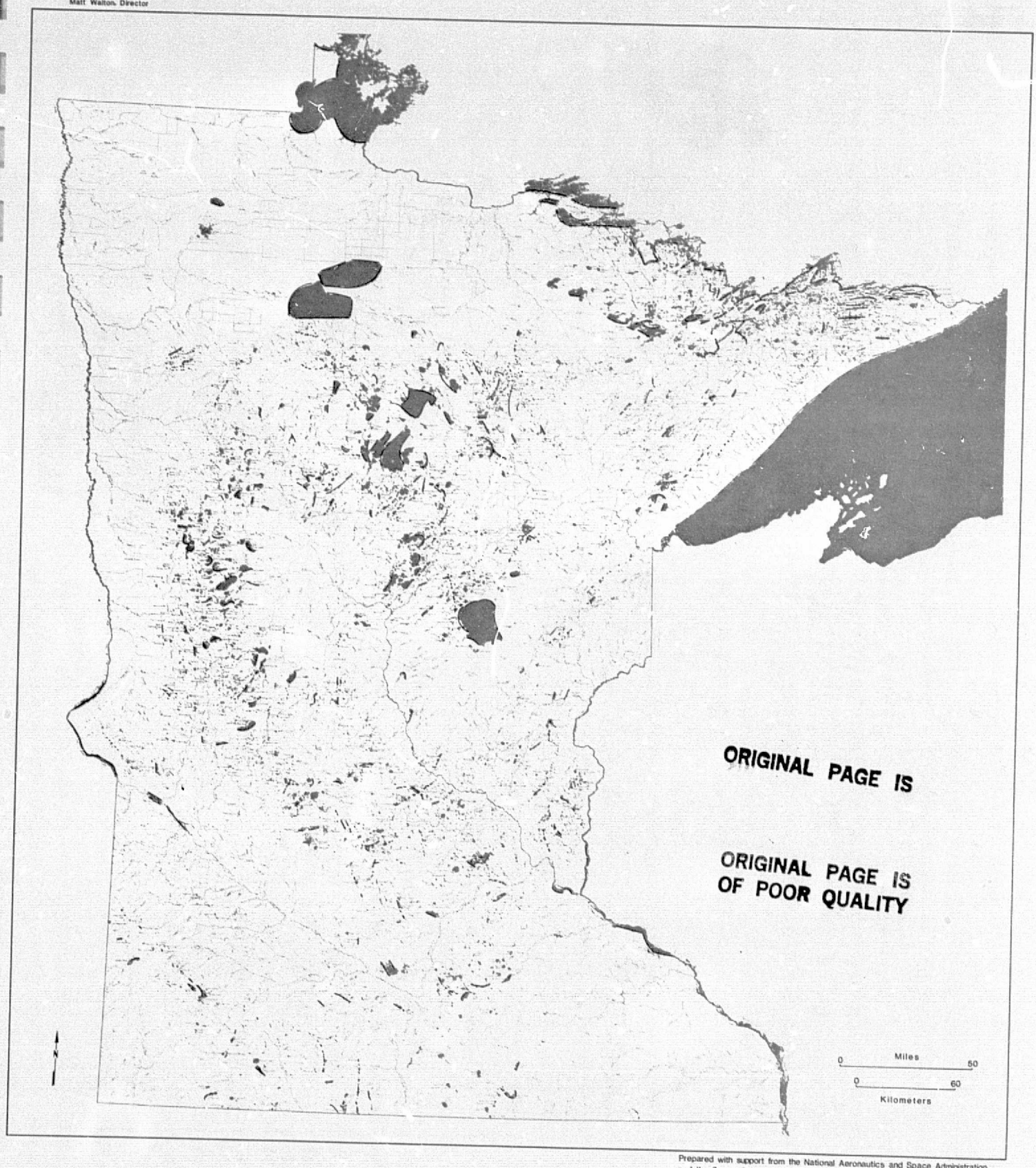

Figure 23: Coincident rectilinear and curvilinear lineaments between lakes of LANDSAT imagery and the lake base.

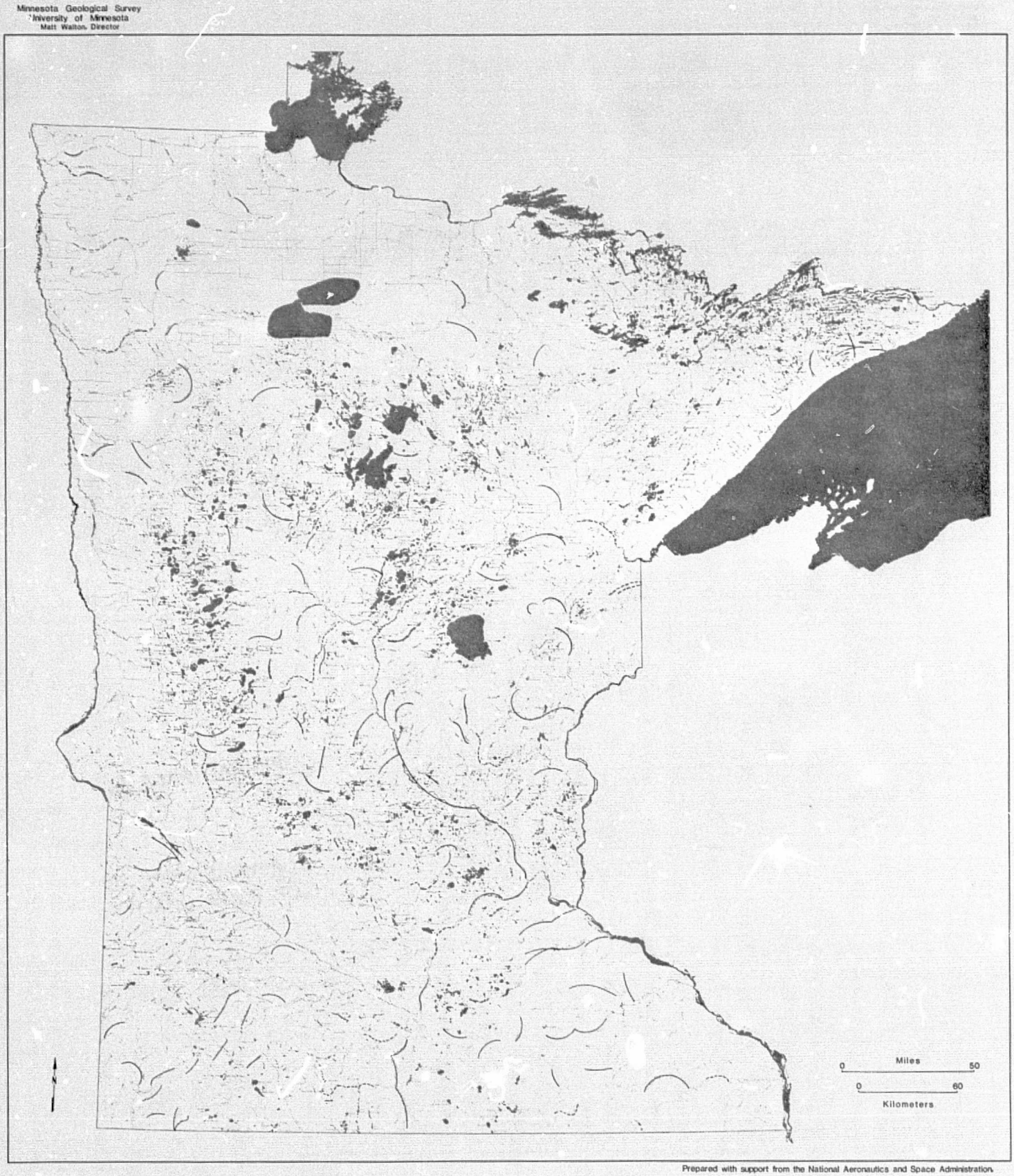

Figure 24: Coincident curvilinear lineaments from rivers on LANDSAT imagery and the rivers and lakes base.

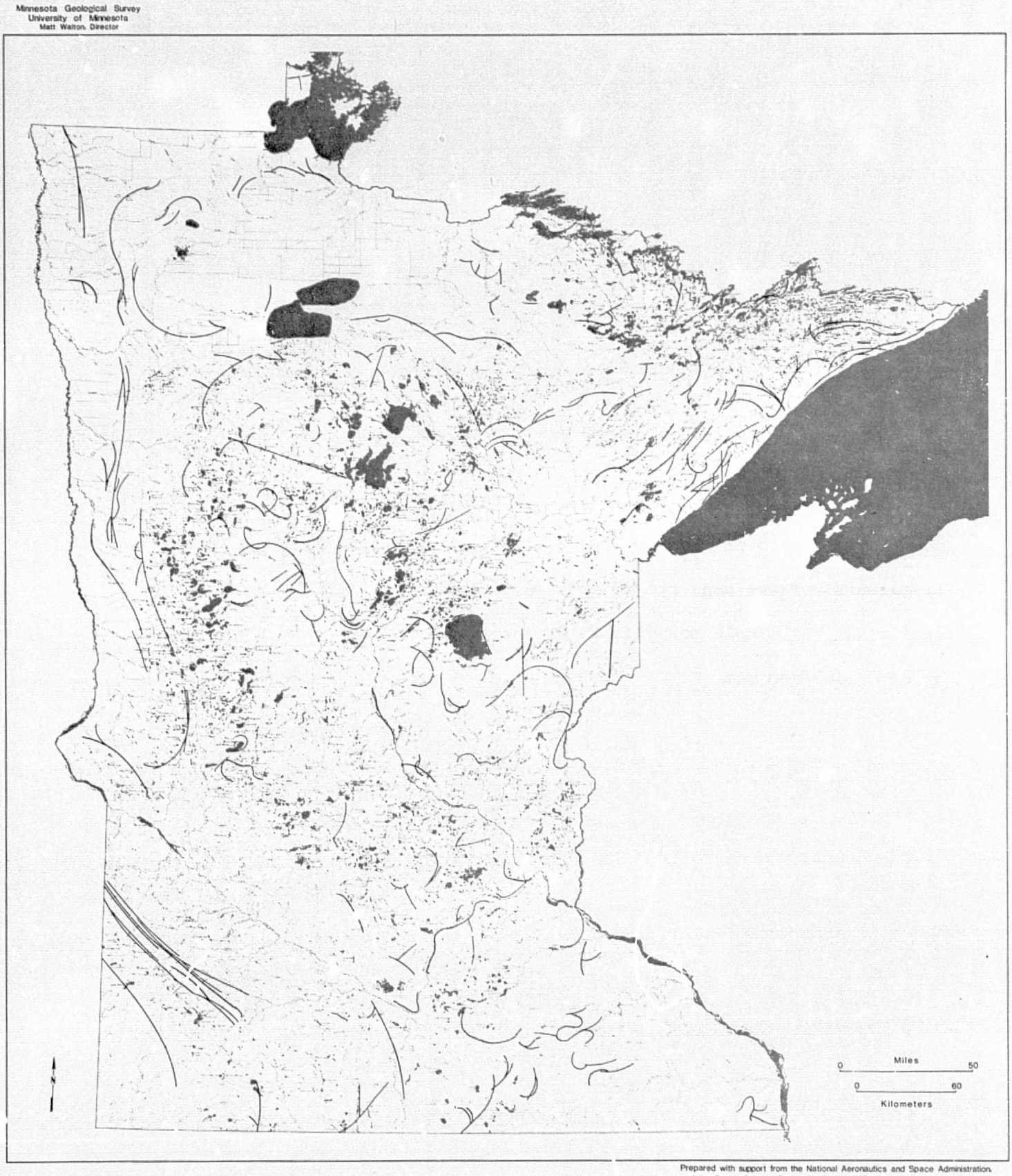

Figure 25: Coincident curvilinear contacts between physiographic areas on LANDSAT imagery and the 50-foot topographic contours.

Significant Coincident Lineaments Maps

These maps, Figures 26 and 27, were generated to show that coincident relationships between lineaments from the various sources of lineaments. These maps are considered to have more significance than the preliminary or simple coincident lineaments because they are supported by more data sources.

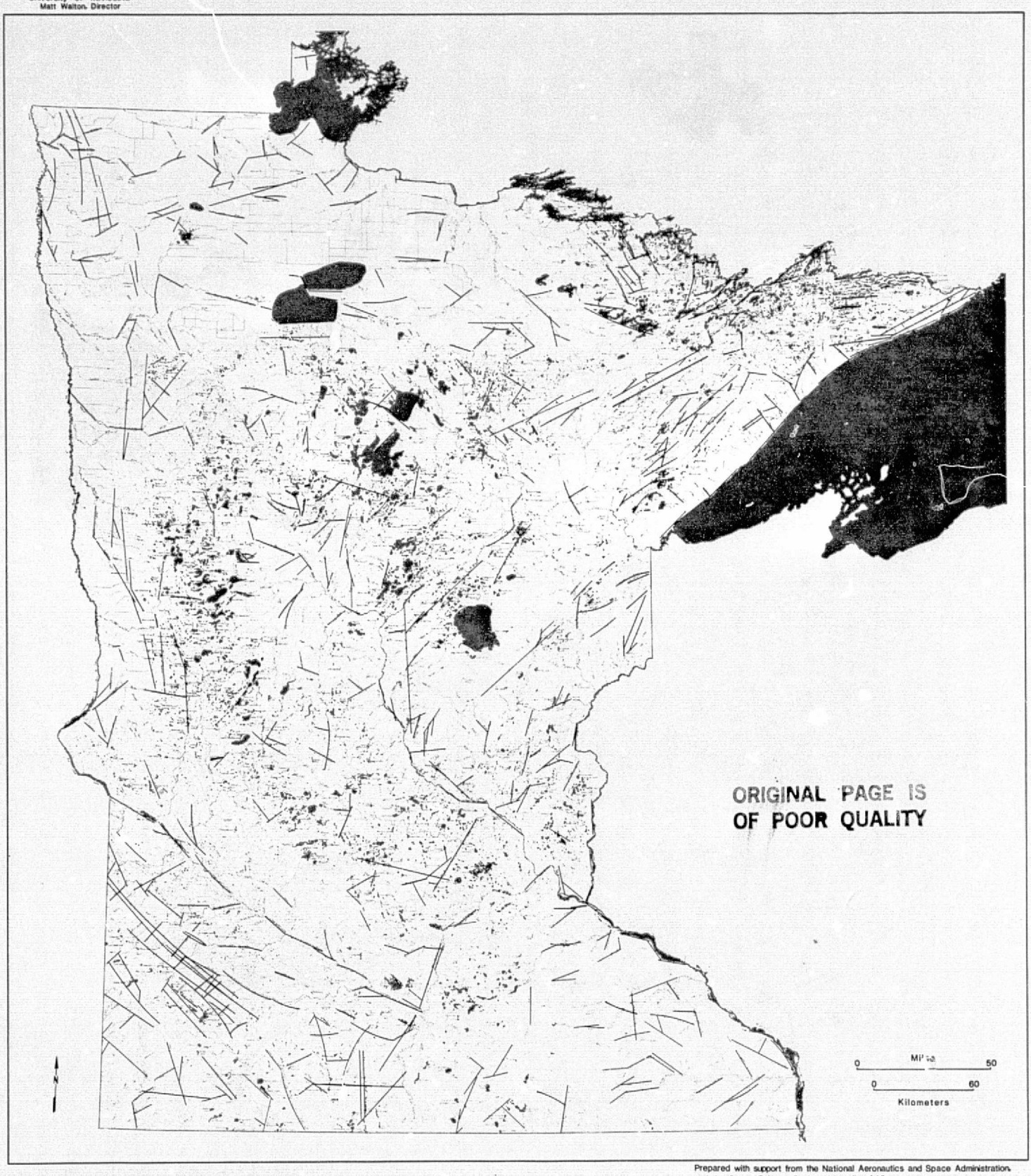

Figure 26: Significant coircident rectilinears.

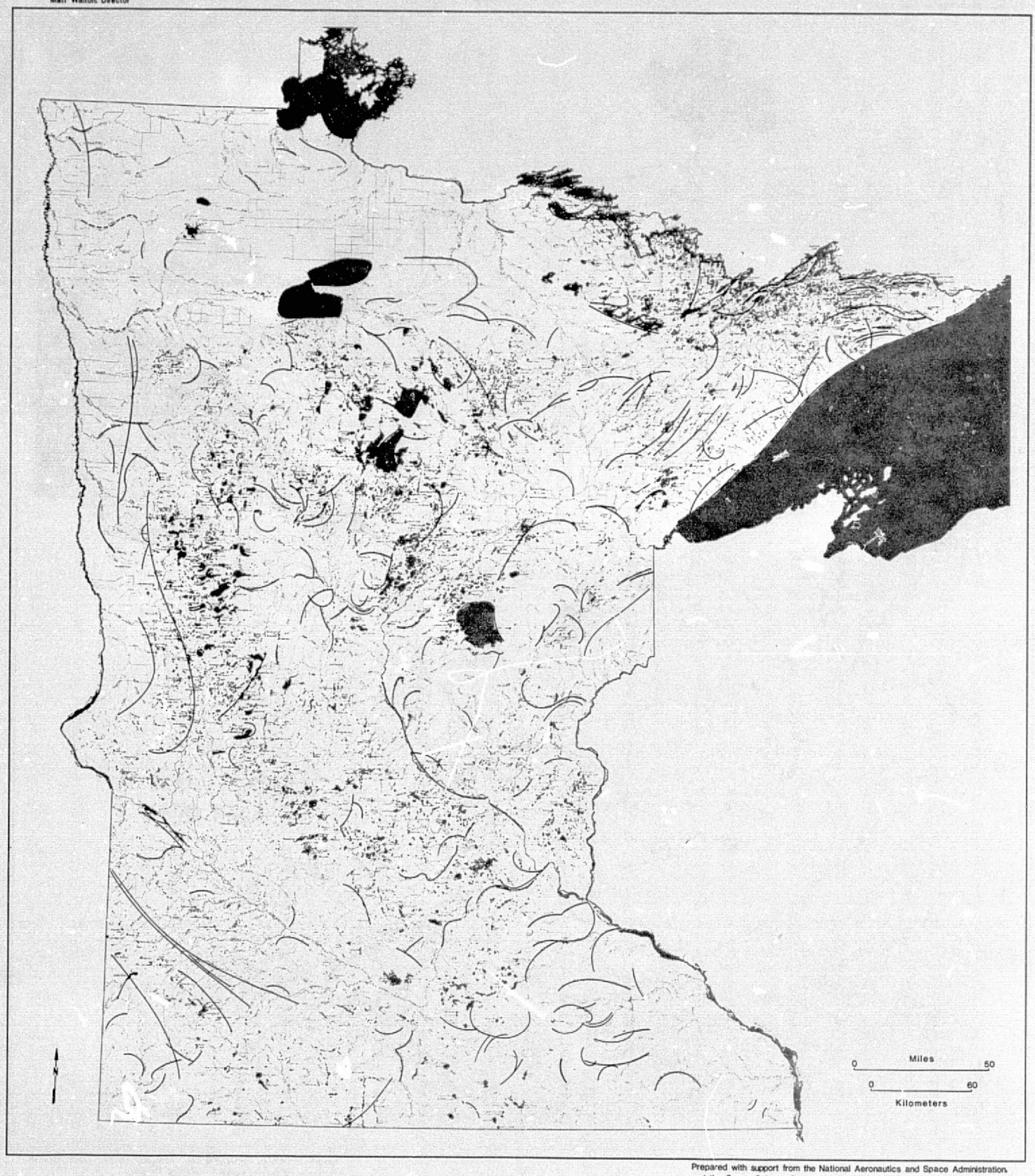

Prepared with support from the National Aeronautics and Space Administration and the Space Science Center, University of Minnesota

Figure 27: Significant coincident curvilinears.

to derive a map of lineaments that should be indicative of geologic conditions. These are the lineaments that either occurred independently on more than one preliminary map or were substantiated by abutment or parallelism with another lineament from another preliminary map. We gave this map the title of Indicative Lineaments, Figure 28.

We placed the map of indicative lineaments on each of the following maps: Quaternary geology, bedrock geology, Bouguer gravity, aeromagnetic, thickness of unconsolidated sediments, bedrock topography and faults with buried valleys. The combined maps will become more useful as geologists who are familiar with each subject evaluate the relationships between the lineaments shown and geologic conditions.

Results

This study resulted in an inventory of lineaments of Minnesota from several data sources. We recorded the lineaments on maps which sequentially displayed synergistic relationships between lineaments from each of the data sets. We isolated those lineaments with the most support based on the comparison of various data bases. We then displayed those lineaments which were probably the most indicative of geologic conditions in Minnesota on geologic maps of the conditions that may be causally related to the lineaments.

Discussion

The lineaments identified in this study are real features, such as slopes and channels, but their geologic significance remains to be evaluated in light of drilling data, outcrops and investigative geologic techniques. The Minnesota Geological Survey will find all of the

Indicative Lineaments Map

Figure 28 shows both the curvilinear and rectilinear lineaments that were supported by lineaments identified on all other independent lineament sources. It is a composite of Figures 26 and 27.

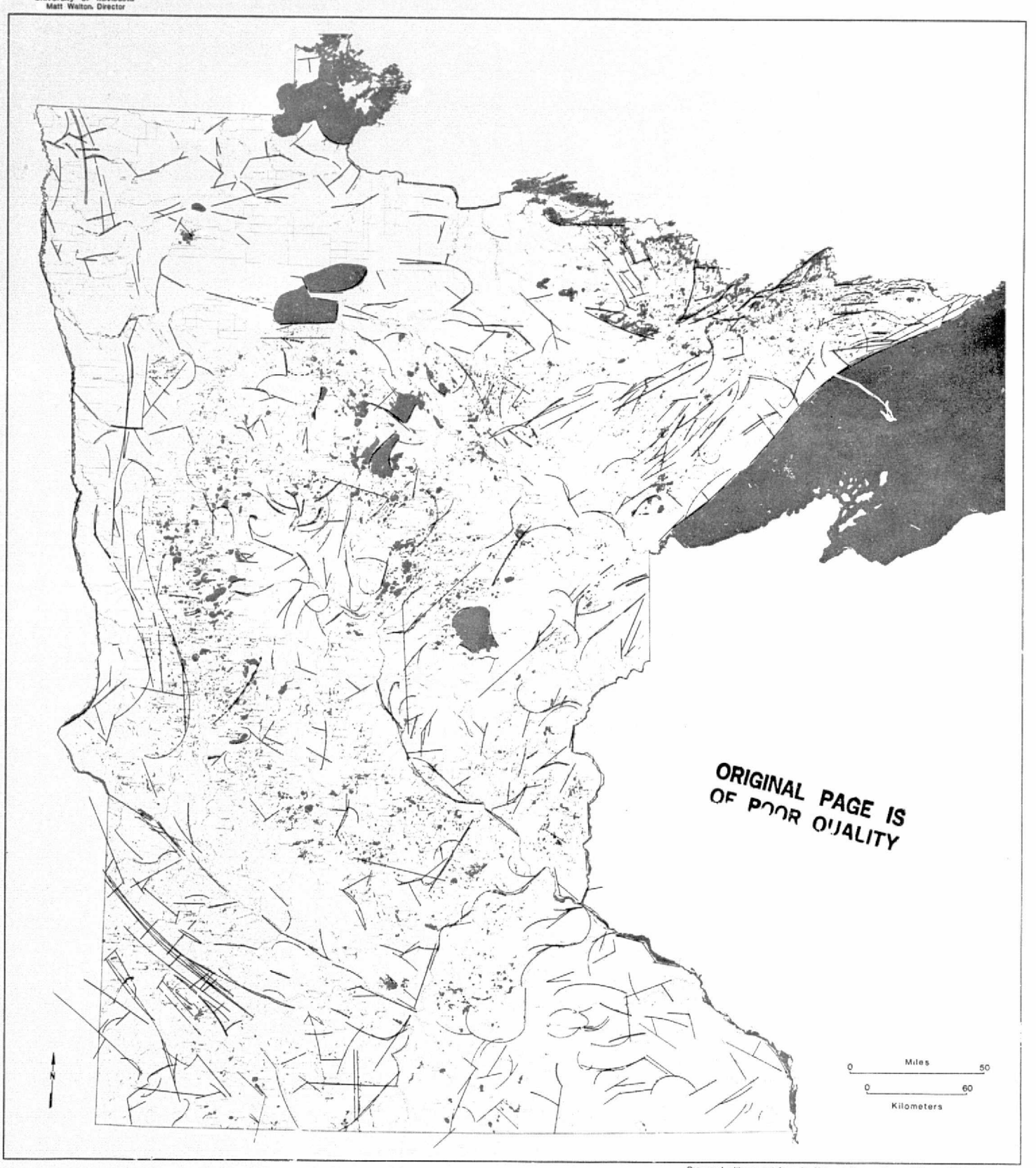

Figure 28: Indicative lineaments.

Maps of Indicative Lineaments and Geologic Conditions

Figures 29 through 35 show Figure 28 superimposed on geologic, aeromagnetic and gravity maps of Minnesota. The maps have been placed in order from highest to lowest probability for association between lineaments and geologic conditions.

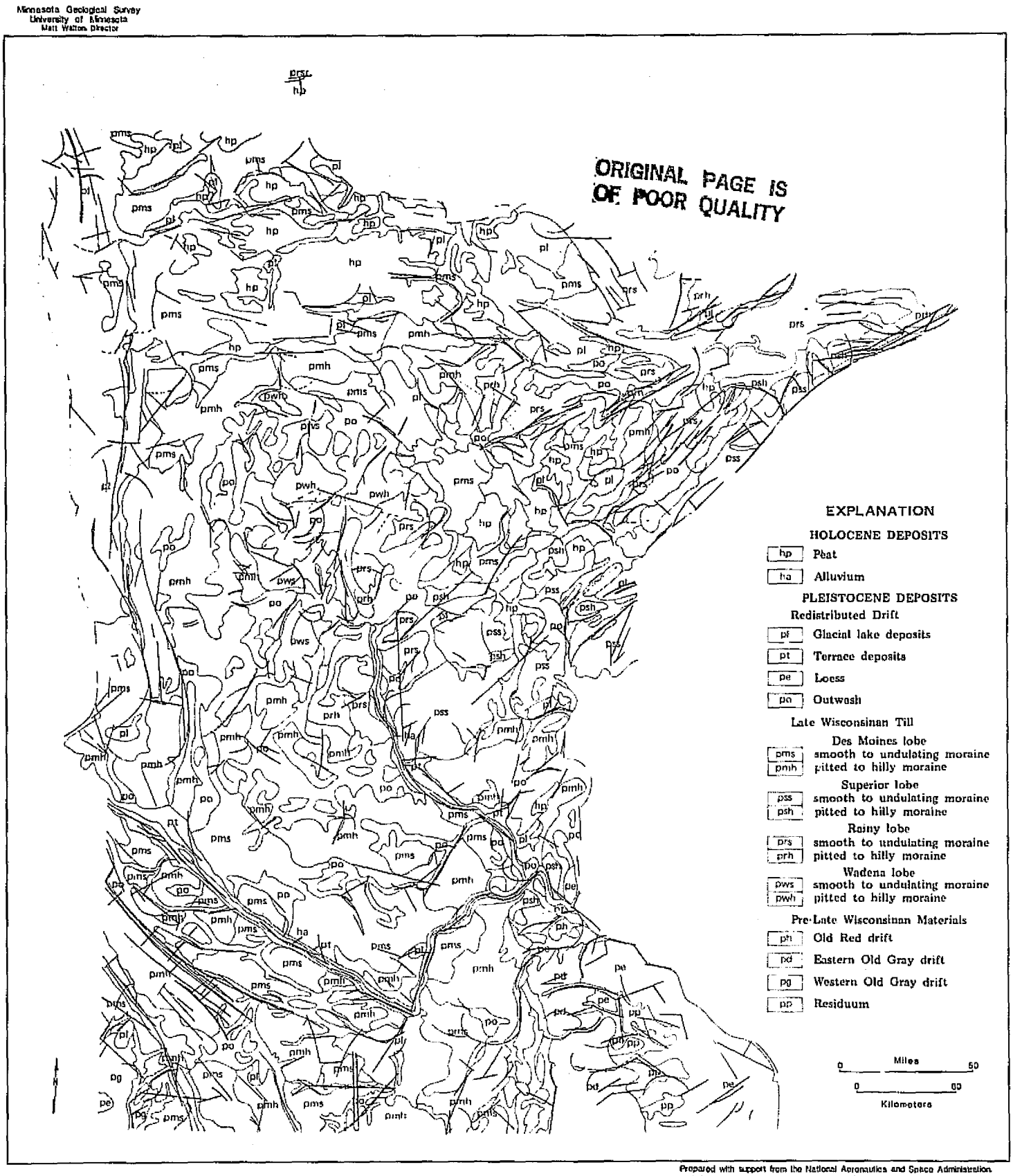

Figure 29: Indicative lineaments superimposed on the Quaternary Geologic map of Minnesota.

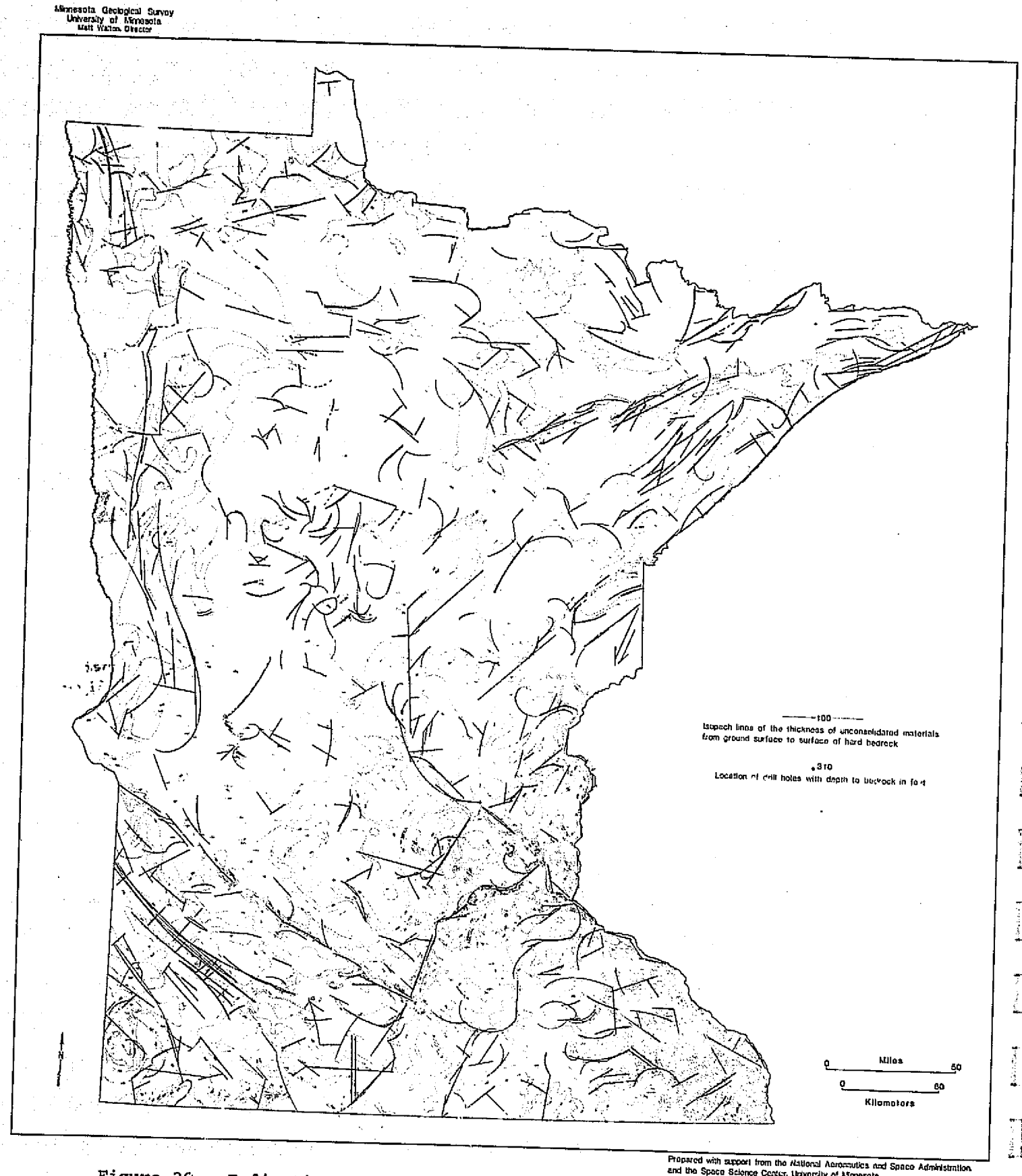

Figure 30: Indicative lineaments superimposed on the Minnesota isopach map of the thickness of unconsolidated sediments.

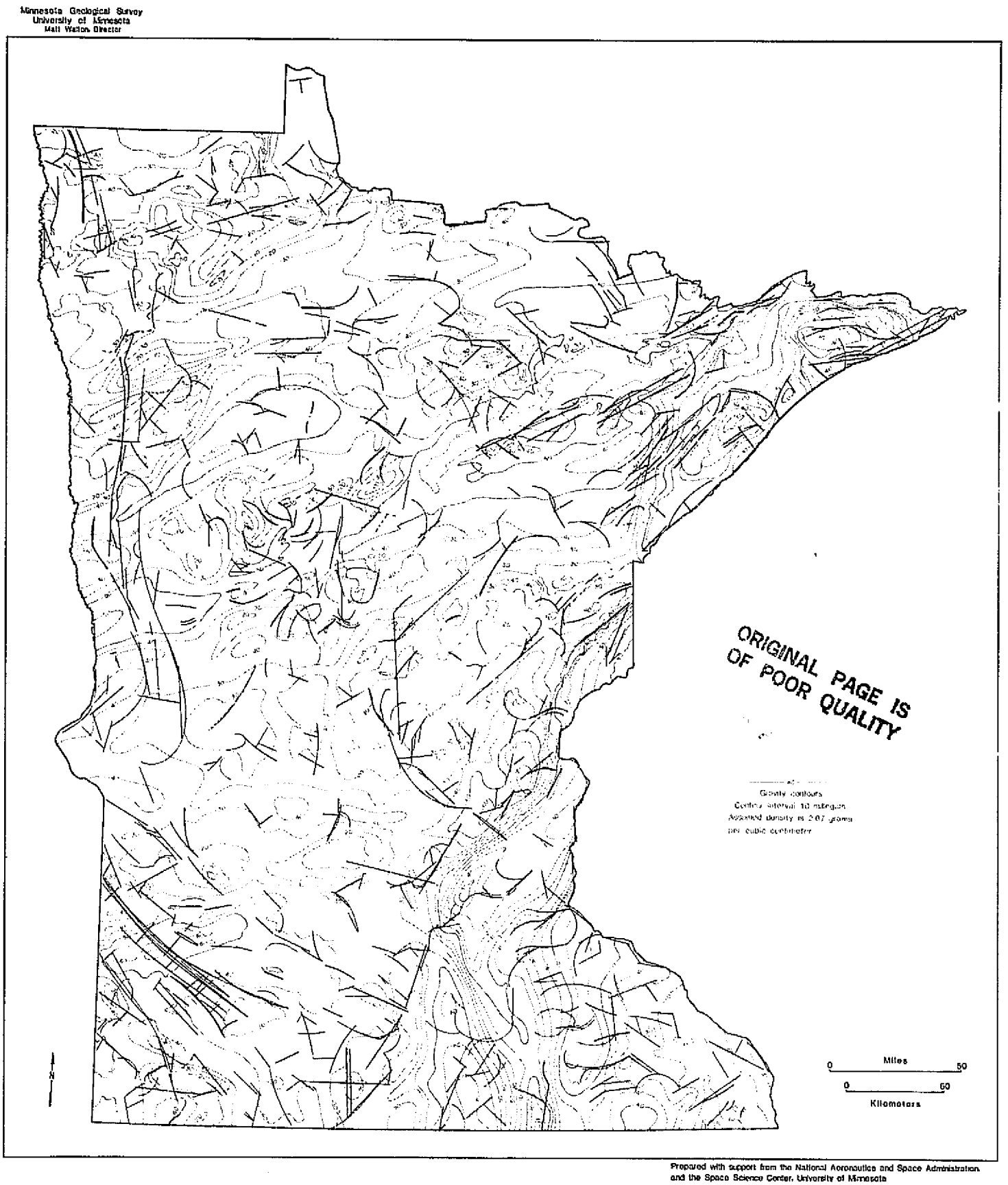

Figure 31: Indicative lineaments superimposed on the Bouguer Gravity map of Minnesota.

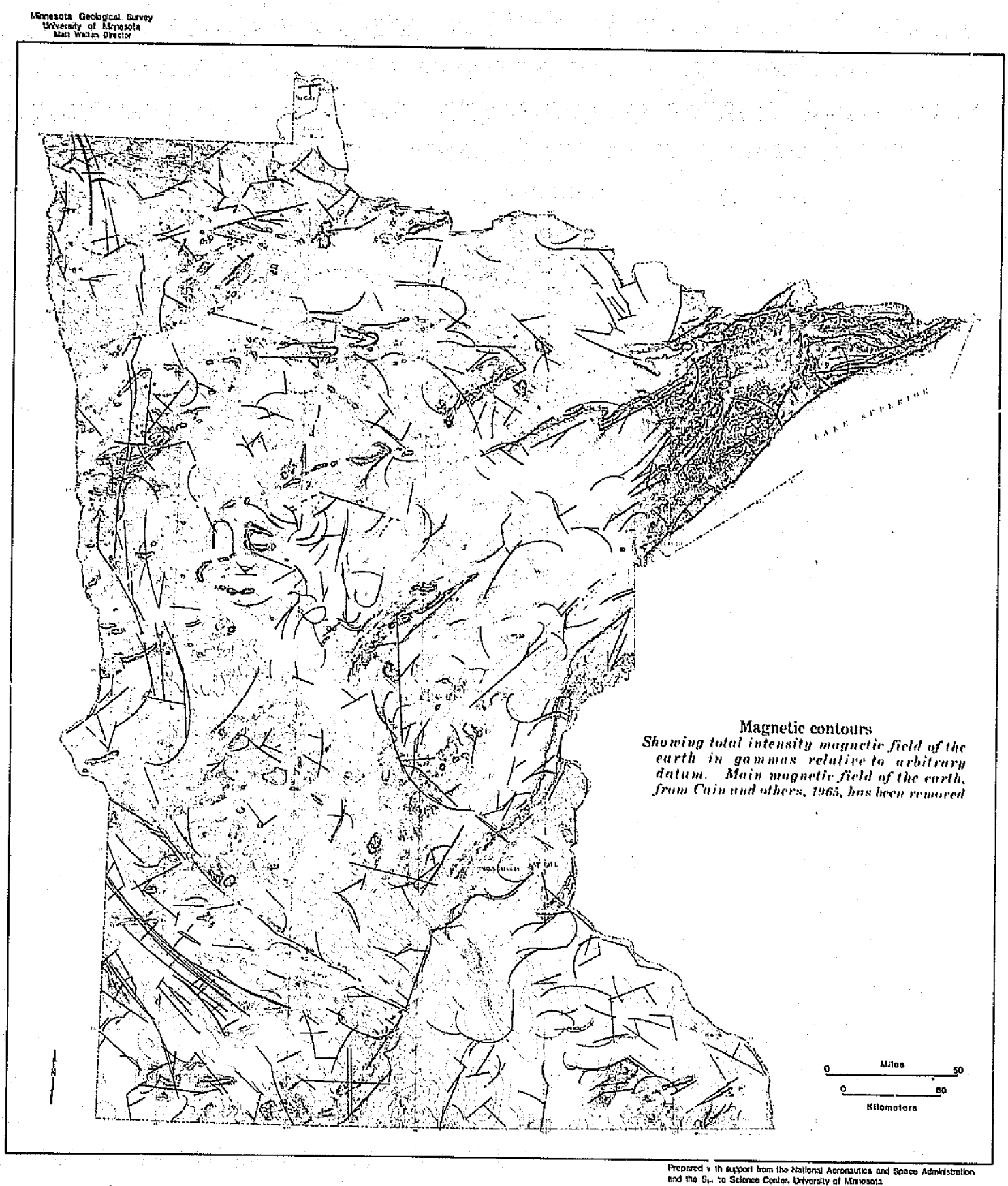

Figure 32: Indicative lineaments superimposed on the Aeromagnetic map of Minnesota.

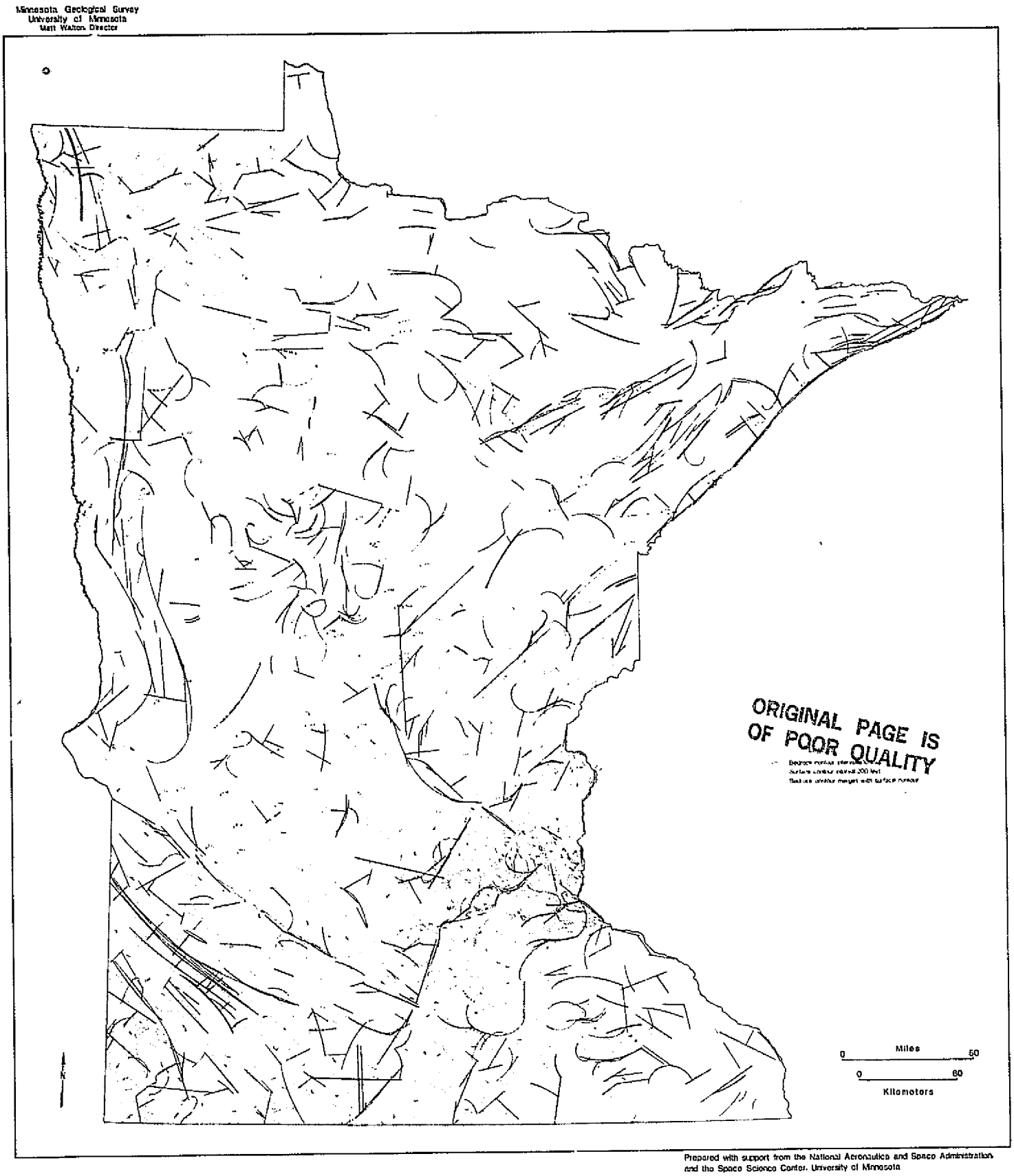

Figure 33: Indicative lineaments superimposed on the Minnesota map of bedrock topography.

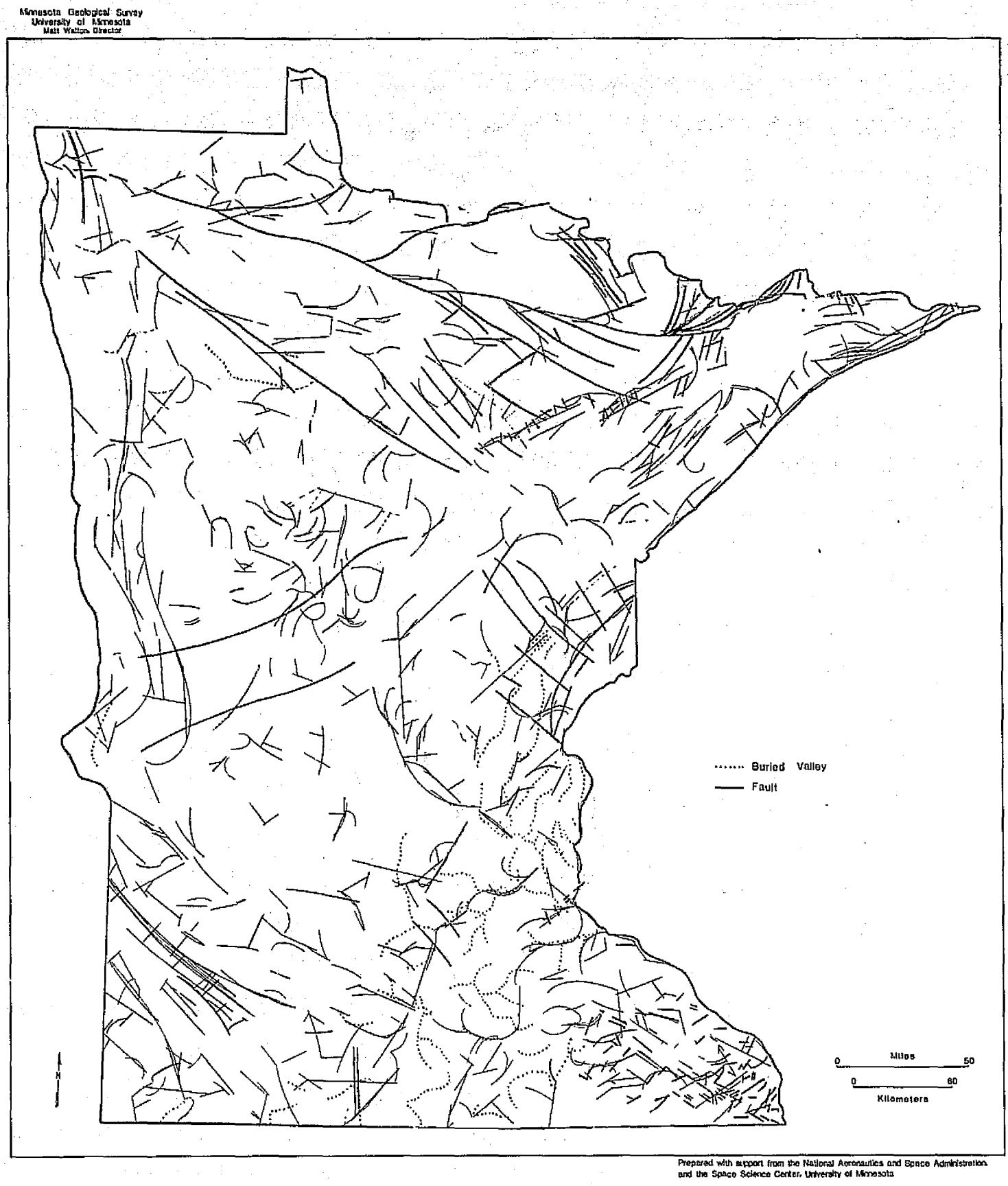

Figure 34: Indicative lineaments superimposed on the map of recognized faults and buried valleys in Minnesota.

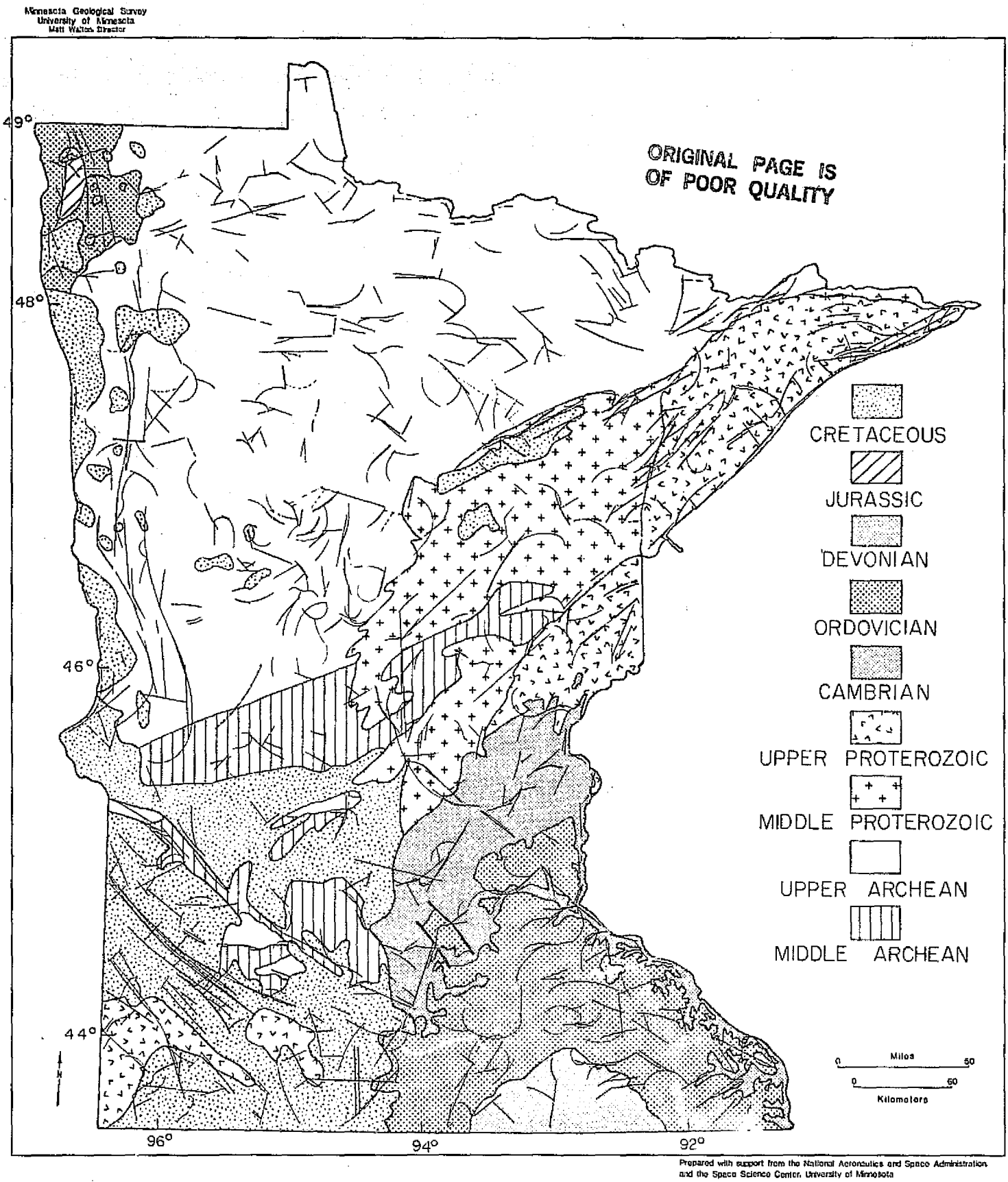

Figure 35: Indicative lineaments superimposed on the Bedrock Geologic map of Minnesota.

lineaments useful in gathering and interpreting data about the geology of the state. When the pattern of interdependence between geologic parameters and the "indicative" lineaments is established, it would be useful to review the preliminary lineaments for similar patterns.

LITERATURE CITED

Goebel, J.E., 1978, Geologic map of Minnesota, Quaternary Geology: Minnesota Geological Survey, SM-4, 1:3,168,000.

Ikola, R.J., 1969, Simple Bouguer gravity map of Minnesota: Minnesota Geological Survey, M-9, 1:250,000.

Morey, G.B., 1976, Geologic map or Minnesota, Bedrock geology: Minnesota Geological Survey, M-24, 1:3,168,000.

Olsen, B.M., 1976, Bedrock topography of Minnesota: Minnesota Geological Survey file map, 1:500,000.

Seitz, I., and Kirby, J.R., 1970, Aeromagnetic map of Minnesota: United States Geological Survey, GP-725, 1:1,000,000.

SECTION D

DETERMINATION OF DETECTABILITY LIMITS IN LAKE SUPERIOR THROUGH THE USE OF LANDSAT DATA

Dr. Michael Sydor
Physics Department
University of Minnesota
Duluth, Minnesota

o

INDEX

Budget of Particulate Matter in Lake Superior..... D1
Literature Cited..... D12

APPENDIX: ANALYSIS OF SUSPENDED SOLIDS BY SINGLE PARTICULATE SCATTERING

Abstract..... D13
Introduction..... D13
Apparatus..... D14
Analysis Method..... D16
Quantitative Fiber Identification..... D23
Figure Captions..... D31
Literature Cited..... D32

o

DETERMINATION OF DETECTABILITY LIMITS IN LAKE SUPERIOR THROUGH THE USE OF LANDSAT DATA

Investigator: Dr. Michael Sydor
Physics Department
University of Minnesota, Duluth

BUDGET OF PARTICULATE MATTER IN LAKE SUPERIOR

Our investigations over the last two summers have been generally directed at a determination of threshold detectibility levels for suspended solids in lakes and the establishment of turbidity reference zones for Lake Superior. The studies were meant to provide preliminary information necessary for the use of LANDSAT data in a determination of the lakewide long term particulate budget.

The need for understanding long term dissipation and budget of particulates in lakes is quite critical. Bierman and Swain (1978) point out that the actual retention times in the Great Lakes for DDT are far shorter than the times previously determined on the basis of the compound's half life. The chief reason for the rapid removal of DDT in the Great Lakes appears to be associated with particulate settling rates. This is not surprising since the association of particulates with contaminant and nutrient concentrations in lakes was reported in studies of the red clay in the extreme western Lake Superior where it has been found that the red clay particles have the ability to scavenge pollutants out of the water column (Bahnick, 1975).

The determination of the concentration levels of organic and inorganic particulates is in general important in the assessment of water

quality and productivity of lakes. It is thus constructive, for resource management purposes, to devise accurate ways for determining the long term balance of particulate matter for the lakes. Numerical modeling of the lakes, backed by remote sensing data to ensure realistic results, is really the only feasible means of addressing the problem in large scale systems such as the Great Lakes and the seacoast. However, before remote sensing data can be utilized effectively, it is necessary to calibrate and interpret the remote sensing data properly. We have shown previously that determinations of suspended loads in clean lakes or in oceans require the establishment of the true background turbidity for an entire system so that the intensity levels above the background in satellite data for any area can be properly correlated with the concentration of the suspended solids above the general background (Sydor, 1978). Small discrepancies in background can produce substantial changes in the estimated contaminant loads. On the other hand, subtle changes in background may provide significant information on the particulate budget balance. This can be seen from our results for the past two summers.

During the Lake Superior cruises (summers of 1977, 1978), turbidity levels for the lake were determined and are shown in Figure 1. The high values near the shores are a consequence of turbidity sources in these areas. The midlake values represent the results of repeated sampling obtained during successive summer cruises and are, therefore, believed to represent true background turbidity levels. It can be seen that this background turbidity decreases from west to east. The difference between the turbidity backgrounds of the western and eastern halves of the lake appears to be persistent and is significant, since it is related to the residual annual input of fine particulates into Lake Superior by the

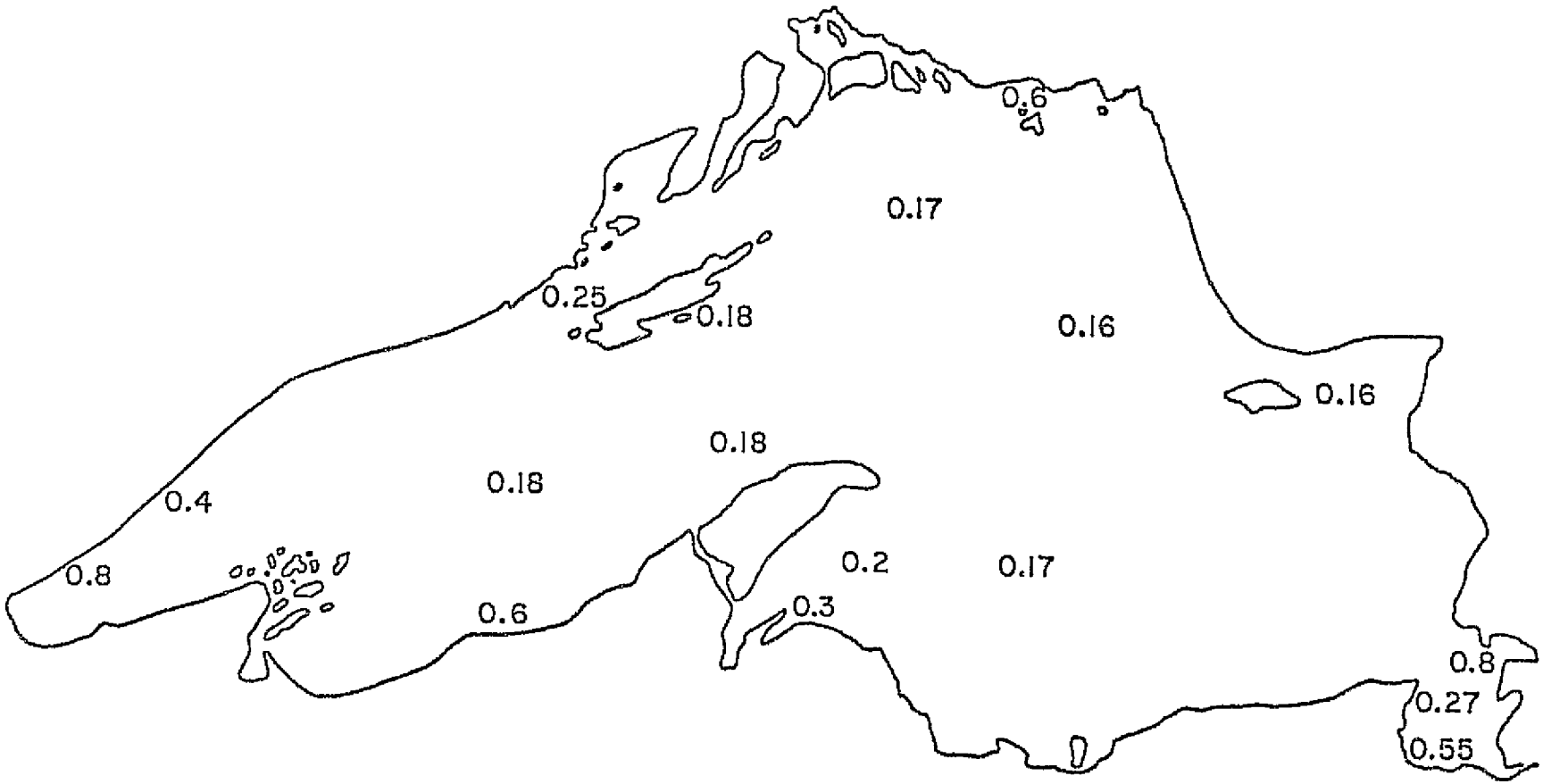

Figure 1. Lake Superior Turbidity (NTU).

turbidity sources in the western half of the lake. The background suspended load in Lake Superior thus appears to have a steady state gradient directed from west to east. The relationship of this background to the residence time for particulates in the lake is a crucial question in studies of particulate budget.

In addition to the determination of the background turbidity levels in the lake, the study of the long term approach to a particulate balance requires the establishment of turbidity reference levels at various points around the lake which can be used to check turbidity calibration curves. Areas useful in establishing these reference levels are found in certain embayments which have broad, reasonably stable suspended loads near the threshold levels. Jackfish Bay, Huron Bay, and Batchawana Bay usually provide good reference areas for Lake Superior. The average suspended loads for several Lake Superior embayments, together with some typical water quality parameters, are shown in Table 1.

Although we have begun addressing some of the basic problems in the threshold for the detectability of suspended solids from LANDSAT observations, much further work is needed before these observations can be applied to an entire lake. Our previous studies have, in general, dealt with problems concerning specific meteorological events. Such investigations examined the onset of turbidity and the transport of turbidity as a function of winds and precipitation. We have shown, for instance (Sydor 1976), that a statistical analysis of LANDSAT data provides the most accurate determination of fine particulate input into large bodies of water, and that remote sensing of the near shore turbidity provides an accurate method for the determination of bank erosion. (The method hinges on the treatment of the shoreline as an ensemble of sources,

which under action of waves and currents contribute to the general turbidity of the near shore zone).

Our present endeavor, the discussion of a long term budget for particulate matter in large water bodies, deals with the dispersal of turbidity as the steady state is approached; that is, the dispersal of turbidity at times long after the effect of an individual meteorological event is discernible. The steady state problem requires, as ground truth information, the backscattering of light by particulates in low concentrations where the origin of the particulates can no longer be traced to specific plumes. Also required is a much more detailed knowledge of the composition of samples in terms of their optical properties, so that threshold detectibility levels from remote sensing can be related to the steady state concentration levels of various species of particulates in the lake. Such detailed information was not needed when working with plumes, where easily measureable parameters such as conductivity and percent volatiles could give a reasonable estimate of the contribution to turbidity due to a particular source or effluent. The methods used for plume studies are not suitable for lakewide studies because of considerations for logistics and cost. Since the steady state problem relates to the overall lake conditions, it is generally necessary to examine a large number of samples. The usual low concentrations of suspended solids in open lake areas also require that the samples be large enough to ensure sufficient quantities for analysis. The usual chemical and electron microscopy methods required for sample analysis are expensive, making costs prohibitive for lakewide studies. Furthermore, chemical analysis is not really appropriate at these low concentrations since the relationship of chemical parameters to the scattered light is statis-

Table 1. Lake Superior Embayments

Location	Sulfate mg/ℓ	Chloride mg/ℓ	Silica mg/ℓ	Total Phosphorous-µg/ℓ	Suspended Solids mg/ℓ
Batchawana	2.9	2.4	1.9	9.0	0.8
	3.0	1.0	1.9	5.8	1.3
	2.9	1.1	2.0	7.0	1.7
	2.8	0.9	1.7	4.5	
	3.2	1.3	1.9	5.0	1.2
Ontonagon	4.8	1.8	7.5	126	
	2.9	2.1	3.2	38.2	
	3.0	1.8	2.5	14.5	2.8
	2.8	2.0	2.1	10.0	1.3
	2.6	1.8	2.4	9.5	1.6
	2.7	1.8	2.0	6.0	0.9
					0.5
Jackfish Bay	2.9		2.7	6.5	0.7
	3.0	2.5	2.4	3.3	0.5
	3.8		2.4	6.5	0.9
					1.8
Whitefish Bay	2.8	1.3	2.4	2.6	0.6
	2.7	5.3	2.1	4.0	
	3.0	2.5	2.2	3.4	0.5
	24.0	3.5	2.3	20.5	1.7
	5.4		2.9	8.0	1.4
Huron Bay	3.0	1.5	2.4	7.2	1.0
	2.6	1.5	2.4	6.1	0.7
					1.0
					0.6
					0.7
	2.8	2.1	1.4	6.5	0.7

Table 1. (continued)

Location	Sulfate mg/ℓ	Chloride mg/ℓ	Silica mg/ℓ	Total Phosphorous-µg/ℓ	Suspended Solids mg/ℓ
			2.4		<0.5
					<0.5
			2.4	2.5	
			2.4	2.6	
Michipicoten					<0.5
Thunder Bay			2.6		0.5
			2.6		0.7
			2.6		0.8
			2.6		0.7
			2.6		0.7
			2.7		0.9
			2.6		0.7
			2.6		0.7
			2.6		0.4
			2.6		0.5
			2.6		0.5
			2.6		0.6
			2.7		0.6
			2.6		0.6
			2.6		0.8
			2.6		0.9
			2.7		0.9
			2.8		0.9
			2.8		3.3
			2.6		0.8
			2.7		0.8
			2.6		0.6
			2.7		0.6
			2.6		
			2.8		

Table 1. (continued)

Location	Sulfate mg/ℓ	Chloride mg/ℓ	Silica mg/ℓ	Total Phosphorous-µg/ℓ	Suspended Solids mg/ℓ
Black Bay*			2.9		2.7
			2.8		2.7
			3.2		2.5
			3.1		1.8
			2.9		3.1
			2.8		3.6
			3.1		4.0
			3.1		4.3

*Black Bay is susceptible to resuspension and as such constitues together with western Lake Superior an interesting system for satellite studies of resuspension due to waves versus resuspension due to currents. This problem is of paramount importance in Lake Erie. But Lake Erie does not have places where the effects can be clearly separated.

tically uncertain and time dependent. Electron microscopy, on the other hand, suffers from statistical uncertainties because of sample preparation and the time required to count statistically meaningful numbers of particles for a determination of the concentrations of various species of particulates.

In order to overcome these difficulties, we have developed a quick, inexpensive optical method for analysis of ground truth data on suspended solids. The method consists of an optical categorization of turbidity samples particle by particle. In this method, particulates are identified by their light scattering pattern. A particle illuminated by a beam of light scatters photons in various directions with intensities which depend on the size of a particle, its shape, its relative index of

refraction, and its orientation in the beam. The scattered light envelope is thus characteristic of the physical properties of the particle. In our apparatus individual particles drifting through a tiny volume of space are viewed simultaneously by several detectors. The set of signals from the detectors are fed into a microprocessor-computer which automatically indentifies the set of simultaneous pulses as those belonging to a specific scattering envelope characteristic of a certain species of particulates. Thus, by counting the abundance of various species of particulates, we can determine the composition of the suspended solids on a statistical basis in terms of broad optical characteristics which relate to categories such as red clay, taconite tailings, and organic fibers associated with tannin water. The apparatus is calibrated using the scattering by samples containing individual species and electron microscope data on the shape of the particulates wthin that species.

The advantage of the optical characterization of samples by this means lies in the fact that the satellite data itself consists of the information which is equivalent to the data observed in the scattering apparatus at one angle (integrated over many particles). Thus the optical scattering apparatus can be arranged to have a detector at an angle relative to the incident beam which corresponds to the angle between the incident sunlight and the light scattered to the satellite. Then the information from the detector can be directly correlated with the satellite data (i.e., the apparatus can predict for any band what fraction of the satellite signal is due to various species of background particulates). The details of the method are given in our paper entitled "Analysis of Suspended Solids by Single Particle Scattering". This paper,

which has been accepted for publication in the Journal of Applied Optics, January 1979, is appended to this report.

The method described has far reaching consequences for the remote sensing of suspended material in lakes. Thus far, we are just beginning to apply the technique to the overall study of the budget for particulates in Lake Superior.

Using laboratory results on backscattering and the information on background intensity levels over Lake Superior determined from LANDSAT observations, we were able to determine threshold detectibility levels for some species of particulates in the lake. The results for red clay are shown in Figure 2. The results indicate that the limit on detectibility of red clay by LANDSAT is 0.5 mg/l.* Thus LANDSAT observations are at the limit of usefulness for particulate budget studies of western Lake Superior, and not useful for midlake studies. LANDSAT observations can, however, provide the geometric resolution and concentration measurements necessary to establish the initial boundary conditions in studies of particulate budgets. Nimbus G data, which provide higher accuracy at low signal levels, can then be used to supply the information needed for numerical simulation of particulate dispersal as steady state conditions are approached. The essential feature of the mathematical treatment of

---

*The turbidity in NTU has been found empirically, to be linearly related to the suspended solids (s.s) for low concentrations of red clay particulates (Sydor NGL 24-005-263). That linear relation will be expected to be approximately true for other types of suspended solids in the concentrations with which we are concerned. We use the emperical relationship

$$SS.(mg/liter) = 0.9 \times NTU + 0.4$$

which has been found to be valid for concentrations of red clay particulates in the range ($0 < NTU \leq 10$) as an approximation for judging the limits of detectability for the suspended solids corresponding to the values in NTU shown in Figure 1. We thus find values for SS ranging from .528 mg/l to 1.12 mg/l.

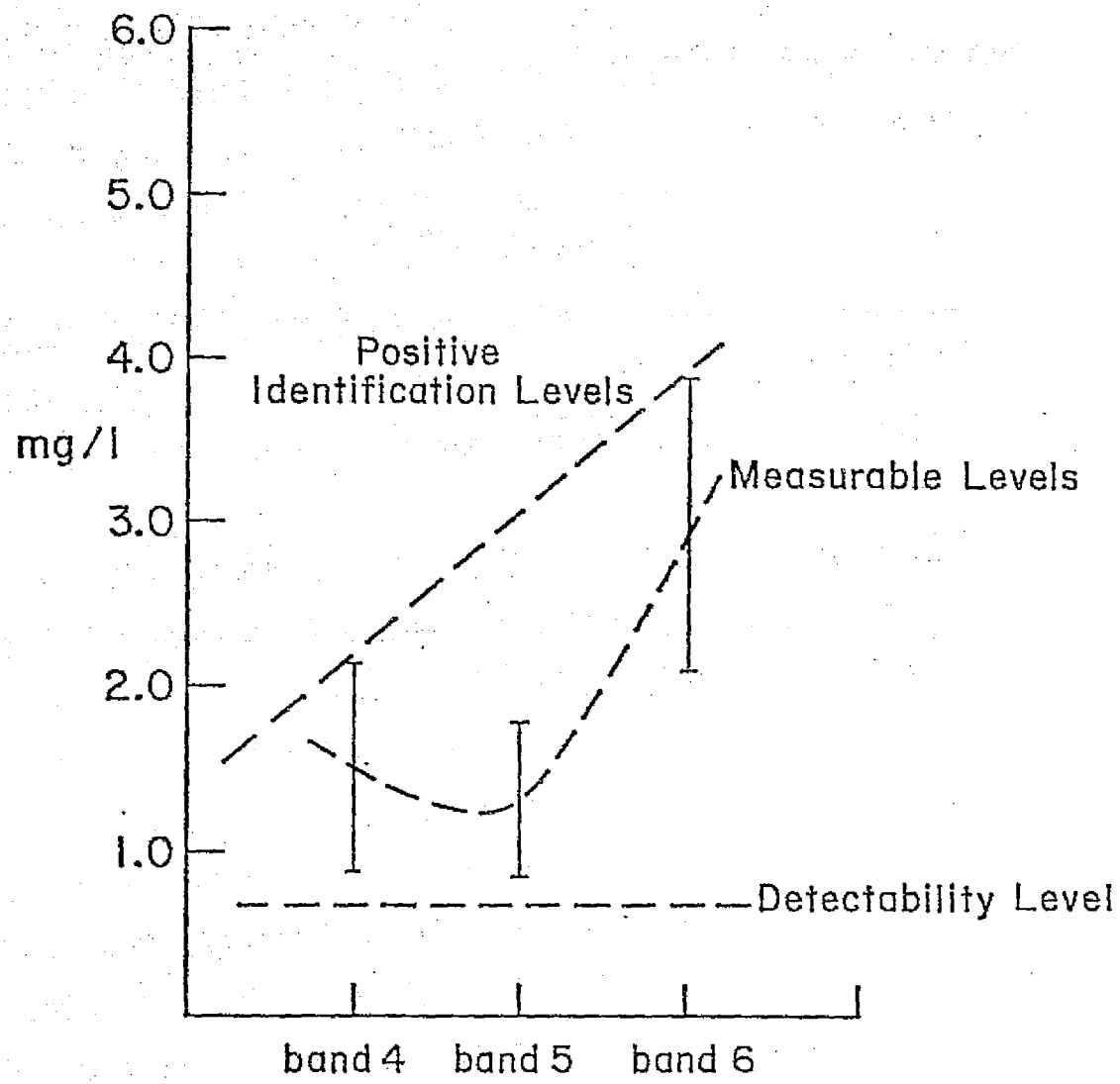

Figure 2. Threshold recognition and detectability levels for red clay particulates in Lake Superior.

the dispersal hinges on the ability to crosscheck the results of numerical models at the intermediate concentration levels. LANDSAT data can provide such a check over western Lake Superior where valid comparison of the LANDSAT and Nimbus G data can be made for common overflight days. This will be the subject of a continuing investigation. If successful, this will give a method and model which will be applicable lakewide at reasonable costs.

LITERATURE CITED

1. Bierman, V.J. and W.R. Swain 1978. DDT Loss in Low Lipid Fishes in Great Lakes, 21st Conference on Great Lakes Research, Windsor, Canada.

2. Bahnick, D.A. 1975. Chemical Effects of Red Clay on Western Lake Superior, Final Report CLSES Contract Publication 35, Univ. of Wisconsin, Superior; Superior, Wisconsin 54880.

3. Sydor, M 1978. Analysis of Suspended Solids in Lakes Using LANDSAT Multispectral Data, Canadian J. of Spectroscopy, v. 23, 3, 91.

4. Sydor, M. 1976. Red Clay Turbidity and its Transport in Western Lake Superior, Final Report E.P.A. Grant R-005175-01, Dept. of Physics, Univ. of Duluth.

APPENDIX A

ANALYSIS OF SUSPENDED SOLIDS BY SINGLE PARTICLE SCATTERING*

ABSTRACT

Light scattering by individual particulates is used in a multiple-detector system to categorize the composition of suspended solids in terms of broad particulate categories. The scattering signatures of red clay and taconite tailings, the two primary particulate contaminants in western Lake Superior, along with two types of asbestiform fibers, amphibole and chrysotile, were studied in detail. A method was developed to predict the concentration of asbestiform fibers in filtration plant samples for which electron microscope analysis was done concurrently. Fiber levels as low as 5×10^4 fibers/liter were optically detectable. The method has application in optical categorization of samples for remote sensing purposes and offers a fast, inexpensive means for analyzing water samples for specific particulate contaminants.

INTRODUCTION

Single particle light scattering has received much attention as a means of sizing, sorting, and identifying microscopic particulates. Techniques have been developed, for example, to identify and size bacterial cells in both flow through systems[1] and suspensions.[2] Scattering as a function of particle size and index of refraction has been extensively studies for spheres,[3,4] circular cylinders,[5,9] and ellipsoids.[6] Recent

---

*Work supported by E.P.A. Contract No. R804361-02-0 NASA Grant NGL 24-005-263.

work has dealt with the dependence upon particle shape and orientation to the illuminating beam.[6,10] Although the theory is complex for particles of widely varying shape and size, the problem can be approached experimentally.

We present here the apparatus and method for determining the concentration of various particulates in an aqueous suspension. The particulates studied are of a type commonly found in Lake Superior and in filtration plant outflow which uses the lake as an intake reservoir. The particulates consist mainly of fine red clay, taconite tailings, asbestiform fibers, and organic debris. The particles are identified on a statistical basis using the relative distribution of light scattered by individual particles drifting through a narrow light beam. The use of two or more simultaneous detectors provides particle shape information which can be utilized to determine the concentration of a specific particulate in a sample of suspended solids.

APPARATUS

A diagram of the apparatus is shown in Figure 1. A laser beam which is focused to a diameter of .1 mm passes through a water sample containing suspended particles. Six photodiode detectors are mounted around the sample at the angles $\pm$ 45°, $\pm$ 90°, and $\pm$ 135° to the indident beam. As individual particles drift through the beam, the resulting scattered light produces a signal at each detector output which appears as a series of pulses of various sizes and shapes with an average width of .2 - .3 seconds.

A lens in conjunction with a narrow aperture increases the light gathering ability of each photodiode yet limits the length of the beam

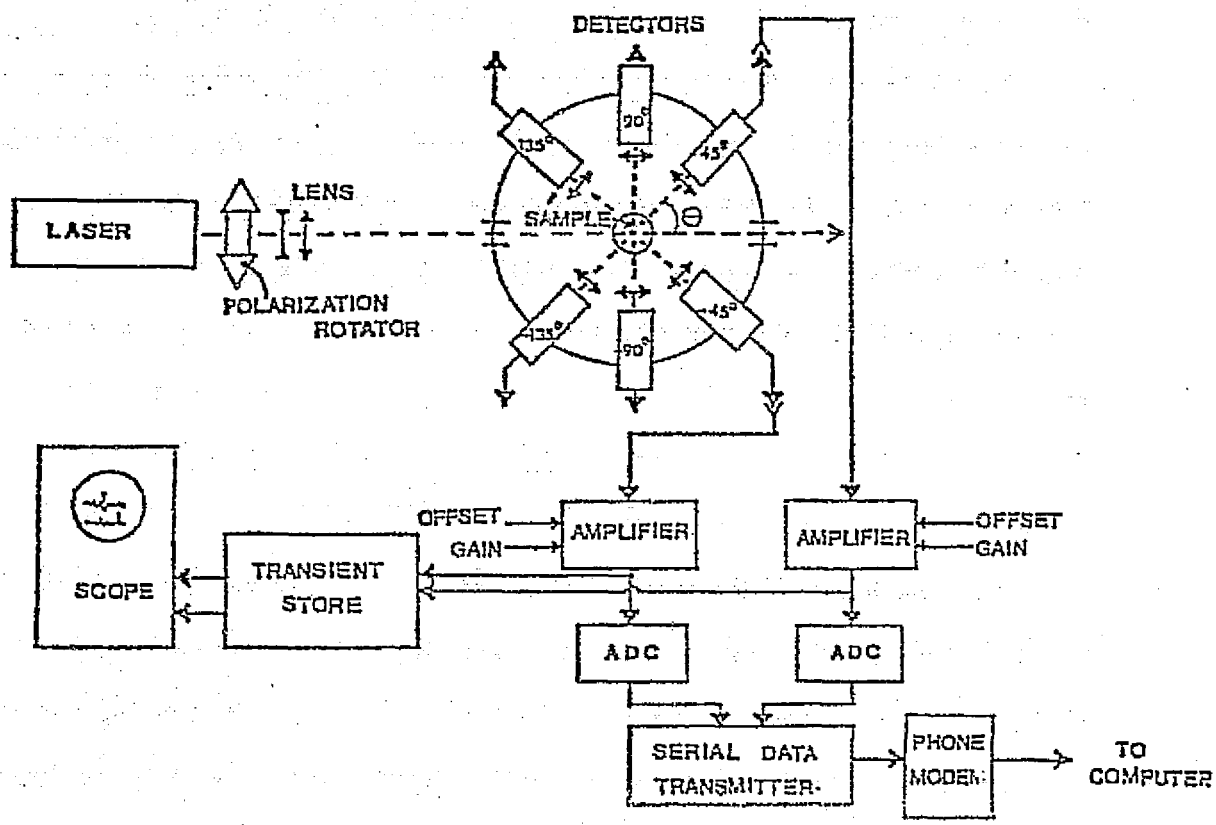

Figure 1. Block diagram of apparatus

viewed by the detectors to 1 mm. This, together with the narrow beam diameter, ensures that usually only single-particle events are viewed by the detectors at any time. In addition, since each lens subtends an angle of about 10°, all the light scattered in a cone toward the lens is detected by the photodiode, producing an integrated signal which smooths out the narrow angular variation in the scattered pattern.

Initially, an analog to digital converter was designed to simultaeously sample any two of the six detectors at a 15 Hz rate (by integrating for 1/15 sec), and transmit the data by telephone directly to a computer where it is stored for analysis. Subsequently, the data recording was extended to three simultaneous detectors and a 60 Hz sampling rate.

ANALYSIS METHOD

In considering the scattered signal by examining simultaneous pulse heights for the six detectors many sampling schemes were possible. Initially, we chose to limit most of our research to the four pairs of viewing angles: $\pm$ 45°, $\pm$ 90°, + 45° with - 135°, and + 45° with + 135°. The polarization plane of the laser beam was always held perpendicular (vertical) to the plane of the detectors. The parallel case was also examined but will not be discussed here.

Once data files were created for a sample, all the advantages and options of the computer were available for data anlysis. A program was written to search each digitized detector output for a repetitive baseline to use for the detector zeros. The program then searched the data for peaks. Once a peak was located, its height and the level of the signal in the accompanying detectors were stored in memory. However,

only events which exceeded a predefined cutoff set sufficiently above the noise level were stored. If the accompanying detectors also produced a peak, i.e., if the peaks occurred simultaneously, the zero-corrected peak heights were stored together and labeled as "coincident." Otherwise, the event for a given detector was labeled as non-coincident. In order to reduce the uncertainty between the measured and actual peak heights due to the finite sampling rate, the stored value for the peak height was averaged over the adjacent digital sampling times.

Computer files containing the peak heights and corresponding coincidence information were created from the original digitized data for a variety of different particle types. Red clay and taconite tailings, the two chief particulate contaminants in western Lake Superior, along with two types of asbestiform fibers, amphibole and chrystotile, were investigated in detail. The average lengths and diameters were respectively 1.7 μm and .2 μm for the amphibole fibers and 2.6 μm and .04 μm for the chrystotile fibers. However, the lengths of both types of fibers were not normally distributed and most of the fibers were under 1 μm in length. Although the tailings consist of roughly 10 - 20 percent asbestiform fibers which are primarily amphibole, most of the tailings particles are blocky irregularly-shaped debris. The red clay and tailings were both roughly sized using centrifuge techniques to less than 2 μm in average dimension. (Particles in the micron size range are of special interest as lake-wide contaminants of drinking water.)

Peak-height frequency distributions for the $\pm$ 45° detector pair can be seen in Figures 2 and 3 for red clay and the chrysotile fibers. The plots were generated by sorting the scattering events into a 21 x 26 element array with maximum peak-height along the vertical axis and peak

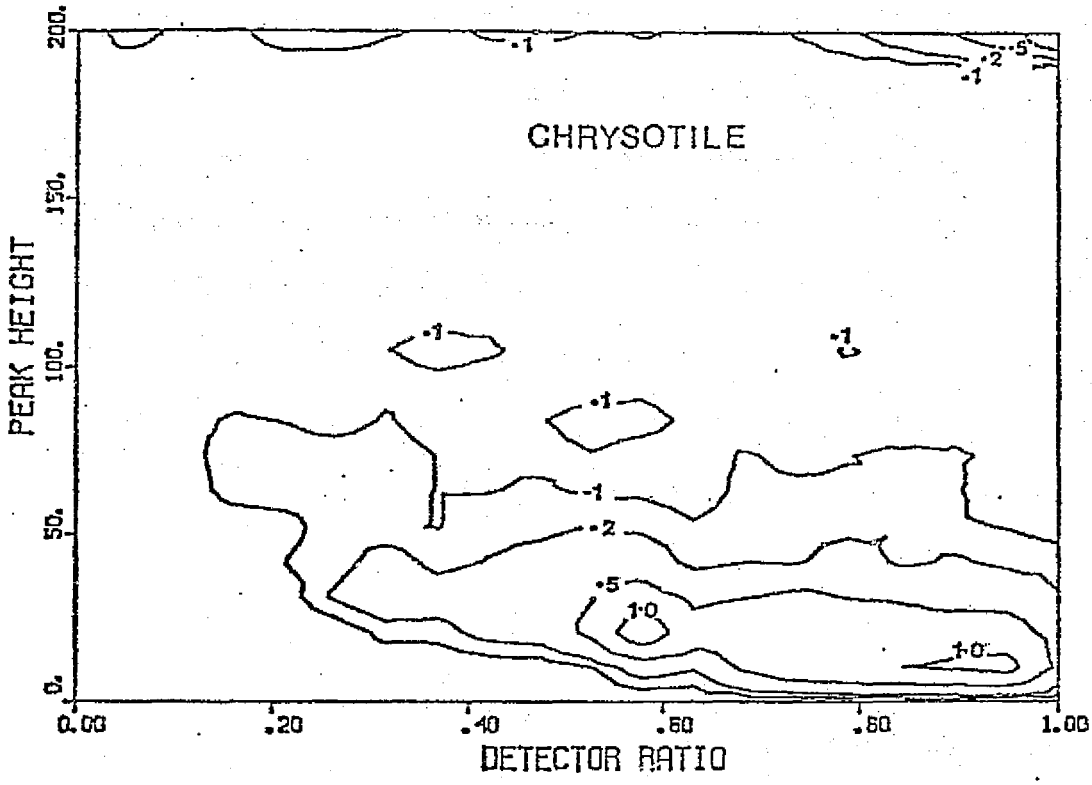

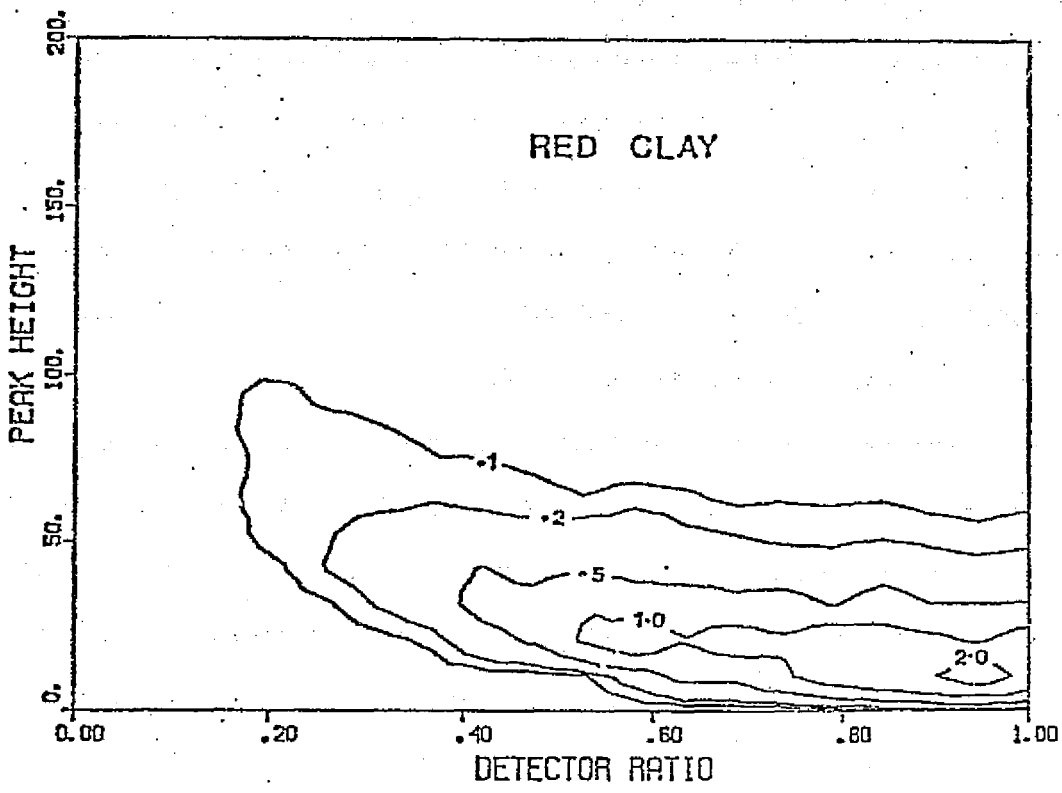

Figure 2. Frequency distribution of coincident events at ± 45° detectors for chrysotile fibers and red clay.

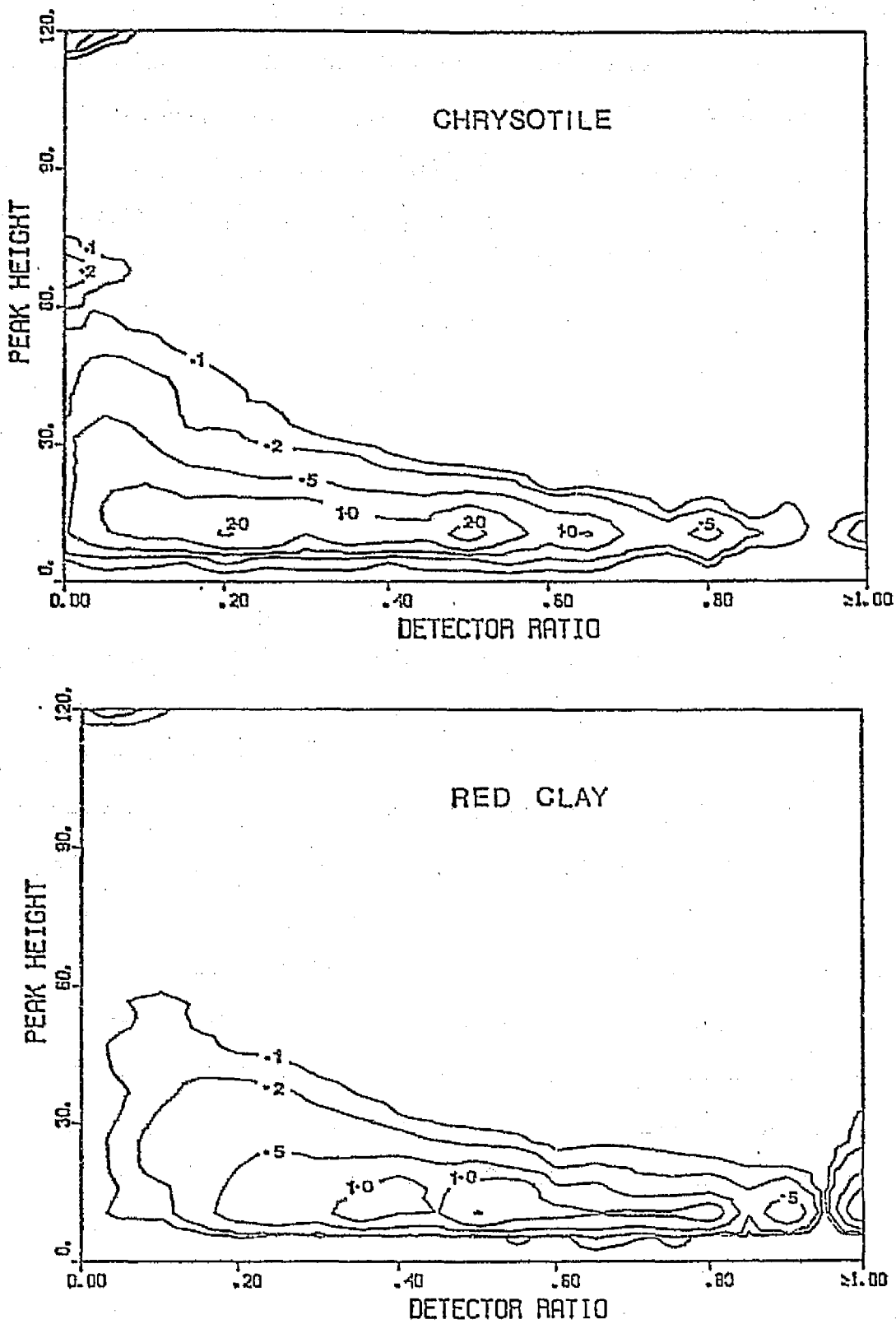

Figure 3. Frequency distribution of non-coincident events at ± 45° detectors for chrysotile fibers and red clay.

ratio along the horizontal axis. For coincident events and symmetrically located detectors the peak ratio was defined as the ratio of the smaller to the larger of the peaks found at the two detectors, resulting in ratios always less than one. For the non-coincident events the ratio values were taken as the level of the detector at which no peak occurred divided by the peak height found at the opposite detector. "Off-scale" events were summed into appropriate locations at the array boundaries. To ease comparison between particle types, the arrays were normalized by dividing the number of events in each element by the total number of events. Thus each contour line in Figures 2 and 3 represents a line of equal event probability given in percent.

The fact that the general shape of the distribution plots of Figures 2 and 3 are similar for the two particle types is not surprising when one considers the irregularity of particle shapes and the character of the scattering distribution for Mie-sized particles. [4,12,13] For instance, under the electron microscope the red clay particles appear as irregularly-shaped globules and platelets which can for some orientations scatter light in a fashion similar to that of the fibers. The wide variation in particle size and shape tends to wash out any pronounced characteristic features of the scattered light unique to each individual category of particles. In addition, the general shape of the plots is in part the result of the apparatus and method of analysis.

However, significant differences do exist between the particle types. As seen in Figure 2, the red clay produced over twice as many coincident events with ratios near 1.0 as did the chrystotile fibers, or either of the other two particle types. This by and large reflects the more spherically-symmetric nature of the red clay particles. In contrast, a

comparison of the non-coincident distributions of Figure 3 reveals a shift toward low ratios for the chrysotile fibers with a concentration of events at the ratios of .2 and .5. The amphibole fibers behaved in a similar but less pronounced manner to that of the chrystotile fibers, yet yielded a few identifying characteristics of their own.

Large differences between the particle types were also observed for each of the other three detector pairs. Peak-height frequency distributions for the + 45° and - 135° detector pair can be seen in Figure 4 for the red clay and chrysotile fibers. (Only plots for the non-coincident events which occurred at the - 135° detector are shown.) The magnitude of the peaks detected at - 135° were plotted against the simultaneous output of the + 45° detector. The large concentration of events at low peak-heights on the fiber plot is over four times greater than that of the same area on the red clay plot.

A comparison between each of the four particle types is shown in Table 1 for the + 45° and - 135° detector pair. The three values listed for each particle type represent the percentage of events located in the high-frequency area of each of the three distribution plots. Thus, for example, the differences seen in Figure 4 between the red clay and chrysotile fibers are evident in the table under the non-coincident at - 135° column where the percentage of chrysotile fibers is over twice that of red clay. As expected, the largest percentage of coincident events belongs to red clay. Actually, the peak-height distributions could be further divided and refined to yield even more pronounced differences between the particle types. Furthermore, the individual constituents of a mixture of these particle types could be identified on a statistical basis using the event rates in the various pulse height regions.

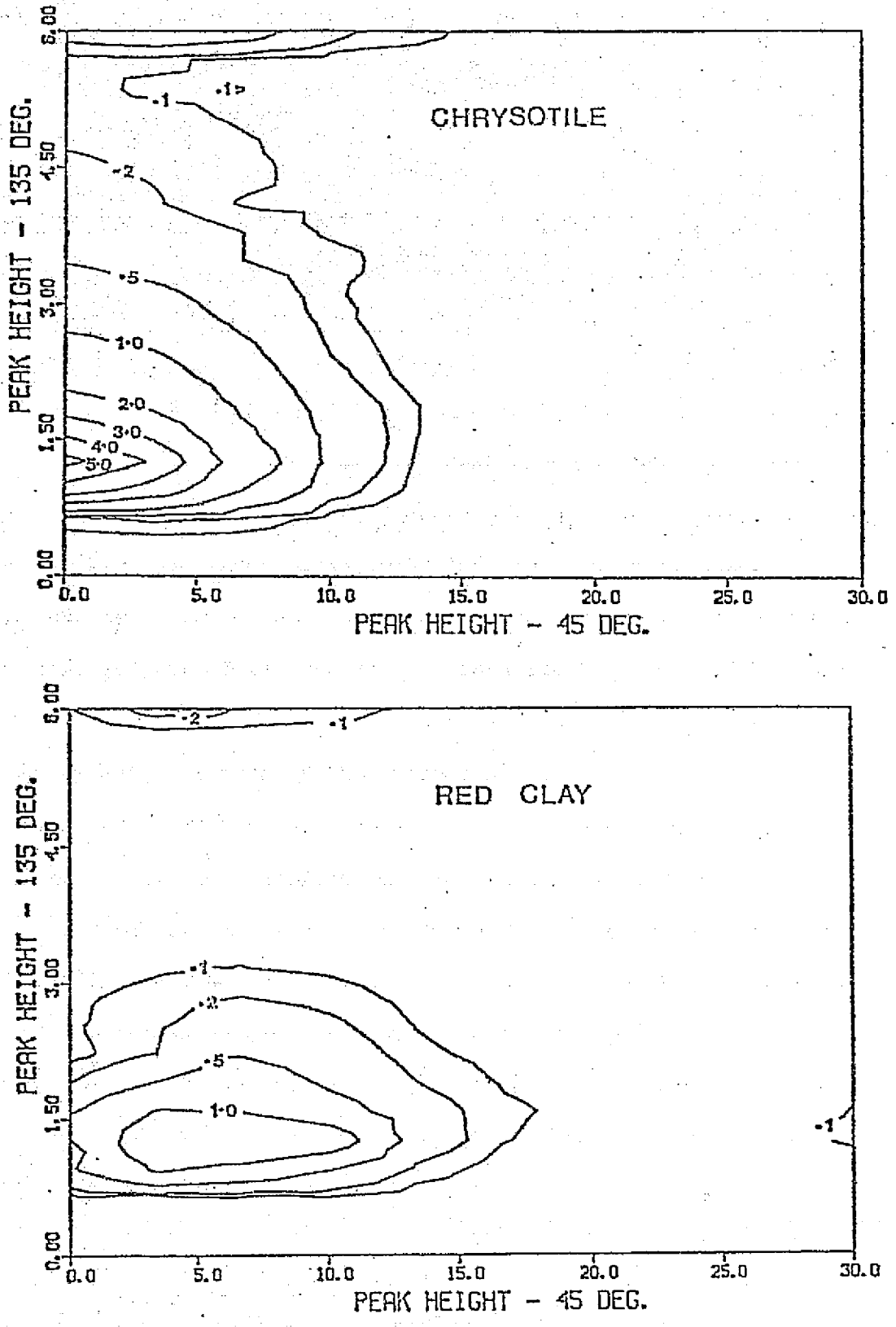

Figure 4. Frequency distributions of events at the + 45° and -135° detector pair for red clay and chrysotile fibers.

Table 1. Detector Pair: + 45° and - 135°

	Coincident Events	Non-Coincident Events at + 45°	Non-Coincident Events at - 135°
Red Clay	21.3%	43.1%	17.1%
Tailings	17.3%	48.0%	10.8%
Amosite Fibers	11.5%	57.1%	12.9%
Chrysotile Fibers	10.1%	23.9%	42.0%

QUANTITATIVE FIBER IDENTIFICATION

Consider subdividing the distribution plots into n regions for a sample containing unknown concentrations of n distinct particle types. Assume the distributions were not normalized and that the regions were chosen so that they behave in a linearly independent fashion when the concentrations of the various particle types are independently varied. Within the accuracy of the event-rate statistics, it can be shown that the concentration of any one of the particle types is given by a linear sum of the n even rates, i.e., the total number of events per unit time obtained in each of the n regions:

1) $$C = aN_1 + bN_2 + cN_3 \ldots + dN_n$$

where C is the concentration of interest, and $N_1, \ldots, N_n$ are the event rates of the n regions.

The necessary coefficients, a, . . . , d, could be obtained by testing each individual particle type present in the unknown sample, and then

solving the resulting set of n simultaneous equations. This would usually be impractical, however, especially if one is only interested in the level of a specific contaminant. Another approach is to test samples which contain various known amounts of the particle type that one desires to identify and which also contain independently varying amounts of the other background particulates. Isolation of the optical characteristics for a given particle category is then possible, provided the number of calibration samples exceeds the number of particle species. Linear-regression analysis can then be used to find the set of coefficients in equation 1) which gives a least-square fit to the measured concentrations of the known particle type. The number and the manner of subdivision of the pulse height regions chosen can be refined until a satisfactory fit is obtained. It should be pointed out that if one uses as many variables, i.e., regions, as there are test samples, the linear regression will produce an exact fit independent of the actual number of particle types. Therefore, to obtain a statistically valid fit, the number of test samples should be at least several times larger than the final number of variables.

One may also increase the number of simultaneous signal combinations by using three or four detectors to establish a region in pulse-height space which is highly selective of one category of contaminant. Increasing the number of detectors is considered later and does produce more accurate identification. However, the advantages of using a minimum of two simultaneous detectors is quite sufficient.

To test the system's ability to measure the concentrations of a specific category of particulate contaminant in samples with varying concentrations of background particulates, we tested over 60 water samples for which electron microscope (EM) fiber counts were available. The

samples were filter effluent from either the main plant which supplies the Duluth drinking water or from an adjoining pilot plant operation.

The primary fiber of interest in the water was amphibole, although chrysotile fibers were also present in smaller amounts. The EM data for the samples included the counting of all amphibole and chrysotile fibers which could be positively identified using selected-area diffraction (SAS). Other fibers were also counted provided they had the correct morphology, such as nearly parallel sides, even though no SAD patterns were observed or the patterns were ambiguous. (The usual 3:1 aspect ratio was used to define the cutoff between fibers and non-fibers.) The total number of fibers that were recorded per sample was usually less than 20, of which only a few were positively identified as amphibole or chrysotile. As pointed out by Leinweber,[14] the statistical uncertainty for such low numbers of fibers is extremely high, and the resulting spread in the data makes it difficult to evaluate the quality of the mathematical fits. To improve the situation, the lower concentration samples were grouped and averaged according to the number of observed fibers. The total number of recorded fibers was used in the calibration procedure.

Trial fits were first computed for each detector combination using all of the coincident and non-coincident pulse height regions. Regions of low significance were eliminated, regions which showed similar coefficients were combined, and the fit was subsequently recomputed. This iterative process was continued until a satisfactory fit was achieved based on as few region combinations as necessary.

The $\pm$ 45° detector pair produced the best attainable least-square fit using only six variables. A plot of the fiber concentrations calculated using the fitting equation versus the actual EF fiber data can

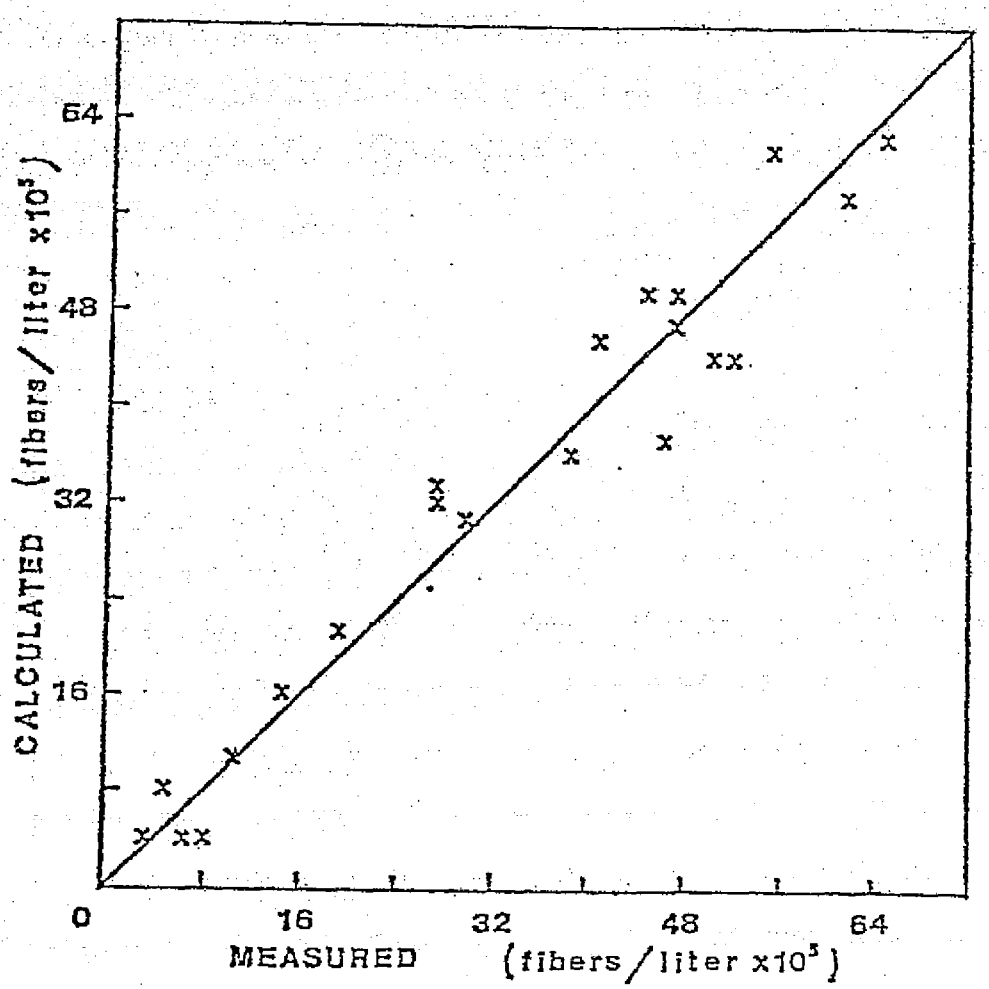

Figure 5. Comparison of fiber concentrations predicted by scattering versus electron microscope measurements.

be seen in Figure 5. With a standard deviation of only .42 million fibers/liter, the quality of the fit is quite good, and suggests that the optical scattering method, once calibrated with a sufficient amount of EM data, is actually more accurate than the EM fiber analysis. When the number of region combinations is reduced still further, the quality of the fit deteriorates somewhat. For instance, a four variable fit was obtained with a standard deviation of .61 million fibers/liter. Even after averaging the samples each data point usually represented fewer than 50 fibers. Assuming that the EM data fluctuations are random and can be described by the usual Poisson statistics, a best-case error of about $\pm$ 15% is implied. A similar source of error results from the statistical uncertainty associated with the number of counts in each pulse height region. Although for a typical sample as many as 1000 events may have been detected, once these are split into their respective regions and inserted into the fitting equation, the possible accumulative error can become appreciable.

To improve the accuracy of the apparatus, the number of simultaneous monitored detectors was increased. A microcomputer with its own multichannel A/D converter was added, and programs were written to simultaneously sample three of the six detectors at a 60 Hz rate instead of only two at 15 Hz as done previously. The subsequent peak-height and coincidence information were used to form three-dimensional event distributions which were then subdivided into regions for use as variables in the linear regression analysis.

A second series of Duluth filter-effluent samples with improved EM data became available and was subsequently tested. Figure 6 shows a six-variable least-square fit to the total fiber concentrations for the second series of samples. For each sample 30 minutes of scattering data

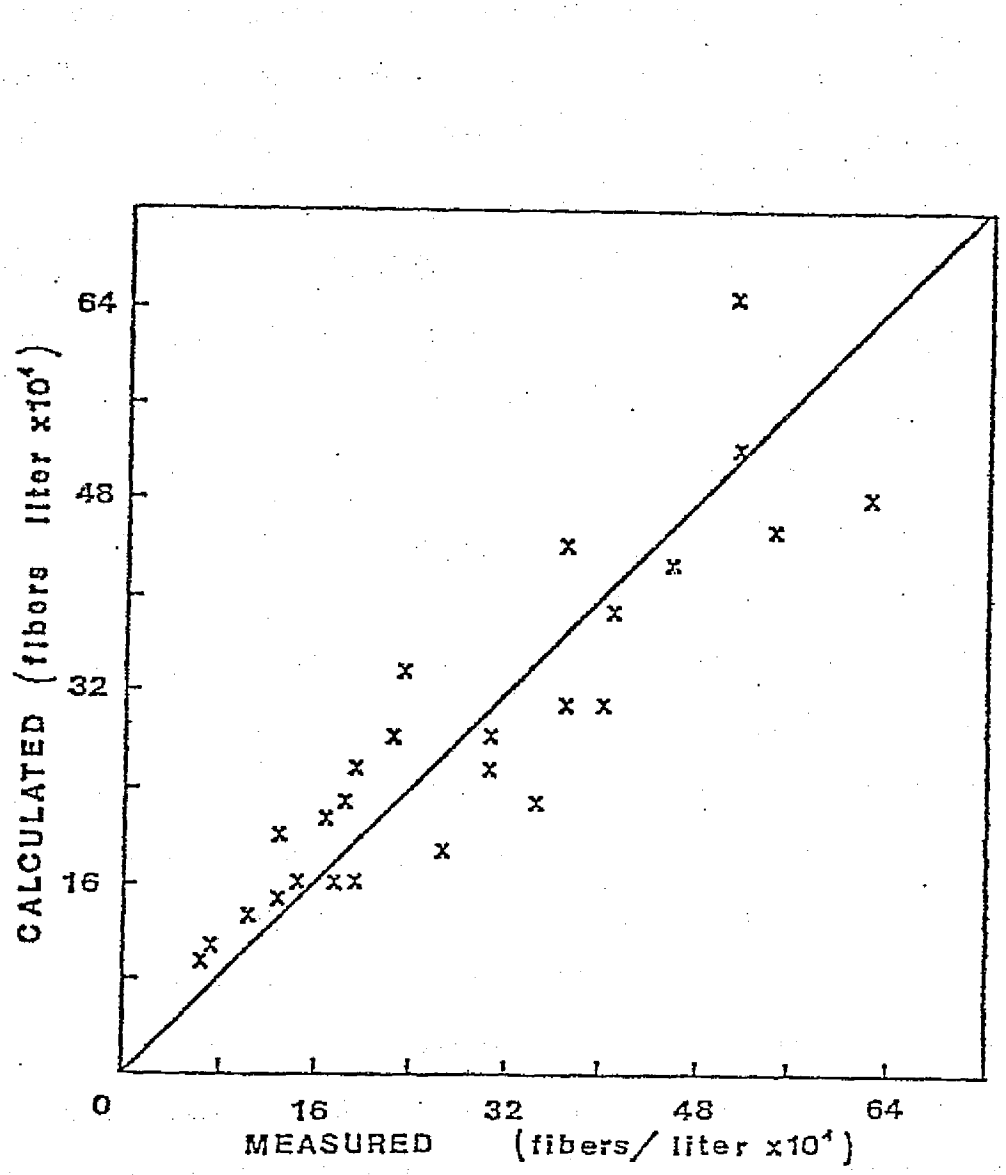

Figure 6. Comparison of predicted fiber concentrations versus electron microscope counts for the 3-detector technique.

was accumulated using the three detectors located at ± 45° and + 135°. Since the samples were not averaged, about 30% of the data points each represent less than 20 EM counted fibers, which accounts for much of the point dispersion. For comparison, a plot of the total fiber concentrations versus total particle concentrations is shown in Figure 7. The total particle counts were obtained using a Hiac, Model PC 320, particle counter operating on forward scattering principle. The minimum particle-size detection limit of the instrument was 1.0 μm (average particle dimension). The results in Figure 7 point out the uncertainty encountered by using a single-detector counter for fiber level measurements and by assuming a fixed ratio between the total particle count and fiber concentration. For example, in Figure 7 two of the points (marked by triangle) which had nearly the same fiber concentrations differed in their total particle count by over a factor of 200. In contrast, the fiber concentrations of these same two samples were predicted accurately using the three-detector fit.

The results show that suspended solids can be characterized optically into broad category types using differential scattering by individual particles. These characteristics can be subsequently used to determine, on a statistical basis, the composition of samples of suspended solids. The results have far reaching applications in the monitoring of filtration plants for specific particulate contaminants and in the optical classification of samples used as ground truth in the remote sensing of suspended solids in lakes. [15,16] Possibilities for the optical analysis of biological contaminants may also be practical.

D30

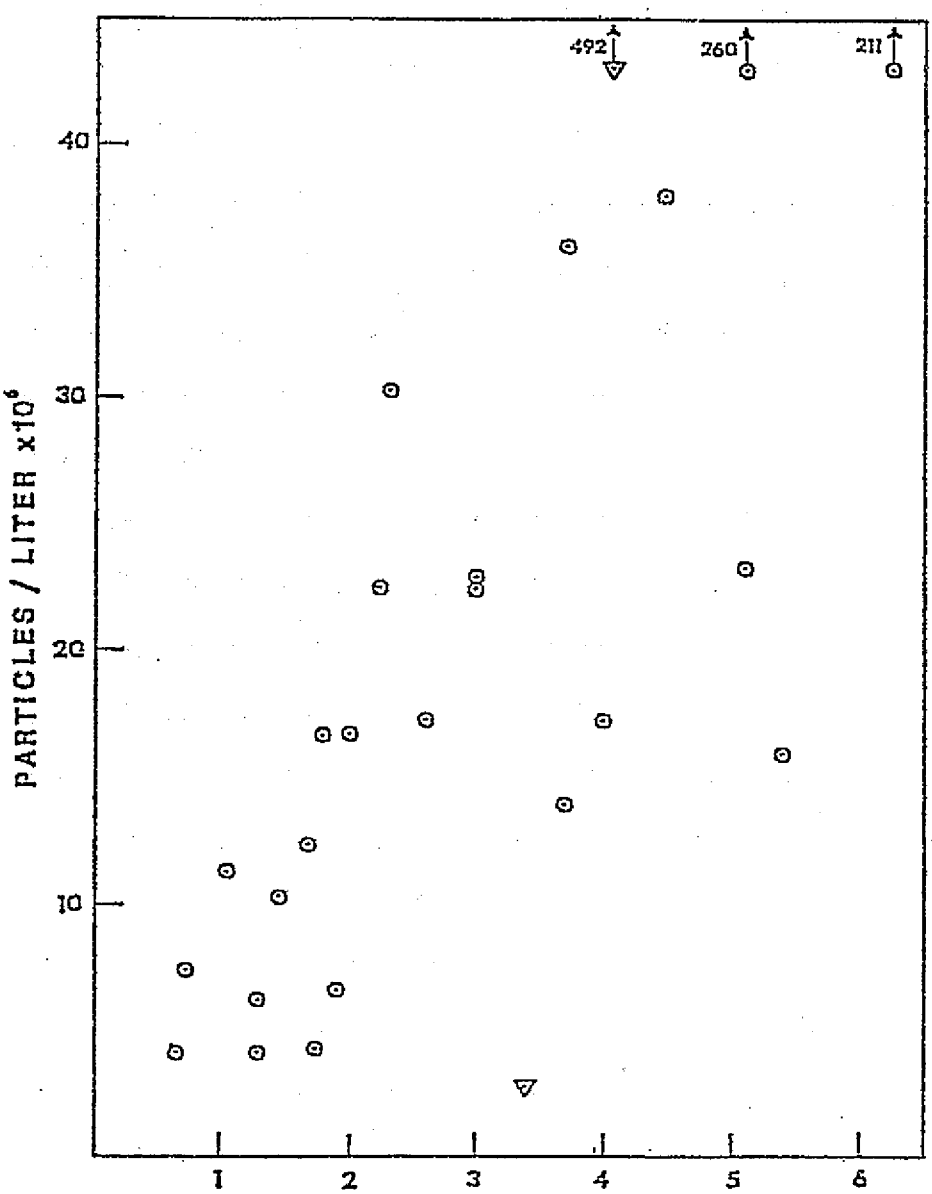

Figure 7. Total particle counts by single-detector forward scattering method versus electron microscope fiber counts.

FIGURE CAPTIONS

Fig. 1. Block diagram of apparatus.

Fig. 2. Frequency distribution of coincident events at ± 45° detectors for chrysotile fibers and red clay.

Fig. 3. Frequency distribution of non-coincident events at ± 45° detectors for chrysotile fibers and red clay.

Fig. 4. Frequency distributions of events at the + 45° and - 135° detector pair for red clay and chrysotile fibers.

Fig. 5. Comparison of fiber concentrations predicted by scattering versus actual electron microscope measurements.

Fig. 6. Comparison of predicted fiber concentrations versus actual electron microscope counts for the 3-detector technique.

Fig. 7. Total particle counts by single-detector forward scattering method versus actual electron microscope fiber counts.

LITERATURE CITED

1. P.F. Mullaney, M.A. Van Dilla, J.R. Coulter, and D.N. Dean, Rev. Sci. Instrum. 40, 1029 (1969).

2. L.W. Casperson, C. Yeh, and W.F. Yeung, Appl. Opt. 16, 1104 (1977).

3. H.C. Van De Hulst, Light Scattering by Small Particles, Wiley, New York (1957).

4. M. Kerker, The Scattering of Light, Academic Press, New York (1969).

5. J.R. Wait, Electromagnetic Radiation from Cylindrical Structures, Pergamon Press, New York (1959).

6. P. Barber and C. Yeh, Opt. 14, 2864 (1975).

7. R.D. Birkhoff, J.C. Ashley, H.H. Hubbel, Jr., and L.C. Emerson, J. Opt. Soc. Am 67, 564 (1977).

8. W.A. Farone and M. Kerker, J. Opt. Soc. Am. 56, 481 (1966).

9. M. Kerker, D. Cooke, W.A. Farone, and R.A. Jacobsen, J. Opt. Soc. Am. 56, 487 (1966).

10. P. Latimer, A. Brunsting, B.E. Pyle, and C. Moore, Appl. Opt. 17, 3152 (1978).

11. S.R. Diehl, D.T. Smith, and M. Sydor, E.P.A. Contract No. R804361-02-0 Report (1978).

12. M.Born and E. Wolf, Principles of Optics, Pergamon Press, New York (1964).

13. G. Kortum, Reflectance Spectroscopy, Springer-Verlag, New York (1964).

14. J.P. Leineweber, Statistics and the Significance of Asbestos Fiber Analysis, Presented at NBS Workshop, July 18 - 20, 1977, Gaithersburg, MD.

15. R.J. Gibbs, J. Geophys. Res. 83, 501 (1978).

16. M. Sydor, Can. J. of Spect. 23, 91 (1978).

SECTION E

ICE COVERAGE OF MINNESOTA LAKES: ASSESSMENT OF FREEZE-OVER FROM LANDSAT IMAGERY AND WEATHER

Dr. H. Stefan and Alec Y.K. Fu
Department of Civil and Mineral Engineering
St. Anthony Falls Hydraulic Laboratory
University of Minnesota
Minneapolis, Minnesota

o

INDEX

Information from LANDSAT Imagery on Freeze-Over..... E1
Theory on Freeze-Over..... E12
Hindcasting of Freeze-Over Dates and Verification Using Memory..... E17
Mean Freeze-Over Dates for Minnesota Lakes..... E18
Information from LANDSAT Imagery on Spring Melting of Lake Ice-Covers..... E18
Conclusions..... E26
Literature Cited..... E28

o

ICE COVERAGE OF MINNESOTA LAKES: ASSESSMENT OF FREEZE-OVER FROM LANDSAT IMAGERY AND WEATHER

Investigators: Dr. H. Stefan
Alec Y.K. Fu
Department of Civil and Mineral Engineering
St. Anthony Falls Hydraulic Laboratory
University of Minnesota
Minneapolis, Minnesota

INFORMATION FROM LANDSAT IMAGERY ON FREEZE-OVER

LANDSAT 1 and 2 images have been used to determine onset of ice coverage of lakes in northern, central and southern Minnesota. The scenes are identified in Figure 1. They carry the identification numbers Path 29, Row 27 (North), Path 30, Row 28 (Central), and Path 29, Row 29 (South). Dates of available LANDSAT scenes and cloud coverage during the period of interest, i.e., from November 11, 1972 through January 17, 1976, are shown in Table 1, (a) through (d).

Although the percentage cloud cover identified in Table 1 has been appreciable, much information could be extracted from LANDSAT scenes. LANDSAT imagery was acquired in the form of 9 x 9 black and white prints (Band No. 6) and for cloud covers up to 90 percent. Examination of the images under a magnifying glass shows ice covers quite clearly.

From 10 to 30 lakes were selected on each LANDSAT scene. The Minnesota Lake Inventory provided the name, the range, township and section, and an identification number for each selected lake. This information was subsequently used to find the median lake depth and the lake surface

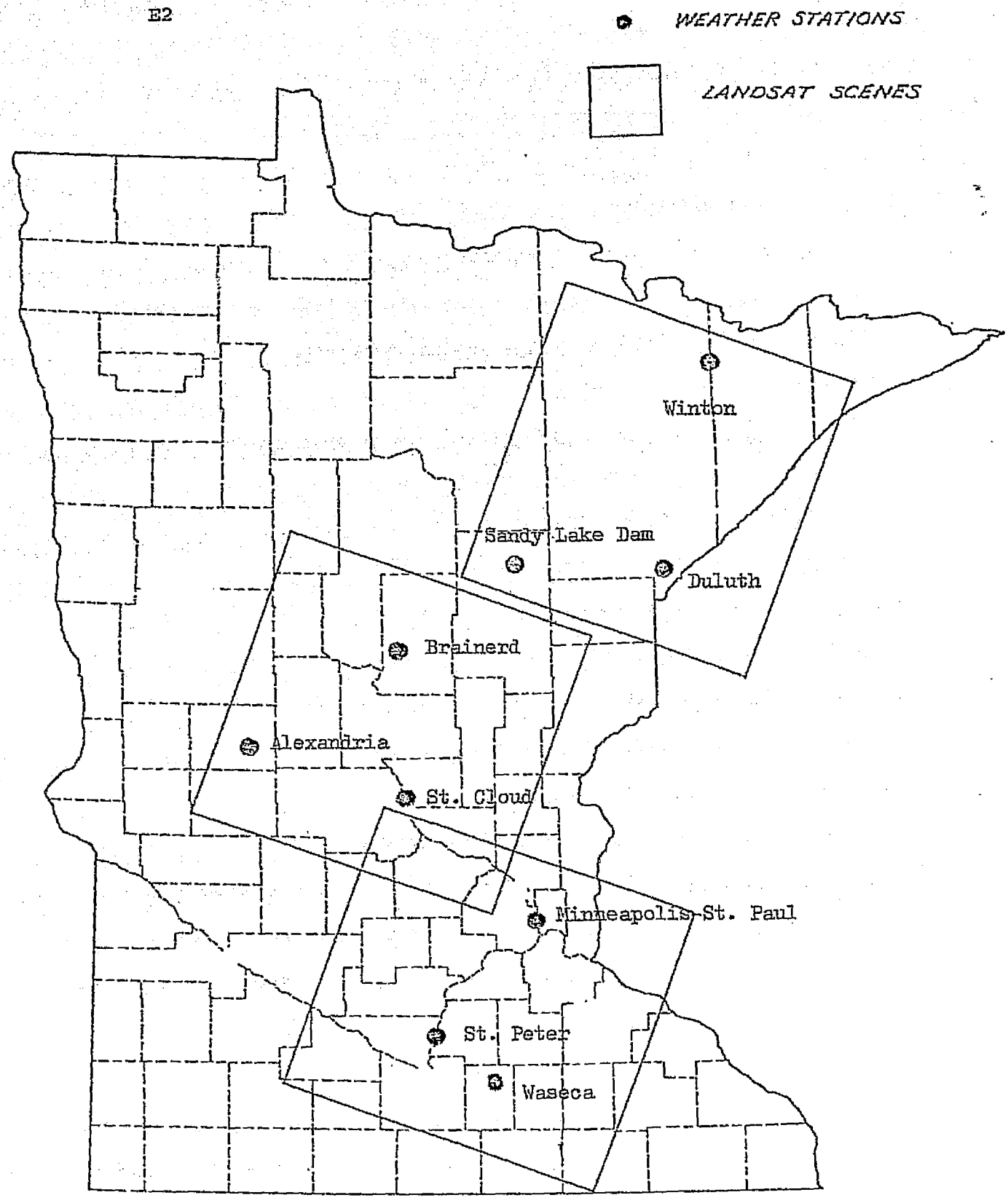

Figure 1. Map of Minnesota showing coverage of selected LANDSAT scenes and locations of weather stations.

TABLE 1 (a). Available LANDSAT Scenes, Fall 1972

North

Date	Quality	Cloud Cover (%)
11/11/72	Excellent	90
11/29/72	Excellent	10
12/17/72	Excellent	90
1/04/73	Excellent	30
	Average	55

Central

Date	Quality	Cloud Cover (%)
11/30/72	Excellent	60
12/18/72	Excellent	50
1/05/73	Excellent	0
	Average	37

South

Date	Quality	Cloud Cover (%)
11/11/72	Excellent	90
11/29/72	Excellent	10
12/17/72	Excellent	20
1/04/73	Excellent	20
	Average	35

TABLE 1 (b). Available LANDSAT Scenes, Fall 1973

North

Date	Quality	Cloud Cover (%)
10/19/73	Excellent	50
11/06/73	Excellent	30
11/24/73	Unavailable	100
12/12/73	Excellent	90
12/30/73	Excellent	10
	Average	56

Central

Date	Quality	Cloud Cover (%)
10/20/73	Unsatisfactory	10
11/07/73	Unavailable	100
11/25/73	Unsatisfactory	90
12/13/73	Excellent	20
12/31/73	Unsatisfactory	20
1/18/74	Unsatisfactory	70
	Average	52

South

Date	Quality	Cloud Cover (%)
10/19/73	Excellent	10
11/06/73	Excellent	20
11/24/73	Unsatisfactory	90
12/12/73	Excellent	50
1/17/74	Excellent	60
	Average	46

TABLE 1 (c). Available LANDSAT Scenes, Fall 1974

North

Date	Quality	Cloud Cover (%)
11/19/74	Fair	90
12/07/74	Excellent	80
1/24/75	Fair	90
	Average	87

Central

Date	Quality	Cloud Cover (%)
11/02/74	Excellent	90
11/20/74	Fair	90
12/08/74	Unavailable	100
12/26/74	Unavailable	100
1/13/75	Unavailable	100
1/31/75	Excellent	40
	Average	87

South

Date	Quality	Cloud Cover (%)
11/01/74	Excellent	50
11/19/74	Fair	90
12/07/74	Excellent	30
1/24/75	Excellent	80
	Average	63

TABLE 1 (d): Available LANDSAT Scenes, Fall 1975

North

Date	Quality	Cloud Cover (%)
10/27/75	Fair	90
11/05/75	Fair	90
11/14/75	Fair	10
11/23/75	Fair	60
12/02/75	Unavailable	100
12/11/75	Unsatisfactory	70
12/20/75	Unavailable	100
12/29/75	Fair	90
1/07/76	Fair	20
	Average	70

Central

Date	Quality	Cloud Cover (%)
10/28/75	Excellent	80
11/06/75	Excellent	90
11/15/75	Fair	90
11/24/75	Fair	30
12/03/75	Unavailable	100
12/12/75	Excellent	20
12/21/75	Excellent	20
12/30/75	Excellent	40
1/08/76	Unavailable	100
1/17/76	Unavailable	90
	Average	66

South

Date	Quality	Cloud Cover (%)
10/27/75	Excellent	0
11/05/75	Fair	10
11/14/75	Excellent	10
11/23/75	Fair	70
12/02/75	Unavailable	100
12/11/75	Unsatisfactory	90
12/20/75	Unavailable	100
12/29/75	Fair	80
1/07/76	Fair	20
1/16/76	Excellent	10
	Average	49

area from the Clean Lakes Inventory File (CLIF) of the Minnesota Pollution Control Agency.

Ice coverage was classified in 5 categories according to which portion of the lake was ice-covered.

(a) open water

(b) nearly fully open

(c) half open

(d) nearly closed

(e) closed

Observations on ice coverage were tabulated.

Under clear sky, no difficulty was encountered in the interpretation. Water appeared black and ice greyish white or white on the images. In cases when light to heavy cloud cover prevailed, it was often difficult to distinguish ice and snow from overlying cloud cover in images. In such circumstances, no interpretation was made.

A.O. Lind (1973) in an early study already indicated the presence of various ice tones, patterns and arrangements of ice as well as open water in a LANDSAT image of Lake Champlain taken on January 8, 1973. In Lind's opinion, MSS band 5 imagery provided the most useful data. Lind states: "While it was not possible to differentiate open water from one - two day old ice, it was possible to interpret the total signatures of the frozen portion in terms of freezing history or age. The dark gray tones of new smooth ice were found to contrast with the medium gray tones of older ice and the rough texture of wind-jammed bay ice."

During the study of the Minnesota lakes, the presence or absence of ice covers was generally well identified and few instances of ambiguity were encountered.

Occasionally, a lake remained open even after all the surrounding lakes were closed in winter and thawed in early spring before all the other lakes did. These lakes were receiving artificial thermal input and must be treated separately in any analysis. A separate list of such water bodies was prepared.

In addition, three weather stations in each LANDSAT frame were identified. They are also shown in Figure 1. Since the objective was to relate weather to ice coverage, results on ice coverage were plotted separately for lakes located in the vicinity of each weather station.

Figures 2a, through 2e give examples of ice coverage for different locations and lakes of different depths. Theoretical predictions for dates of freeze-over are also plotted. The theoretical analysis is discussed in Theory on Freeze-Over. The effect of lake depth on the delay in freeze-over is quite apparent. That delay was also determined theoretically. Not expected was the dependence on lake surface area. A sample graph showing the dependence of ice conditions on lake surface area was given in an earlier report. Sometimes lake depths and lake surface areas are related to each other in the sense that larger lakes are also deeper. This is, however, not generally true. It may be that wind effects also have an important role. Wind can prevent formation of a coherent ice cover and wind effects are stronger on lakes with larger fetch (surface area). Ice movement by wind is readily observed in large lakes and has been described e.g., by Tsang (1974). A graph in which the lake volume instead of the lake depth is plotted, was also found to be useful.

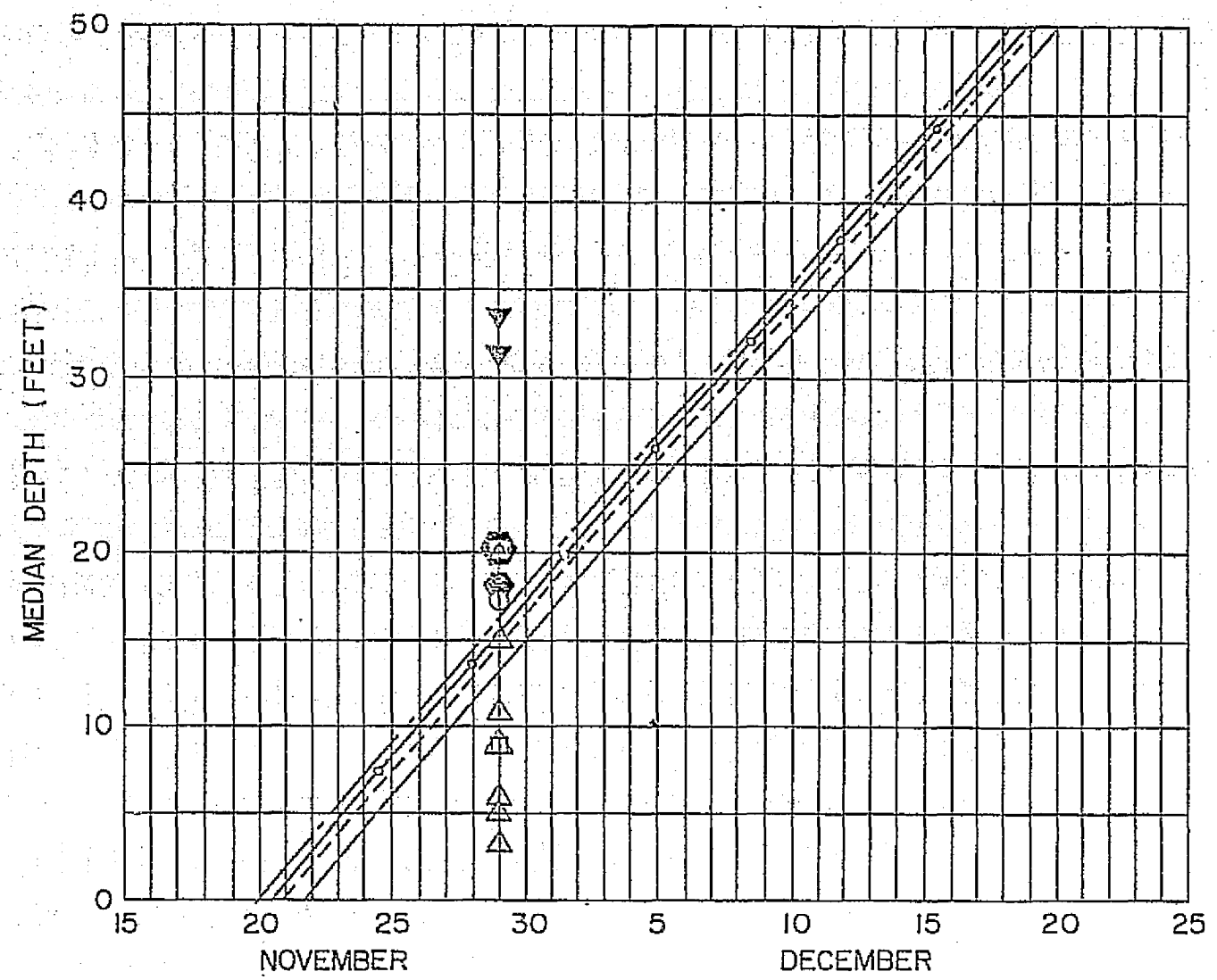

Figure 2a. Theoretically predicted dates of freeze-over for lakes as a function of their depth in the vicinity of Minneapolis/St. Paul in the Fall of 1972 (plotted lines) and the observed condition of a number of lakes determined from LANDSAT imagery on the indicated date.

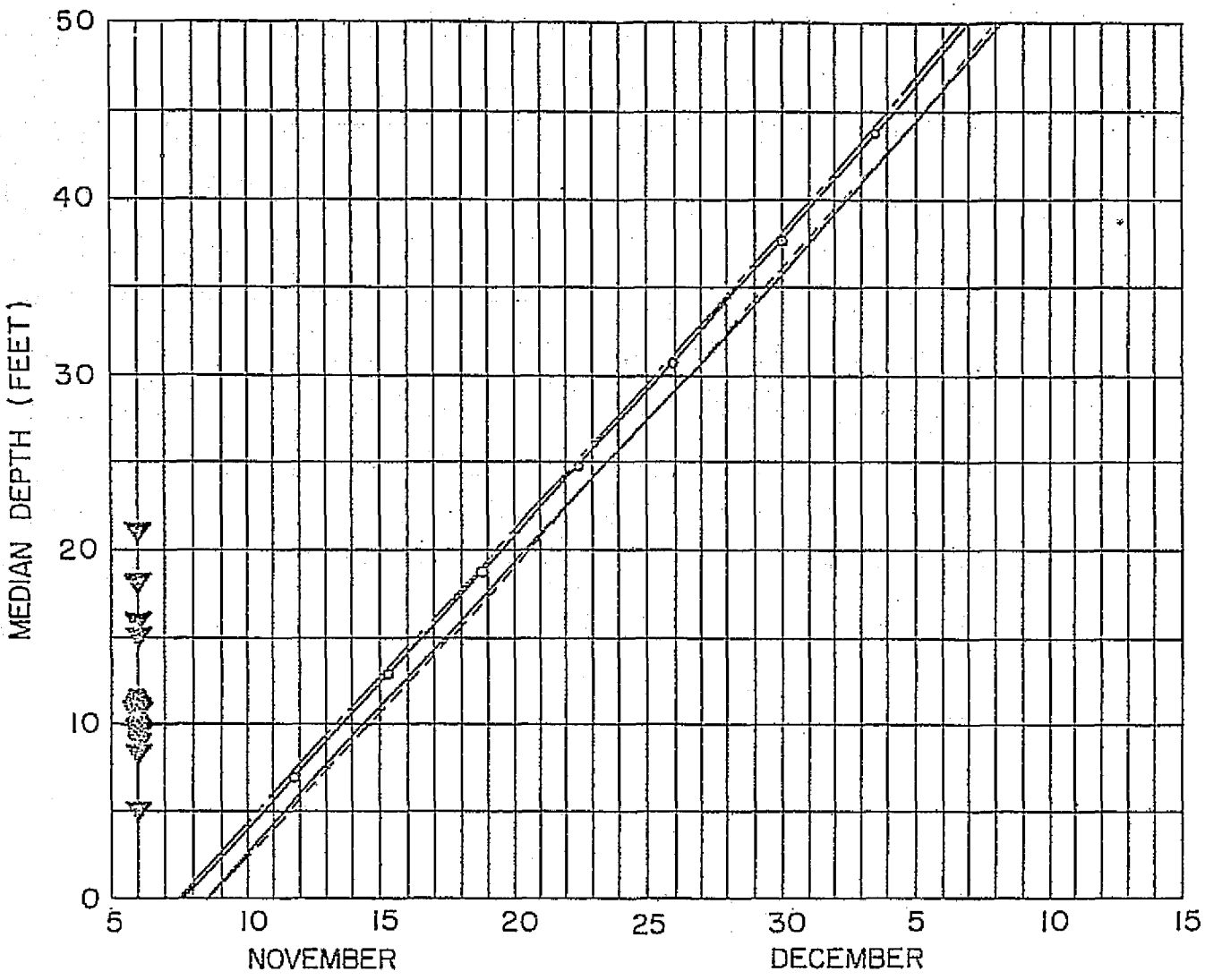

Legend

Month at the end of which prediction was made

- August
- September
- October
- November and December

Figure 2b. Theoretically predicted dates of freeze-over for lakes as a function of their depth in the vicinity of Sandy Lake Dam Libby in the Fall of 1973 (plotted lines) and the observed condition of a number of lakes determined from LANDSAT imagery on the indicated date.

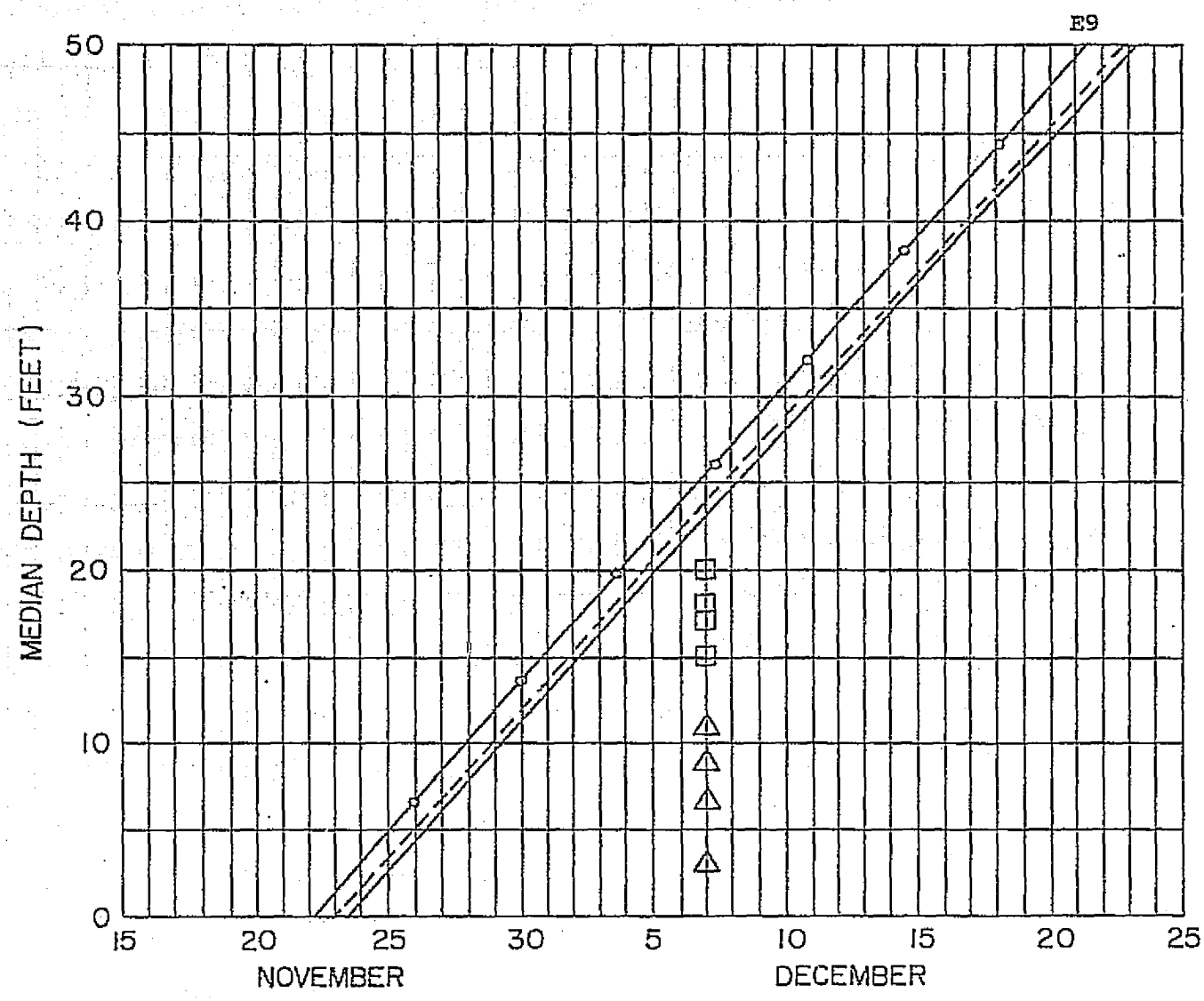

Legend

Month at the end ofwhich prediction was made

August and September

October

November and December

Figure 2c. Theoretically predicted dates of freeze-over for lakes as a function of their depth in the vicinity of Minneapolis/St. Paul in the Fall of 1974 (plotted lines) and the observed condition of a number of lakes determined from LANDSAT imagery on the indicated date.

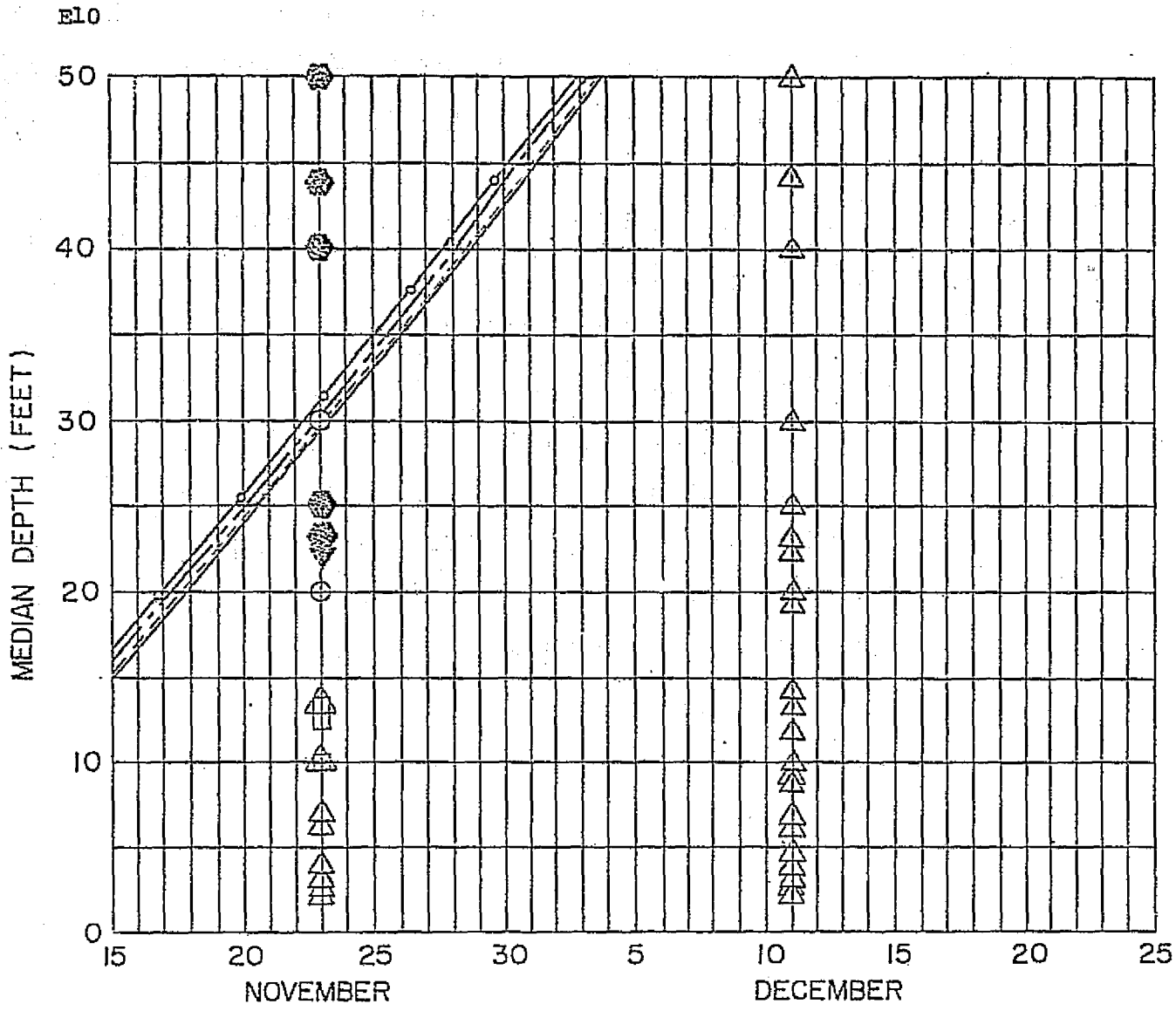

Legend

Month at the end of which prediction was made

- August
- September
- October
- November and December

Figure 2d. Theoretically predicted dates of freeze-over for lakes as a function of their depth in the vicinity of Winton Power Plant in the Fall of 1975 (plotted lines) and the observed condition of a number of lakes determined from LANDSAT imagery on the indicated date.

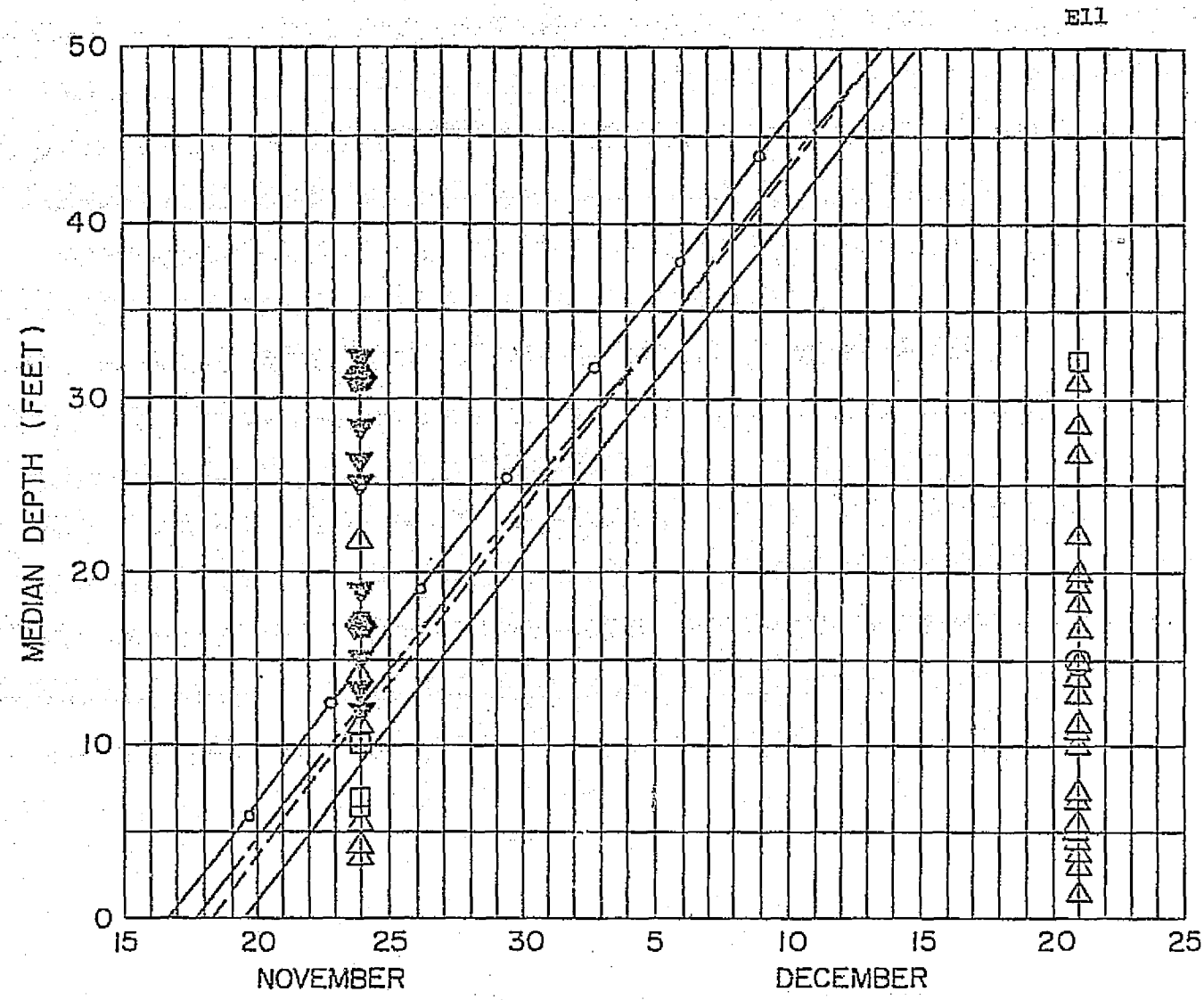

Legend

Month at the end of which prediction was made

- August
- September
- October
- November and December

Figure 2e. Theoretically predicted dates of freeze-over for lakes as a function of their depth in the vicinity of Alexandria Airport in the Fall of 1975 (plotted lines) and the observed condition of a number of lakes determined from LANDSAT imagery on the indicated date.

THEORY ON FREEZE-OVER

A mean seasonal water temperature cycle of a lake can be approximated by the relationship

$$T = E_m + \frac{I}{m} + \Delta E \left(1 + \left(\frac{\omega}{m}\right)^2\right)^{-1/2} \sin(\omega t - \delta)$$

Equation (1) is valid only for temperatures $T \geq 32°F$ (0°C) (1)

The foregoing equation is derived from the mean annual equilibrium temperature cycle

$$E = E_m + \Delta E \sin(\omega t) \quad (2)$$

Equations (1) and (2) have been plotted in Figure 3. Equilibrium temperature E is by definition that water temperature at which the net heat transfer through the water surface is zero. Equilibrium temperature can be computed from weather data, specifically air temperature, solar radiation, dew point temperature, wind velocity and cloudiness ratio. Some actual data from an Environmental Protection Agency report (1971) are given in Figure 4.

In Equation (1) t = time in days, $\omega = 2\pi/365$, $m = K/\rho ch$, where K = annual bulk surface conductance, ρc = specific heat per unit volume, h = mean depth of water body, I = the daily rate of artificial heat input, if any and $\delta = \arctan\left(\frac{\omega}{m}\right)$. Typical values for central Minnesota conditions are $E_m = 49°F$, $\Delta E = 28°F$, $K = 80$ BTU ft^{-2} day^{-1} $°F^{-1}$, $\rho c = 62.4$ $ft^{-3}°F^{-1}$ and $I = 0$.

A lake will freeze over, when $T = 32°$ is reached during the cycle of decreasing water temperature (3rd quadrant of the sinusoidal temperature

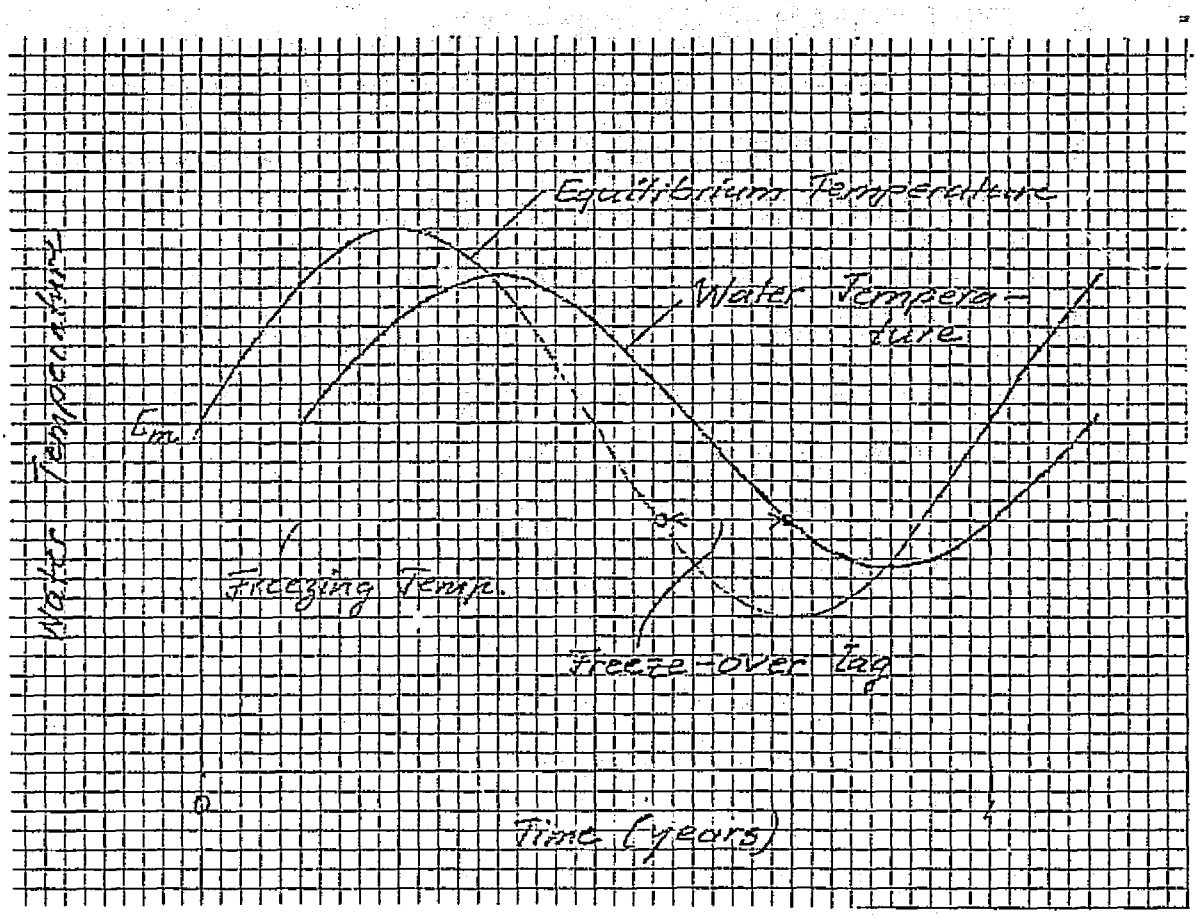

Figure 3. Schematic mean annual water temperature and equilibrium temperature cycles.

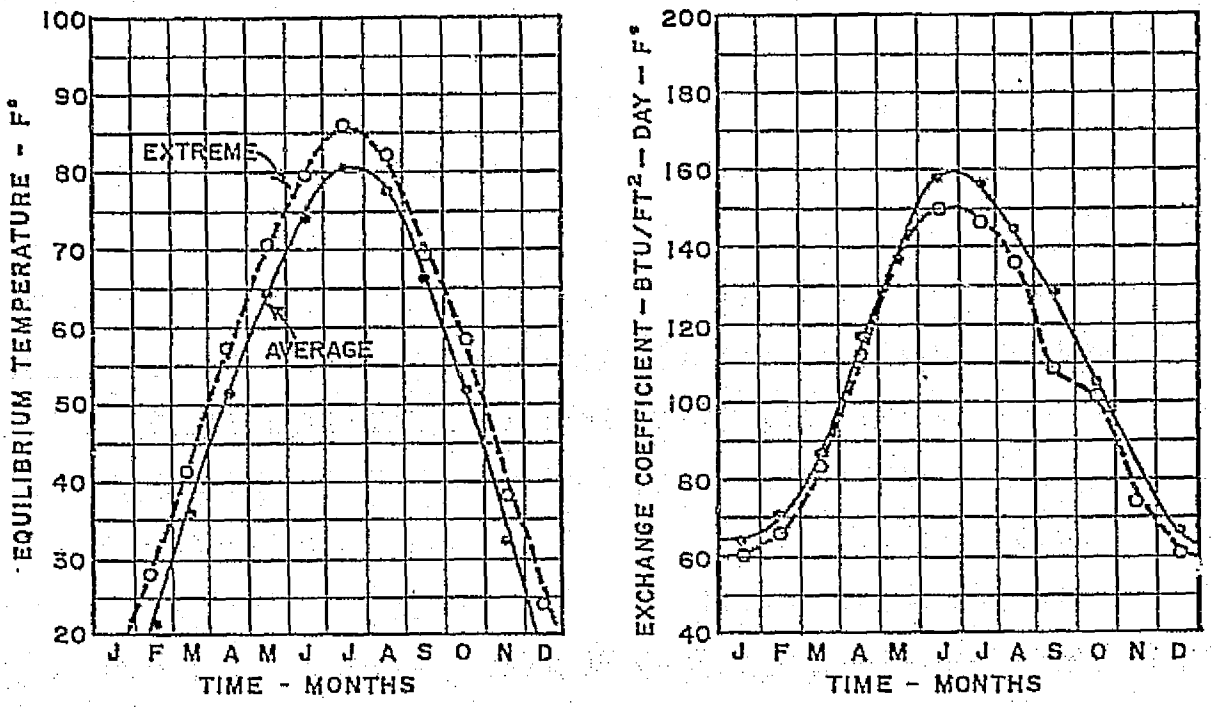

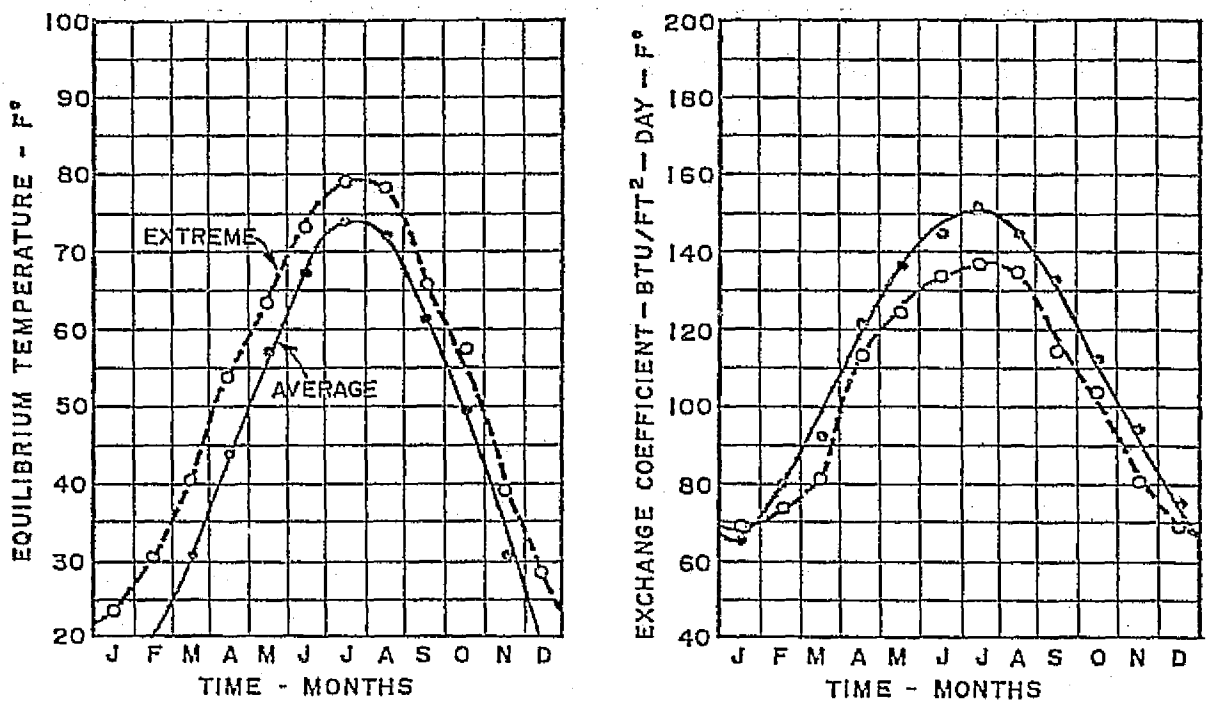

Figure 4. Actual mean monthly values of equilibrium temperature and bulk surface heat exchange coefficients.

cycle). If Equation (1) is solved for t at T = 32°F, the result is

$$t = \frac{1}{\omega} \arcsin \frac{32 - E_m - \frac{I}{m}}{\Delta E} \left(1 + \frac{\omega}{m}^2\right)^{1/2} + \delta \qquad (3)$$

The right-hand side of Equation (3) depends on lake depth h. A lake of depth h = 0 freezes over when equilibrium temperature reaches 32°F or when

$$t = \frac{1}{\omega} \arcsin \frac{32 - E_m - \frac{I}{m}}{\Delta E} \qquad (4)$$

Lake depth produces a lag in the freeze-over date. The lag is

$$\text{lag} = \frac{1}{\omega} \arctan \frac{\omega}{m} + \frac{1}{\omega} \arcsin \frac{32 - E_m - \frac{I}{m}}{\Delta E} \left(1 + \frac{\omega}{m}^2\right)^{1/2}$$

$$- \frac{1}{\omega} \arcsin \frac{32 - E_m - \frac{I}{m}}{\Delta E} \qquad (5)$$

Function (5) has been plotted in Figure 5

The relationship shown in Figure 5 is for specified values of $E_m = 49°F$, $\Delta E = 28°F$, $K = 80$ BTU ft^{-2} day^{-1} $°F^{-1}$ and $I = 0$, which in essence describe mean climatological conditions in central Minnesota. For other regions and specific years other numerical values would be obtained. Figure 5 does specify an order of magnitude for the lag time. Since it reflects a nearly linear relationship it may be interpreted to mean that for every foot of median depth the freeze-over date will be delayed by approximately one day. Obviously, the total lag between lakes of different depths can add up to considerable lengths of time in terms of days and weeks. Information from satellite imagery given in Figures 2a through 2e corroborates this information.

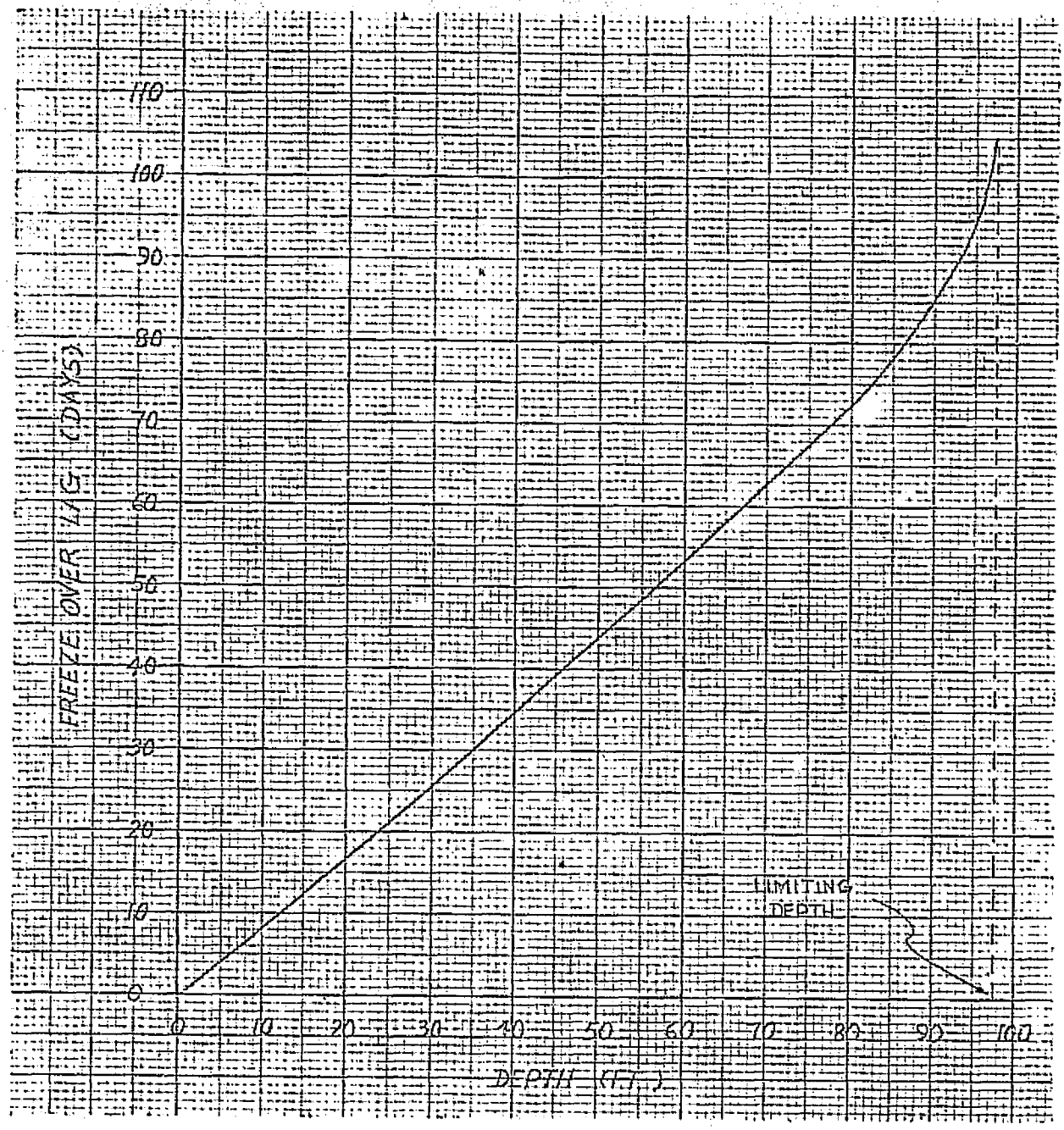

Figure 5. Theoretical time lag of freeze-over date as a function of mean lake depth.

The theory also indicates that a lake will not freeze over at all if its depth exceeds a value which can be derived from the relationship

$$E_m + \frac{I}{m} - 32°F = \Delta E \left[1 + \left(\frac{\omega}{m}\right)^2\right]^{-1/2} \quad (6)$$

The critical depth is

$$h_{cf} = \frac{K}{\omega \rho c} \left[\frac{\Delta E}{E_m + \frac{I}{m} - 32}\right]^2 - 1\Bigg]^{1/2} \quad (7)$$

HINDCASTING OF FREEZE-OVER DATES AND VERIFICATION USING IMAGERY

LANDSAT imagery provided the only means to verify the relationships derived for forecasting freeze-over dates. Satellite imagery does not provide a continuous freeze-over history of a lake. It rather provides an occasional glimpse at ice conditions in an entire region. Typically lakes of many different sizes and depths are found in a region, and those which have open water can be distinguished from those which are ice-covered. This information can be presented in the form already shown in Figures 2 (a-e) and can be superimposed and compared with the theory presented.

The forecasting of ice-covers would be made sometime in fall, when the annual weather cycle is still incomplete. Estimates of the parameters E_m, ΔE and K would be based on weather data available at the time of forecasting. Details on the relationships used to compute values of the parameters E_m, ΔE and K from the individual weather station data can be found in A. Fu's M.S. Thesis (1979).

The effect of weather data limitations on the forecasting is shown in Figures 2 (a-e) where forecasts (hindcasts) at the end of four different months are compared with information from satellite imagery. It can be seen that the forecast freeze-over date shifts generally by one to seven days as the season progresses.

The agreement between hindcasts and satellite observations was generally satisfactory. The effect of lake depth on freeze-over described by the theory was also found in the satellite observations.

MEAN FREEZE-OVER DATES FOR MINNESOTA LAKES

The forecasting procedure verified by using information from the LANDSAT scenes (Figure 1) for four years of observations was subsequently applied to all of Minnesota. The number of weather stations was expanded from 9 to 19 to cover all of the state. The results of the weather data analysis applied to the freeze-over theory are shown in Figure 6 and Figures 7 (a-e). Figure 6 gives an approximate minimum depth i.e., minimum mean depth of a lake which is unlikely to freeze over completely in an average year. The value is an average of those found for the years from 1972 through 1977 and reflects the weather conditions during that time. Figures 7 (a-e) give the average freeze-over dates for lakes of different mean or median depths.

Figure 6 presents one number at the location of each weather station used. In addition interpretated lines are shown.

INFORMATION FROM LANDSAT IMAGERY ON SPRING MELTING OF LAKE ICE-COVERS

The melting of ice covers on Minnesota lakes in the spring occurs typically between March and May. LANDSAT images for March, April and

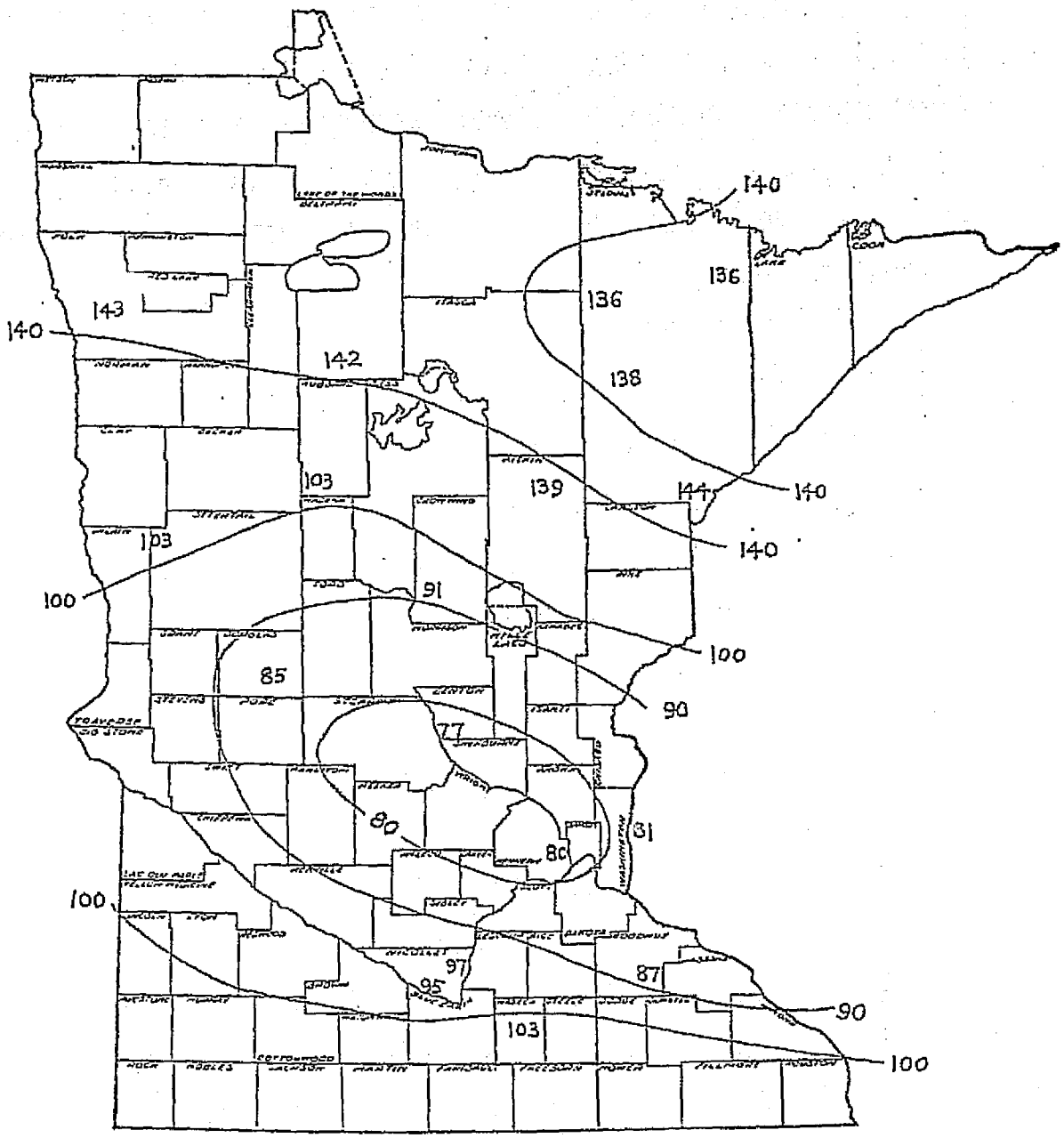

Figure 6. Distribution of no-freeze-over depths of completely mixed lakes in Minnesota.

E20

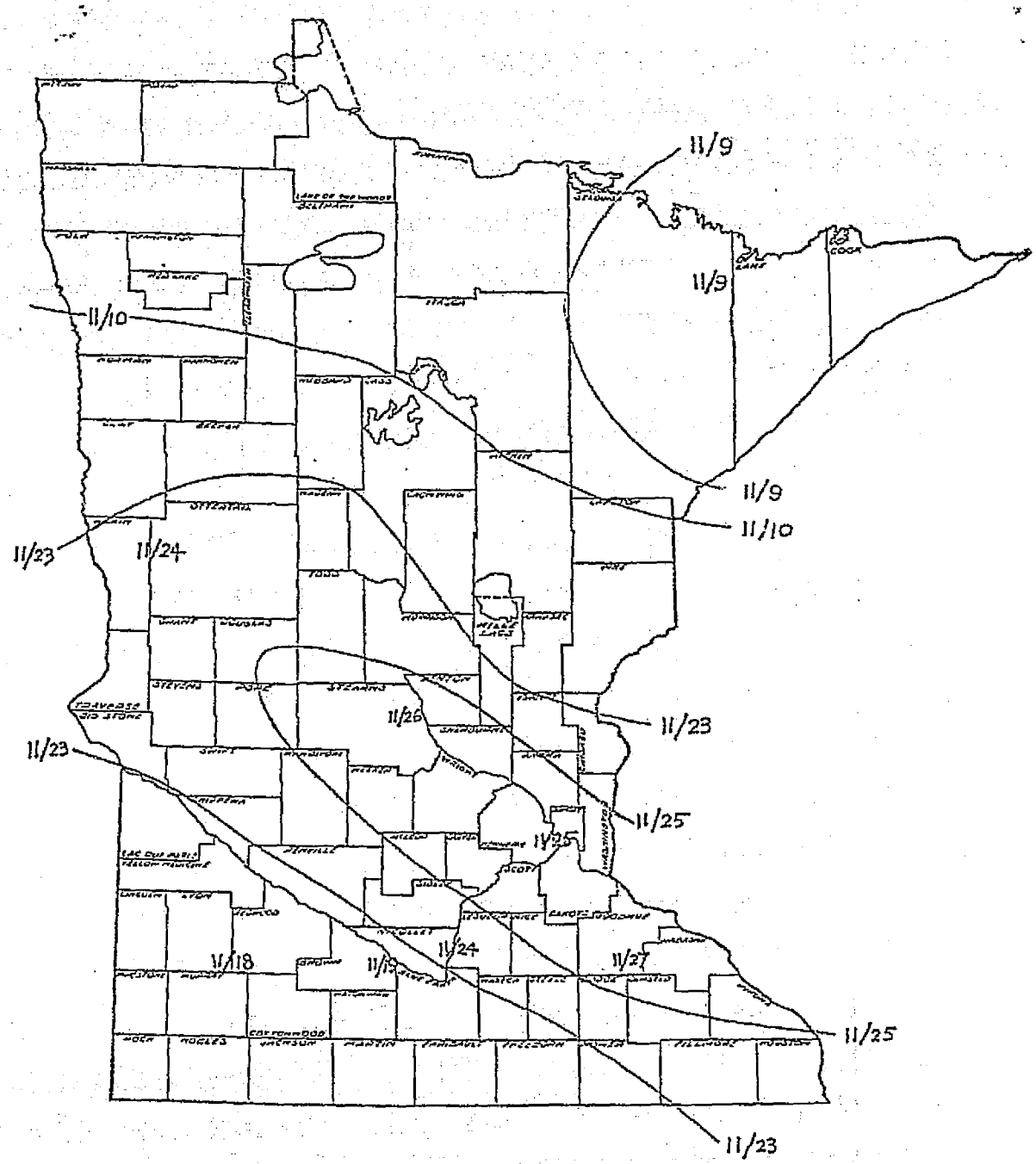

Figure 7a. Average freeze-over dates of lakes having mean or median depths less than or equal to 5 feet.

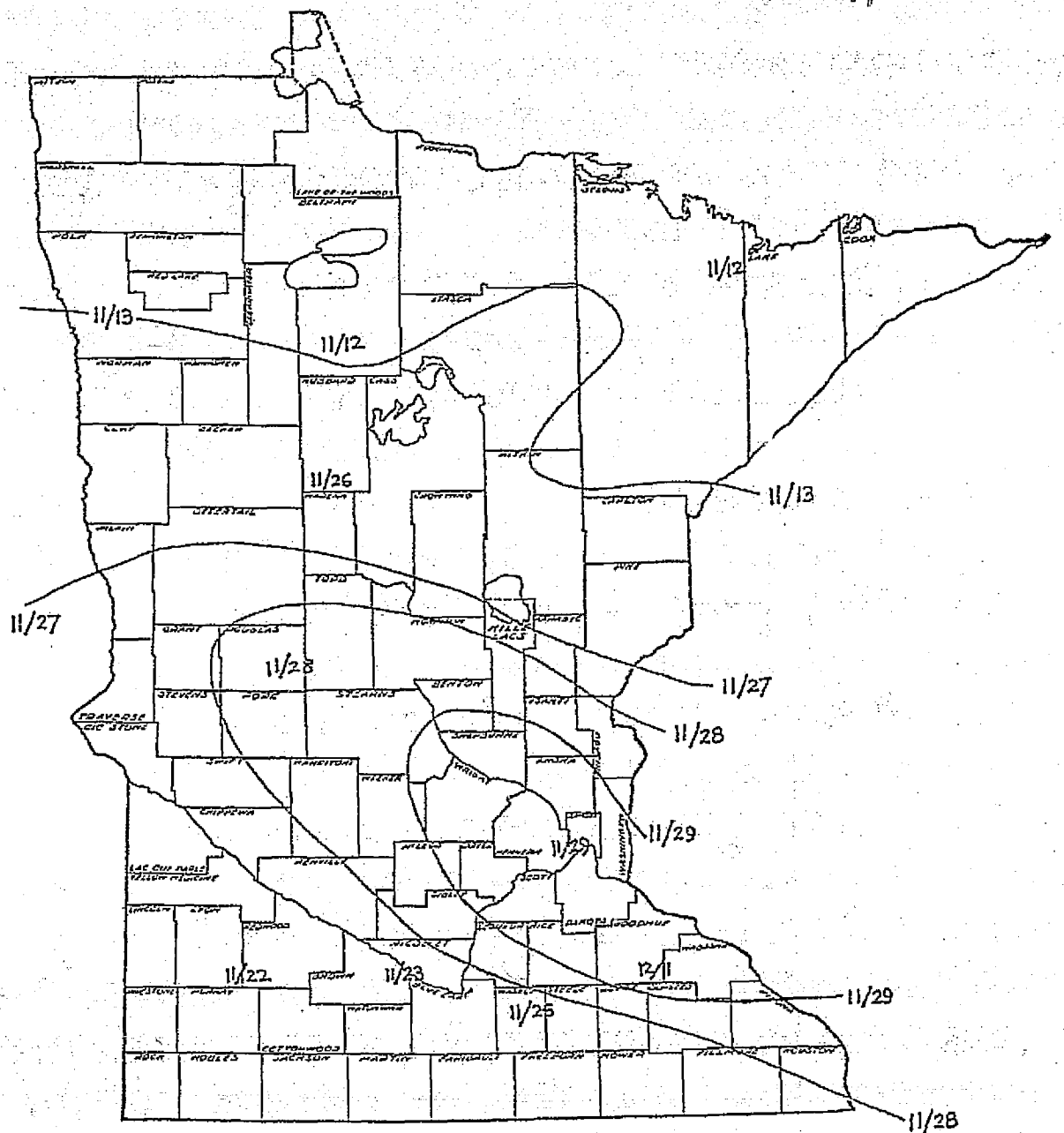

Figure 7b. Average freeze-over dates of lakes having mean or median depths less than or equal to 10 feet.

E22

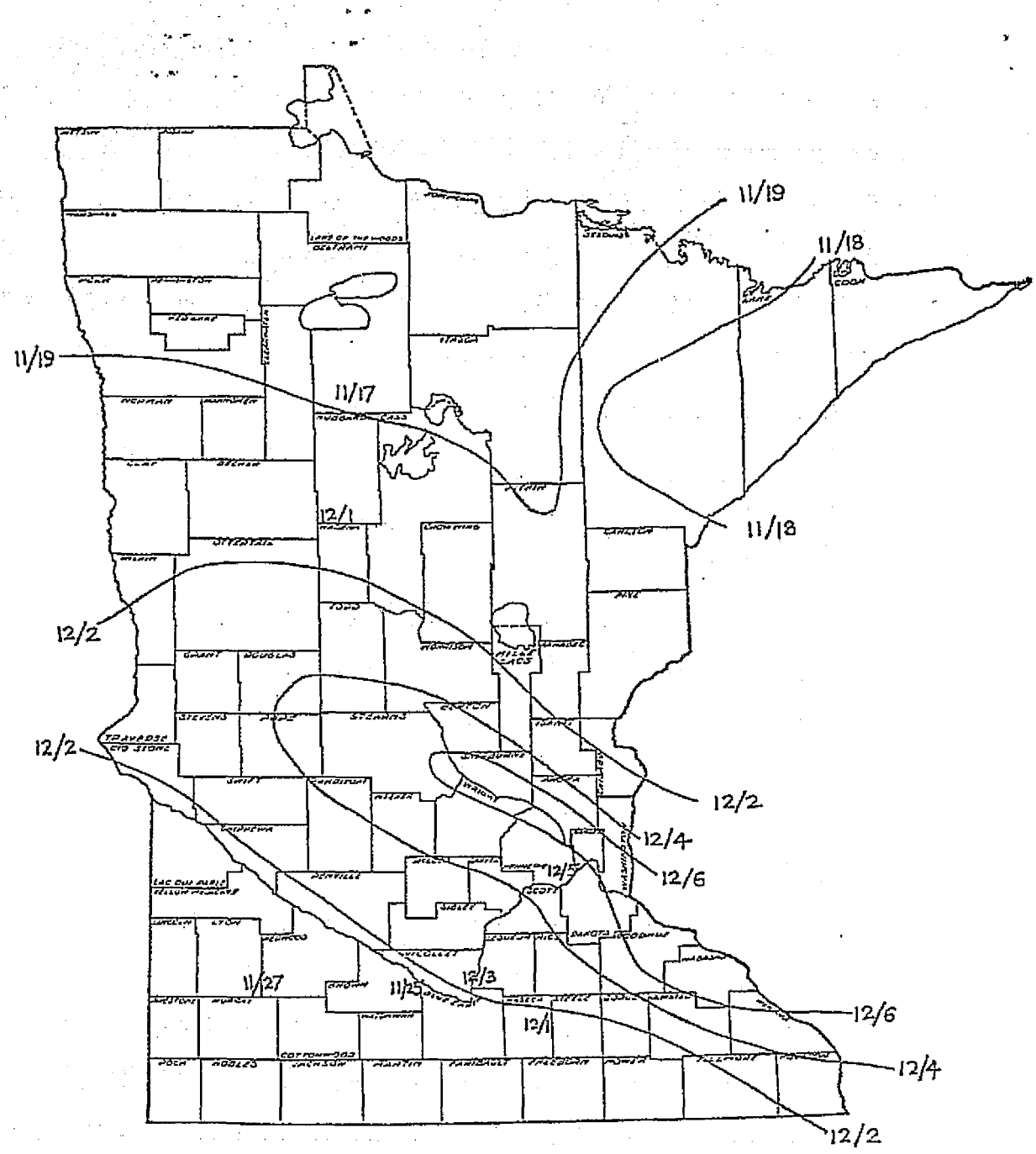

Figure 7c. Average freeze-over dates of lakes having mean or median depths less than or equal to 20 feet.

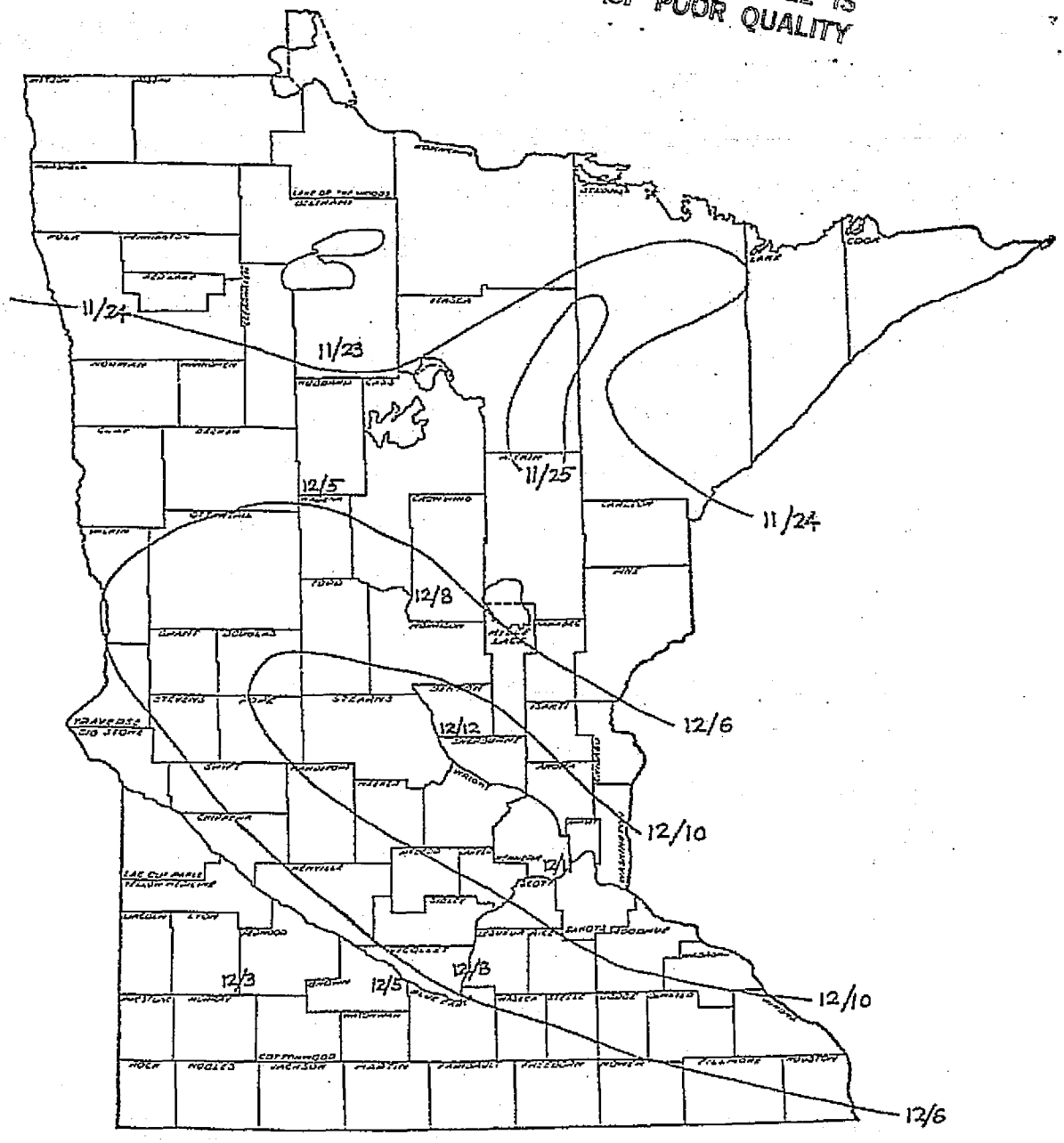

Figure 7d. Average freeze-over dates of lakes having mean or median depths less than or equal to 30 feet.

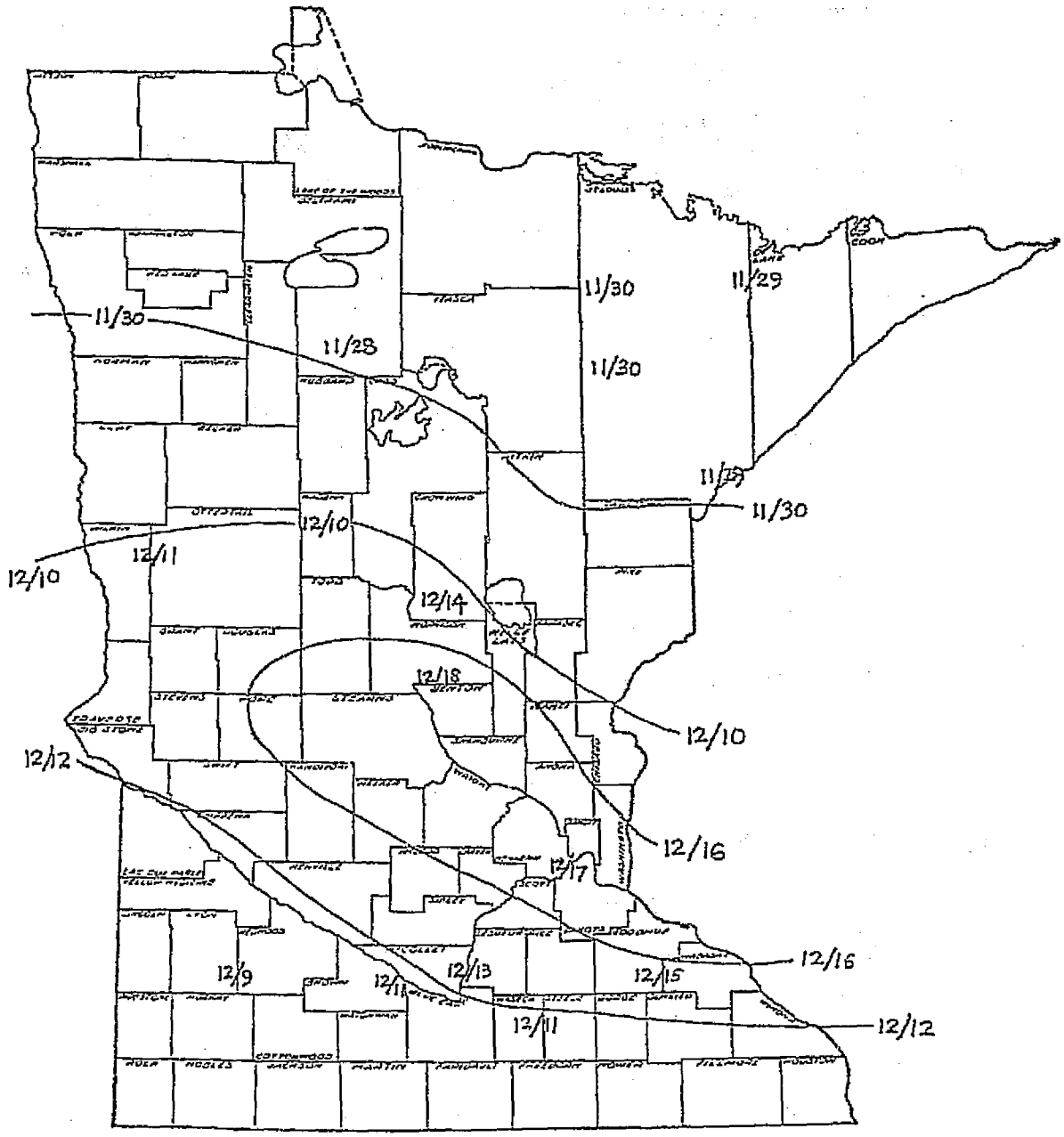

Figure 7e. Average freeze-over dates of lakes having mean or median depths less than or equal to 40 feet.

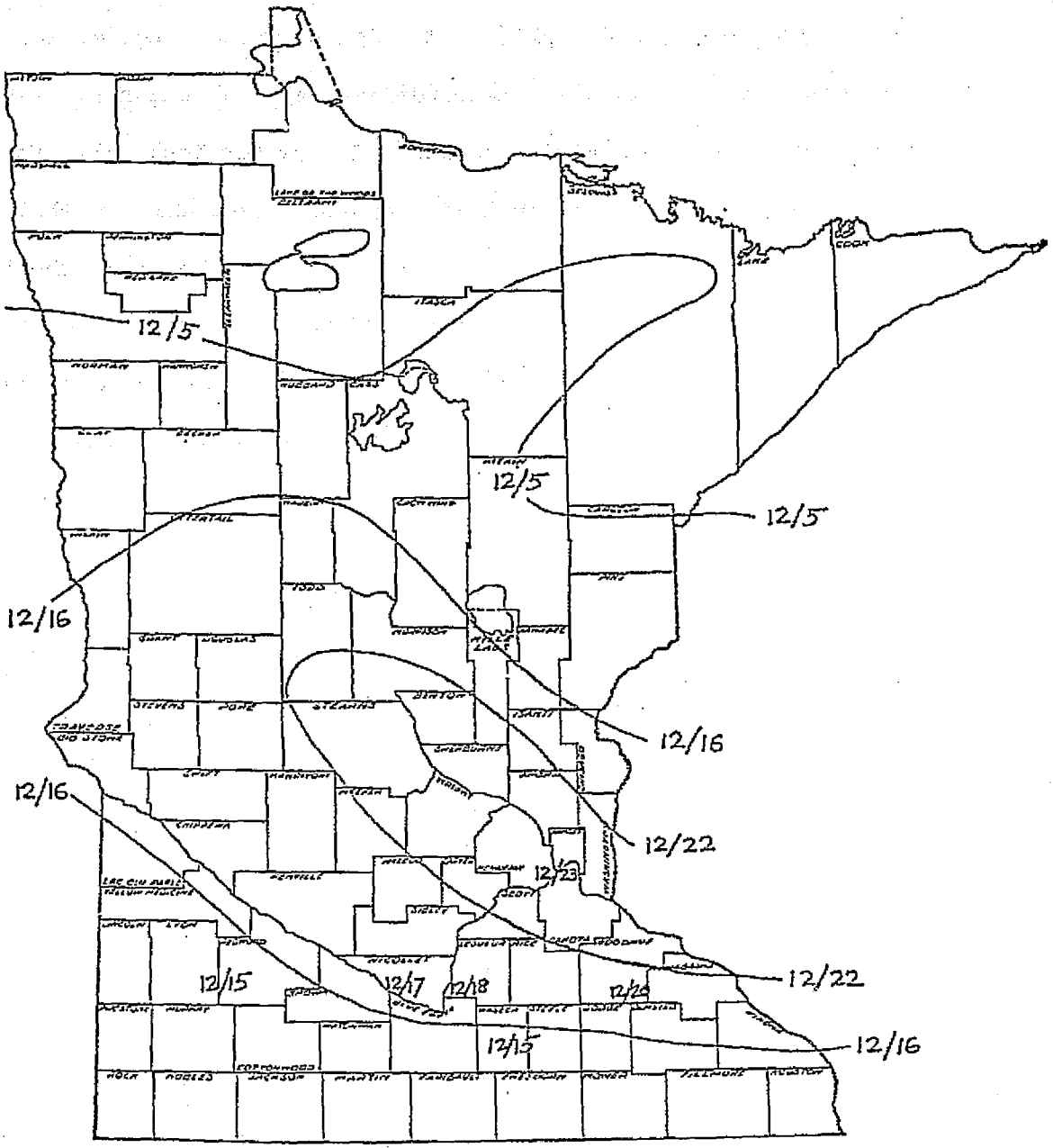

Figure 7f. Average freeze-over dates of lakes having mean or median depths less than or equal to 50 feet.

May 1976 have been used to extract information on ice conditions in spring. Average cloud cover in spring of 1976 was less than in the fall of 1975. This is typical also for other years. The procedure for LANDSAT image interpretation was similar to that described earlier for the fall of 1975. Results showing ice conditions as a function of lake depth and date similar to those given in Figure 2 were plotted. They showed a very poor correlation of ice cover with depth. The reason is that the melting of the ice cover is only to a minor degree related to the heat budget of the lake water beneath the ice. The radiation balance on the ice as well as along the shorelines, and inflow of water from minor tributaries and overland flow are much more important. Radiation and overland flow, if at all related to lake morphology, would depend on lake surface area. Observations on ice coverage were therefore plotted versus lake surface area. It appears that the spring ice melting is very uniform in time and pretty much independent of lake size. A theory very different from that used for the freeze-over prediction is needed.

CONCLUSIONS

a) LANDSAT imagery is the only easily accessible and extensive source of information on ice coverage of Minnesota lakes.

b) Ice coverage affects water quality of lakes e.g., through oxygen depletion, enhancement of sedimentation and interaction with groundwater. It is a potential factor in toxic material transport. Certain lake surveys require an ice cover. Removal of rough fish from lakes is often done just prior to ice formation.

c) Cloud coverage hinders the use of LANDSAT imagery. Usefulness of satellite imagery in the falls of 1972, 73, 74 and 75 is summarized

in Table 1. Average cloud coverage during the period of lake ice formation in those four years was 59 per cent. Nevertheless, enough information was available to verify a theoretical model for the prediction of freeze-over dates of Minnesota lakes.

d) The model is based on a seasonal heat budget and takes into consideration lake depth. It was found that as a rule of thumb freeze-over date was delayed by three days for every additional meter of mean depth. A lake of 40 ft. mean depth would therefore freeze about 27 days later than a lake of 10 ft. depth.

e) The predictive model was applied to different regions of Minnesota. The results are summarized in Figures 6 and 7 (a-e). Lakes in the northeastern part of Minnesota are predicted to freeze over first, those in the Metropolitan-St Cloud area last. The lag for lakes of equal mean depth but located in those two extreme regions was predicted to be about 18 days.

f) The lag-times due to depth and due to latitude are cumulative. A very shallow northwestern Minnesota lake would therefore freeze 26 days before a 20 ft. (mean) deep lake in the Metropolitan area.

g) The prediction of freeze-over dates at the end of the summer or in fall may miss the real date by as much as a week due to the uncertainty of the weather between the date of the forecasting and the freeze-over date.

h) Spring melting of icecovers observed on LANDSAT imagery bears little relationship to lake morphology. A separate theory needs to be considered.

LITERATURE CITED

1. Lind, A.O., Ice Development on Lake Champlain, Remote Sensing Lab., Vermont University, Burlington, Ontario, July 1973.

2. Minnesota Department of Conservation, Division of Water and Soils, An Inventory of Minnesota Lakes, Bulletin No. 25, St. Paul, Minnesota, 1968.

3. Tsang, Gee, Ice Piling on Lakeshores, with Special Reference to the Occurrences on Lake Simcoe in the Spring of 1973, Scientific Series No. 35, Canada Centre for Inland Waters, Burlington, Ontario, 1974.

4. Vanderbilt University, Department of Environmental and Water Resources Engineering, Effect of Geographical Location on Cooling Pond Requirements and Performance, U.S. Environmental Protection Agency, Water Pollution Control Research Series, 16 130 FQD 03/71.

5. Fu, Alec Y.K., Analysis and Prediction of Freeze-Over Dates of Minnesota Lakes Using LANDSAT Imagery and Weather Information, Master of Science Thesis, University of Minnesota, Minneapolis, Minn., March 1979.